Volume 34 No. 2 | JNSChE Sep/Oct 2019 | ISSN 0794-6759

JOURNAL OF THE NIGERIAN SOCIETY OF CHEMICAL ENGINEERS

Published by,
THE NIGERIAN SOCIETY OF CHEMICAL ENGINEERS
National Secretariat: Infinite Grace House, Plot 4, Oyetubo Street,
Off Obafemi Awolowo Way, Ikeja, Lagos State, Nigeria.
E-mail: nationalhqtrs@nsche.org, nsche_headquarters@yahoo.com
Website: http:www.nsche.org.ng
Submission of Manuscripts: nschejournal@yahoo.com and copy: stevmomoh@yahoo.com

JOURNAL OF THE NIGERIAN SOCIETY OF CHEMICAL ENGINEERS
A Publication on the Science and Technology of Chemical Engineering

EDITORIAL BOARD

2019 NIGERIAN SOCIETY OF CHEMICAL ENGINEERS

BOARD OF DIRECTORS AND OFFICIALS

Engr. O. A. Anyaoku, *FNSChE*	National President
Engr. S. A. Mohammed, *FNSChE*	Deputy National President
Prof. Sam S. Adefila, *FNSChE*	Immediate Past President
Engr. D. Uweh, *MNSChE*	Publicity Secretary
Engr. Ben Akaakar, *FNSChE*	Asst. Publicity Secretary
Engr. Anthony Ogheneovo, *MNSChE*	National Treasurer
Engr. (Mrs.) Edith A. Alagbe, *MNSChE*	Asst. National Treasurer
S. O. Bosoro, *MNSChE*	Executive Secretary

INTERNAL AUDITORS

Engr. Dr. Mrs. G. Akujobi-Emetuche, *FNSChE*
Engr. Edwin N.Ikezue, *FNSChE*

SUBSCRIPTION

a.	**Individual Member**	₦3,000.00
b.	**Overseas Subscribers**	US$100.00
c.	**Institution, Libraries, etc**	₦5,000.00

CHAPTER CHAIRMEN

Engr. G. H. Abubakar, *MNSChE*	Kogi
Engr. (Mrs.) Rosemary O. Imhanwa, *MNSChE*	Edo/Delta
Engr. I. A. Dirani, *MNSChE*	ABBYGOT
Prof. I. A. Mohammed-Dabo, *MNSChE*	Kaduna
Dr. M. S. Nwakaudu, *FNSChE*	Imo/Abia
Prof. G. O. Mbah, *FNSChE*	Anambra/Enugu/ Ebonyi
Dr. A. A. Ujile,*FNSChE*	RIVBAY
Engr. N. A. Akanji, *MNSChE*	Niger
Engr. O. O. Onugu, *FNSChE*	FCT/Nasarawa
Prof. E. A. Taiwo, *FNSChE*	Oyo/Osun/Kwara
Dr. K. F. K. Oyedeko, *FNSChE*	Lagos/Ogun
Engr. T. S. Soom, *MNSChE*	Benue Industrial
Dr. I. O. Oboh , *MNSChE*	Akwa Ibom/Cross River
Prof. E. I. Dada, *FNSChE*	USA

EXPERIMENTAL INVESTIGATION OF THE DEHYDRATION KINETICS OF WHITE YAM (*DIOSCOREA ROTUNDATA*) USING A REFRACTANCE WINDOW™ DRYER

***Akinola, A. A. and Ezeorah, S. N.**
Chemical and Petroleum Engineering Department
University of Lagos, Akoka, Lagos
*Email of the Corresponding author: akinjideakinola@gmail.com

ABSTRACT

The objective of this study is to investigate the dehydration characteristics of yams slices at different drying temperatures and for different thicknesses of yam slices. Yam slices 1.5, 3.0, and 4.5 mm thick were dehydrated in a laboratory-scale Refractance Window™ dryer at 65, 75, 85, and 95°C. During the drying operations, moisture content data were recorded. The experimental moisture content data were fitted into empirical and semi-theoretical thin-layer drying models. For the process conditions studied, the drying data fitted all the thin-layer drying models considered in this report, with a correlation coefficient greater than 98%. However, the Haghi and Ghanadzadeh model gave a higher correlation than the other models implying that the model predicts the drying kinetics of yam better than other models. The data was also used to plot the drying curve and the drying rate curve. The drying times to dehydrate the yam slices to a moisture ratio of 0.11g-water/g-solid varied between 25 to 320 minutes. The drying times were observed to decrease as the temperature increased for a given slice size. Also, the drying times increased with slice size for a given temperature. This study was performed to facilitate the understanding of the dehydration characteristics of the Refractance Window™ (RW) drying operations for yam slices, with the intentions of designing, modelling, and operating a continuously operating RW dryer.

Keywords: Yams; Thin-Layer Drying Models; Drying Curves; Refractance Window™ Dryer

INTRODUCTION

Yams produce elongated large cylindrical-shaped tubers which are grown bi-annually in tropical regions of the world. Yams are from the plant species whose genus is *Dioscorea* (family *Dioscoreaceae*) and white yams, *Dioscorea rotundata*, are the most popular species especially in the dominant yam production zones in Africa (IITA, 2009). Raw yams constitute, 69.60 % water, 27.88 % carbohydrates, and 1.53 % protein; 100g of yam provides 118 kcal of energy (Cock, 1985; USDA, 2017).

Yam tubers, processed into powdered form, are used to prepare many cuisines around the world (Hudgens and Trillo, 2003). The powder preparation process involves washing, peeling, slicing, and dehydrating. The process is a labour-intensive process (Lancaster *et al.,* 1982), which may take about 3 to 5 days in regions where sun-drying is the dehydration method. Also, dirt and microorganisms may cause degradation of the quality of the dehydrated yams (Agoreyo et al., 2011). A fast-drying process producing a suitably dry final product can prevent the degradation of dehydrated yams (Maskan, 2000). There is, therefore, a need to find an alternative drying method to reduce significantly, the time taken to dry yam tubers.

The Refractance Window™ drying technique patented by Magoon (1986) and fully developed by MCD Technologies Inc., Tacoma, WA, USA, is increasingly being used in dehydrating food. Studies using a Refractance Window™ dryer conducted by Nindo and Tang, (2007) indicated that purees and juices prepared from fruits, vegetables, or herbs could be dehydrated to 10% within 3 -5 minutes. Akinola *et al.,* (2016) using a Refractance WindowT^{M} drying dryer, demonstrated that carrot slices, 3 mm thick, could be dried to a moisture content of less than 10% within 200 minutes. Akinola *et al.,* (2018) demonstrated that at 60°C, a laboratory-scale Refractance Window™ dryer would dehydrate 3 mm-thick cucumber slices to a moisture content of less than 10% within 120 minutes. These times are considerably less than the 3 – 5 days taken for sun-drying of yams.

The article reports the dehydration characteristics of yam under varied conditions, using a laboratoryscale Refractance Window™ dryer. The dehydration characteristics determined are the drying curve and the drying rate curve, which are essential characteristics

required in the design, modelling, operations of dryers, in this case, the Refractance Window^{TM} dryer.

METHODS AND MATERIALS

Drying Apparatus

The drying of yam slices was investigated using a laboratory-scale Refractance Window^{TM} dryer fabricated at the University of Lagos, Lagos, Nigeria. The apparatus is similar to those used by Akinola *et al.* (2018). The apparatus, presented in Figure 1, consists of a 1 cm thick stainless steel shallow water tub, 1.0 meter in length, 0.5 meters wide, and 75 mm deep. A 0.15 mm thick transparent polyethylene terephthalate (PET) Mylar plastic film covered the water tub.

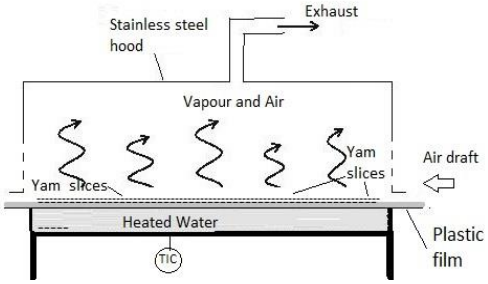

Fig. 1 A Schematic Diagram of a Refractance Window Dryer (Akinola *et al.*, 2018)

The water in the equipment was heated with a 2.5 kW heater which was controlled using a Bayite BTC201 Pre-Wired Digital Temperature Controller. The lower surface of the PET film was always in contact with the water, and the film was secured, with metal brackets. The moist air above the drying film was extracted using a suction fan in the hood above the dryer; this was to ensure that the moist air does not inhibit the drying process.

Sample Preparation and Experimental Procedure

White yam tubers bought from a local market were used, in this study. The yam tubers had lengths between 45 cm to 60 cm and maximum diameters between 11.3 and 16.4 cm; they had elongated cylindrical shapes with tapered ends. For experimentation, the yam tubers were cut, into 1.5, 3.0 and 4.5 mm thick slices, using a mechanical Mandolin slicer and then carefully cut into 2.54 cm squares with a sharp knife. Thin slices were used because they have higher drying rates than thicker slices (Azizi *et al.*, 2017). Also, the 1.5 to 4.5 mm yam slices size range used in this study is within the 1.0 - 6.0 mm slice sizes for most experiments done in the literature (Madamba *et al.*, 1996; Azizi et al., 2017).

Experiments were performed for each set of slice size, with water temperatures of 65^{o}C, 75^{o}C, 85^{o}C, and 95^{o}C in the Refractance Window^{TM} dryer. The high temperature of 95^{o}C was selected to be slightly lower than the maximum possible operating temperature (100^{o}C) for a Refractance Window^{TM} dryer. The low temperature of 65^{o}C was selected to have a reasonable drying time. The 75^{o}C and 85^{o}C temperatures were selected to study the kinetics within the lower and upper boundaries.

The initial moisture content of yam slices was determined to be 65.98% wet basis, using an OHAUS moisture analyser (OHAUS Corporation, 2011). A dozen sets of experiments were performed, each for a combination of a temperature and a slice size. The drier was started and allowed to attain the desired temperature before loading of samples on the heated transparent polyethylene terephthalate (PET) Mylar plastic film. At 5-minute intervals, during the experiments, some yam slices were removed and their moisture content determined. All drying operations were performed 3 times.

Determining the Moisture Ratio

The moisture ratio at given drying period was determined using Equation 1(Akgun and Doymaz (2005); Doymaz (2004); Sharifian *et al.*, 2012).

$$MR = MC_t/MC_i \quad (1)$$

where

MC_t is the moisture content of the sample after drying for time t and

MC_i is the initial moisture content of the fresh sample, all in the unit of grams of water removed/grams of solids.

Thin-Layer Drying Models

The experimental data were fitted to 9 common empirical, and semi-theoretical thin-layer drying models used in the dehydration of roots, corms, bulbs, fruits and vegetables; these thin-layer models are presented in Table 1 (Ezeorah, 2018).

Table 1 Thin-Layer Drying Models Used in this Study (Akinola *et al.*, 2018)

No.	Model Names	Models
1.	Newton model	$MR = \exp(-kt)$
2.	Page model	$MR = \exp(-kt^n)$
3.	Modified Henderson and Pabis model	$MR = a\exp(-kt) + b\exp(-gt) + c\exp(-ht)$
4.	Logarithmic model	$MR = a\exp(-kt) + c$
5.	Demir *et al.* model	$MR = a\exp(-kt)^n + b$
6.	Verma *et al.* model	$MR =$

Table 1 Thin-Layer Drying Models Used in this Study (Akinola *et al.*, 2018)

No.	Model Names	Models
		$a\exp(-kt) + (1 - a)\exp(-gt)$
7.	Weibull model	$MR = a - b\exp(-k_0 t^n)$
8.	Peleg model	$MR = 1 - t/(a + bt)$
9.	Haghi & Ghanadzadeh	$MR = a\exp(-bt^c) + dt^2 + et + f$

Where

MR is the moisture ratio,

t is the drying time and,

a, b, c, d, e, f, k, k_0, and n are all constant determined by regression analysis.

RESULTS AND DISCUSSION

Experimental Environment

During the drying operations, the surface of the dryer was exposed to ambient conditions. The ambient conditions in the laboratory, over the several days of experimental work, were such that the temperature ranged from 29 to 31^{o}C, while the humidity varied between 53 to 62%.

Moisture Ratio and Drying Time Relationship

The thin layer drying model that best describes the relationship between moisture ratio and drying time, the drying kinetics, was determined by fitting the experimental drying data to the models presented in Table 1. The thin-layer drying model that best describes the drying kinetics of the yam slices is the one in which the following three criteria are satisfied. The criteria are the coefficient of determination (R^2), is to be closest to unity, the sum-of-square-error (SSE), and the root mean-square-error (RMSE) are closest to zero. The method of estimating R^2, SSE and RMSE are discussed extensively in literature (Ogunnaike, 2011; Johnson, 2017), and have been used in works on drying kinetics of agricultural food materials (Ertekin and Yaldiz, 2004; Kabiru *et al.*, 2013, Sanful et al., 2015; Akinola et al., 2016). The Matrix Laboratory software (MATLAB) was used to perform the statistical analysis.

The results of the statistical analysis for fitting the thin-layer drying models are presented in Tables 2, 3, 4, and 5.

For the 12 sets of experiments performed, all the 9 models were observed to fit the experimental data with a coefficient of variance R^2, better than 0.96. However, the Haghi and Ghanadzadeh (2005) thin-layer drying model was found to fit because it had an R^2 value closest to unity. The constants obtained for the Haghi and Ghanadzadeh model at different slice sizes and the drying temperature are presented in Table 6.

Validation of Selected Models

To corroborate that the Haghi and Ghanadzadeh (2005) thin-layer drying model best fits the drying kinetics, the relationship between the predicted (PMR) and experimental moisture ratio (EMR) values were determined. Table 7 shows that in all cases, the linear relationship had slopes close to unity and intercepts close to zero. Also, in all cases, the coefficient of variance (R^2), was better than 0.99 (Table 7). The implication is that there was no significant difference between moisture ratios determined by performing experiments and the predicted moisture ratios for the process conditions considered when modelling using the Haghi and Ghanadzadeh (2005) thin-layer drying model.

Table 2: Result Summary of the Statistical Curve Fitting Analysis at 65^{o}C For 1.5, 3.0 and 4.5 mm Yam Slices

Slice Thickness →		**1.5 mm**			**3.0 mm**			**4.5 mm**		
No.	**Model Name**	R^2	**SSE**	**RMSE**	R^2	**SSE**	**RMSE**	R^2	**SSE**	**RMSE**
1	Haghi & Ghanadzadeh	0.998	0.002	0.016	0.999	0.001	0.016	1.000	0.001	0.007
2	Verma et al	0.997	0.003	0.019	0.997	0.003	0.021	0.998	0.003	0.014
3	Modified Henderson & Pabis	0.997	0.004	0.023	0.989	0.011	0.048	0.998	0.003	0.016
4	Page	0.995	0.005	0.021	0.997	0.003	0.018	0.999	0.001	0.008
5	Logarithmic	0.995	0.006	0.024	0.995	0.006	0.026	0.998	0.003	0.013
6	Demir et al	0.995	0.006	0.025	0.995	0.006	0.028	0.998	0.003	0.014
7	Peleg	0.994	0.006	0.024	0.986	0.015	0.041	0.998	0.002	0.011
8	Newton	0.994	0.007	0.024	0.994	0.007	0.026	0.990	0.012	0.027
9	Weibull	0.992	0.008	0.030	0.998	0.002	0.017	1.000	0.001	0.007

Table 3: Result Summary of the Statistical Curve Fitting Analysis at 75^{o}C For 1.5, 3.0 and 4.5 mm Yam Slices

Slice Thickness →		1.5 mm			3.0 mm			4.5 mm		
No.	**Model Name**	R^2	**SSE**	**RMSE**	R^2	**SSE**	**RMSE**	R^2	**SSE**	**RMSE**
1	Haghi & Ghanadzadeh	1.000	0.000	0.005	0.998	0.002	0.016	0.999	0.001	0.009
2	Verma et al	1.000	0.000	0.004	0.995	0.006	0.023	0.997	0.003	0.017
3	Modified Henderson & Pabis	1.000	0.000	0.005	0.913	0.102	0.113	0.991	0.008	0.035
4	Page	0.999	0.001	0.009	0.994	0.007	0.024	0.996	0.004	0.019
5	Logarithmic	0.993	0.006	0.026	0.995	0.006	0.024	0.992	0.008	0.028
6	Demir et al	0.993	0.006	0.028	0.995	0.006	0.025	0.992	0.008	0.029
7	Peleg	1.000	0.000	0.005	0.993	0.008	0.026	0.997	0.003	0.016
8	Newton	0.969	0.026	0.051	0.994	0.007	0.023	0.978	0.021	0.042
9	Weibull	1.000	0.000	0.008	0.991	0.011	0.033	0.989	0.010	0.034

Table 4: Result Summary of the Statistical Curve Fitting Analysis at 85^{o}C For 1.5, 3.0 and 4.5 mm Yam Slices

Slice Thickness →		1.5 mm			3.0 mm			4.5 mm		
No.	**Model Name**	R^2	**SSE**	**RMSE**	R^2	**SSE**	**RMSE**	R^2	**SSE**	**RMSE**
1	Haghi & Ghanadzadeh	1.000	0.000	0.010	0.998	0.002	0.019	0.999	0.001	0.016
2	Verma *et al*.	0.999	0.001	0.011	0.997	0.002	0.017	0.998	0.002	0.017
3	Modified Henderson & Pabis	0.999	0.001	0.015	0.998	0.002	0.019	0.998	0.002	0.018
4	Page	0.999	0.001	0.013	0.996	0.004	0.021	0.998	0.002	0.014
5	Logarithmic	0.994	0.004	0.029	0.990	0.009	0.033	0.998	0.002	0.015
6	Demir *et al.*	0.994	0.004	0.032	0.990	0.009	0.036	0.998	0.002	0.016
7	Peleg	0.999	0.001	0.011	0.994	0.005	0.024	0.995	0.006	0.025
8	Newton	0.976	0.018	0.050	0.982	0.016	0.040	0.998	0.002	0.016
9	Weibull	0.999	0.001	0.015	0.980	0.017	0.050	0.998	0.002	0.016

Table 5: Result Summary of the Statistical Curve Fitting Analysis at 95^{o}C For 1.5, 3.0 and 4.5 mm Yam Slices

Slice Thickness →		1.5 mm			3.0 mm			4.5 mm		
No.	**Model Name**	R^2	**SSE**	**RMSE**	R^2	**SSE**	**RMSE**	R^2	**SSE**	**RMSE**
1	Haghi & Ghanadzadeh	0.998	0.002	0.040	0.998	0.003	0.020	0.999	0.002	0.014
2	Verma et al	0.997	0.003	0.025	0.994	0.007	0.026	0.998	0.004	0.016
3	Modified Henderson & Pabis	0.989	0.008	0.091	0.994	0.007	0.031	0.998	0.004	0.018
4	Page	0.996	0.003	0.023	0.994	0.007	0.025	0.997	0.004	0.016
5	Logarithmic	0.994	0.004	0.033	0.994	0.007	0.026	0.997	0.004	0.018
6	Demir et al	0.994	0.004	0.038	0.994	0.007	0.027	0.997	0.004	0.018
7	Peleg	0.996	0.003	0.025	0.991	0.010	0.030	0.992	0.012	0.028
8	Newton	0.988	0.009	0.038	0.994	0.007	0.024	0.997	0.005	0.018
9	Weibull	0.997	0.003	0.029	0.994	0.007	0.027	0.997	0.004	0.017

Table 6 Constants for the Haghi & Ghanadzadeh for Yam Drying at Different Temperatures and Sizes

	Parameters		Constants					
No.	Temperature (oC)	Slice Size (mm)	a	b	c	d	e	F
1	65	1.5	0.605	0.216	0.520	2.061E-4	-0.020	0.395
		3.0	2.032	0.008	1.072	-8.908E-6	0.006	-1.036
		4.5	0.674	0.026	0.941	2.488E-6	-0.002	0.327
2	75	1.5	0.715	0.237	0.956	7.913E-5	-0.009	0.285
		3.0	0.286	0.350	0.357	5.756E-5	-0.013	0.714
		4.5	0.555	0.011	1.405	5.676E-6	-0.003	0.445
3	85	1.5	0.673	0.033	2.474	2.057E-4	-0.016	0.327
		3.0	2.709	0.071	0.377	5.179E-5	-0.006	-1.709
		4.5	1.313	0.015	0.920	5.047E-6	0.000	-0.315
4	95	1.5	1.839	0.238	0.263	5.645E-4	-0.022	-0.839
		3.0	0.342	0.012	2.013	1.623E-4	-0.020	0.653
		4.5	1.049	0.022	0.911	1.574E-5	-0.003	-0.048

Table 7 Experimental and Predicted Moisture Ratio at Different Temperatures

S/N	Temperature (oC)	Slice Size (mm)	Relationship	R^2
1	65	1.5	PMR = 0.9957EMR + 0.0007	0.9981
		3.0	PMR = 0.9987EMR + 0.0030	0.9984
		4.5	PMR = 1.0038EMR - 0.0012	0.9994
2	75	1.5	PMR = 0.9985EMR + 0.0016	0.9998
		3.0	PMR = 0.9990EMR + 0.0006	0.9990
		4.5	PMR = 1.0026EMR + 0.0003	0.9996
3	85	1.5	PMR = 0.9965EMR + 0.0027	0.9996
		3.0	PMR = 1.0052EMR - 0.0025	0.9979
		4.5	PMR = 1.0000EMR + 0.0011	0.9986
4	95	1.5	PMR = 0.9967EMR + 0.0023	0.9982
		3.0	PMR = 0.9978EMR + 0.0004	0.9975
		4.5	PMR = 0.9987EMR + 0.0011	0.9982

The Drying Curves

Line plots of the drying curves, i.e., the variation of moisture content with time, for the different yam slice sizes, at 65°C, 75°C, 85°C, and 95°C are shown in Figures 2, 3, 4, and 5 respectively. Figures 2 – 5 shows that for a given temperature of water in the Refractance Window™ dryer, the moisture content decreased exponentially with time. Meanwhile, as the yam thickness increased from 1.5mm to 4.5mm, an increase in drying time occurred. This is because, as the yam's thickness increases, there is an increase in the amount of moisture that has to be removed from the slice. Therefore, the drying process is prolonged.

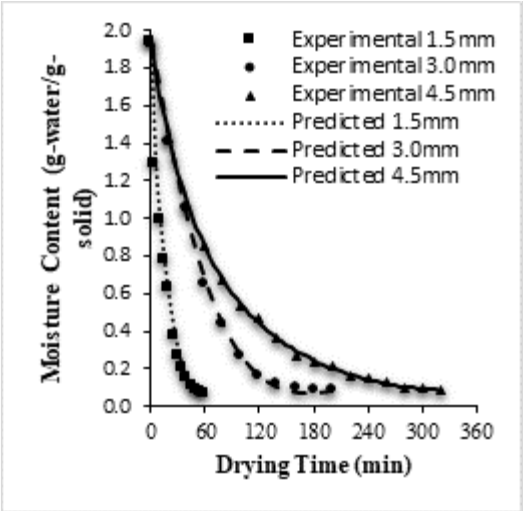

Figure 2 Experimental Drying Curves for Different Yam Slices at 65^0C

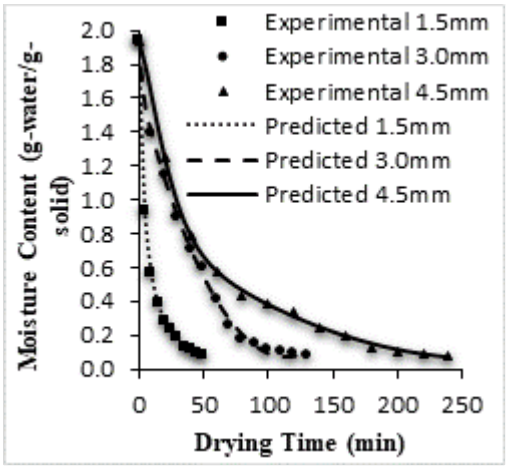

Figure 3 Experimental Drying Curves for Different Yam Slices at 75^{0}C

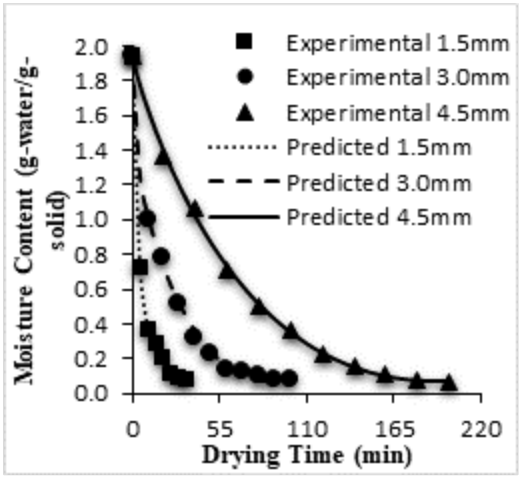

Figure 4 Experimental Drying Curves for Different Yam Slices at 85^{0}C

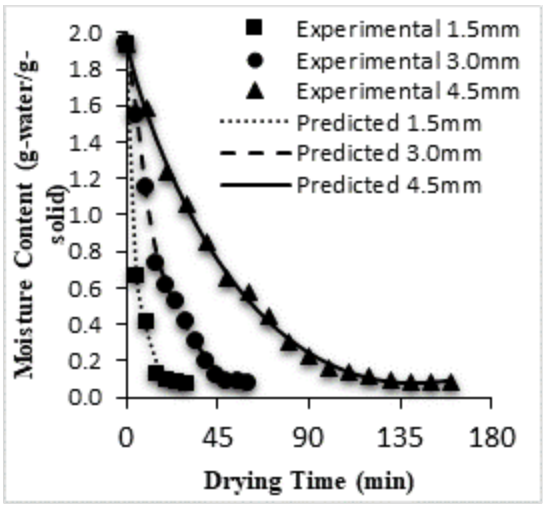

Figure 5 Experimental Drying Curves for Different Yam Slices at 95^{0}C

From the drying curves presented in Figures 2 to 5, the drying times required to dehydrate the yam slices to 0.10g-water/g-solid increases with increasing yam slices thickness for a given temperature. Also, as the drying temperature increases, the drying times decreases for a given yam slice size. Table 8 presents quantitative values of the drying times for different yam slice sizes at different temperatures.

Table 8 Drying Times for Different Yam Slice Sizes at Different Temperatures

	Temperature ^{o}C			
	65	75	85	95
Size	Minutes			
1.5 mm	60	45	35	25
3.0 mm	200	130	90	55
4.5 mm	320	240	180	160

Drying Rate Curve

Line graphs for the drying rate curves, i.e., graphs of drying rate against drying time for the 1.5, 3.0, and 4.5 mm thick yam slices with water temperatures of 65^{o}C, 75^{o}C, 85^{o}C, and 95^{o}C in the Refractance Window™ dryer is shown in Figs. 6, 7, and 8, respectively. The line plots were obtained by differentiating the equations for the respective Haghi and Ghanadzadeh (2005) models that fit the experimental data points, as suggested by Kemp *et al.*, (2001). The drying data values were limited; they were, therefore, not used in plotting the drying rate curves. Figs. 6-8 shows that the drying rate rises initially then reaches a peak value and then fall; these are characteristics of a typical drying rate curve (Traub, 2002). In the initial drying rate period, the latent heat of evaporation is transferred to the slice to remove the moisture. In a typical drying curve, the peak drying rate remains constant for a specified period. However, in these set of experiments, this peak drying rate remains constant for a short period, and even appears to be absent. This phenomenon occurs because the unbound moisture on the surface of the slice structure is almost instantly expelled. When the drying rate falls, this is the falling rate period. In the falling rate period, moisture migrates from the inner spaces of each slice to the outer surface before being released. As the free moisture content approached zero, drying rates at 65^{0}C, 75^{0}C, 85^{0}C, and 95^{0}C also gradually dropped to zero, signifying the end of a drying process.

CONCLUSIONS

Thin layer slices of white yam tubers, 1.5, 3.0 and 4.0 mm thick were dried using a Refractance Window™ dryer in which the dehydrating water temperature was

65, 75, 85, and 95^{o}C. The yam slices determined to have an initial moisture content of 1.94 g-water/g-solid, were dehydrated to a moisture ratio of about 0.1 g-water/g-solid. Recorded were the variation in moisture content with dehydration time of the samples during the drying operations. The conclusions are,

1. For a given slice size, an increase in dehydrating temperature causes a decrease in drying time. Also, for a given temperature, an increase in slice size causes an increase in drying time.
2. At 65^{o}C the drying time when dehydrating 1.5, 3.0 and 4.5 mm thick yam slices was determined to be 60, 200, and 320 minutes respectively.
3. At 75^{o}C the drying time when dehydrating 1.5, 3.0 and 4.5 mm thick yam slices was determined to be 45, 130, and 240 minutes respectively.
4. At 85^{o}C the drying time when dehydrating 1.5, 3.0 and 4.5 mm thick yam slices was determined to be 35, 90, and 180 minutes respectively.
5. At 95^{o}C the drying time when dehydrating 1.5, 3.0 and 4.5 mm thick yam slices was determined to be 25, 55, and 160 minutes respectively.
6. An increase in temperature causes an increase in dying rate. This is expected as moisture movement is higher at elevated temperatures, which consequently, will cause moisture to be expelled faster for the yam sample.
7. In predicting the drying kinetics of the yam slices dehydration process, while regression analysis indicated that no significant difference exists in any of the thin-layer models tested. However, the Haghi & Ghanadzadeh thin-layer model was the most appropriate to use, as it had R^2 closest to unity, and both SSE and RSME closest to zero.
8. As most of the dehydration took place during the falling rate period, the controlling mechanism for the drying is the moisture movement through the interstices of the yam slabs. Hence, internal diffusion may be considered the mechanism by which dehydration occurs during Refractance Window^{TM} drying.

The drying curve and the drying rate curves are fundamental characteristics used in the design and modelling of dryers in the food industry. As limited literature was found on the attributes for the Refractance Window^{TM} drying of yams, this work presents features that will be useful for designing, modelling, and operating such equipment.

ACKNOWLEDGEMENT

The authors are grateful for the financial support provided by the Tertiary Education Trust Fund (TETFund), Nigeria under Grant CRC/TETFUND/NO.2018/04

REFERENCES

Agoreyo, B. O., Akpiroroh, O., Orukpe, O. A., Osaweren, O. R., & Owabor, C. N., (2011), The effects of various drying methods on the nutritional composition of *Musa paradisiaca*, *Dioscorea rotundata* and *Colocasia esculenta*. *Asian Journal of biochemistry*, 6(6), 458-464.

Akgun, N.A. and Doymaz, I., (2005), Modelling of olive cake thin-layer drying process, *Journal of Food Engineering*, 68(4), 455-461.

Akinola, A. A., Ayo, D. B. and Ezeorah, S. N., (2018), Temperature Dependence of the Effective Moisture Diffusivity of Yam (*Dioscorea rotundata*) Slices Dried Using a Refractance Window^{TM}, *The Journal of the Association of Professional Engineers of Trinidad and Tobago*, ISSN 1000 7924, 46(1).

Akpinar, E. K., Bicer, Y. and Yildiz, C., (2003), Thin layer drying of red pepper, *Journal of Food Engineering*, 59(1), 99-104.

Akinola, A. A., Malomo, T. O. and Ezeorah, S. N., (2016), Dehydration characterisation of carrot (Daucus carota) slices dried using the refractance window™ drying technique, *Zimbabwe Journal of Science and Technology*, 11, 28-37.

Akpinar, E. K., (2010), Drying of Mint Leaves in a Solar Dryer and Under Open Sun: Modelling, Performance Analyses, *Energy Conversion and Management*, 51(12), 2407-2418. DOI: 10.1016/j.enconman.2010.05.005.

Ayensu, A., (1997), Dehydration of Food Crops Using a Solar Dryer with Convective Heat Flow, *Solar Energy*, 59(4-6), 121-126.

Azizi, D., Jafari, S. M., Mirzaei, H., & Dehnad, D., (2017), The Influence of Refractance Window Drying on Qualitative Properties Of Kiwifruit Slices. *International Journal of Food Engineering*, 13(2).

Cock, J. H., 1985, *Cassava: New Potential for a Neglected Crop.* pp. 191. Westview Press, Boulder, Co.

da Silva, W. P., Rodrigues, A. F., e Silva, C. M. D., de Castro, D. S., & Gomes, J. P. (2015). Comparison between continuous and intermittent drying of whole bananas using empirical and diffusion models to describe the processes. *Journal of Food Engineering*, 166, 230-236.

Doymaz, I., (2004). Convective Air Drying Characteristics of Thin Layer Carrots. *Journal of Food Engineering*, 61(3), 359-364.

Ertekin, C. and Yaldiz, O., (2004), Drying of eggplant and selection of a suitable thin layer drying model. *Journal of Food Engineering*, 63(3), 349-359.

Ezeorah, S. N., (2018), *Evaluation of Refractance Window[TM] Drying technology for Yam Dehydration*, M.Sc., Research Report, Department Chemical and Petroleum Engineering, Lagos, Nigeria.

Haghi, A. K. and Ghanadzadeh, H., (2005), A Study of Thermal Drying Process, *Indian Journal of Chemical Technology*, 12(1), 654-663.

Hudgens, J., and Trillo, R., (2003), The Rough Guide to West Africa, *Rough Guides* (p. 1012). ISBN 1-843-53118-6.

International Institute of Tropical Agriculture (IITA), (2009), IITA, Research to Nourish Africa; Yam, Retrieved August 1, 2016 from http://www.iita.org/yam.

Johnson, R. A., (2017), *Miller and Freund's Probability and Statistics for Engineers*. Pearson Education © 2017. ISBN 10: 1-292-17601-6, ISBN 13: 978-1-292-17601-7.

Kabiru, A. A., Joshua, A. A. and Raji, A. O. (2013). Effect of Slice Thickness and Temperature on the Drying Kinetics of Mango (*Mangifera Indica)*, *International Journal of Research and Review in Applied Sciences*, 15(1), 41-50.

Karathanos, V. T., (1999), Determination of Water Content of Dried Fruits by Drying Kinetics, *Journal of Food Engineering*, 39(4), 337-344.

Kemp, I. C., Fyhr, B. C., Laurent, S., Roques, M. A., Groenewold, C. E., Tsotsas, E., Sereno, A. A., Bonazzi, C. B., Bimbenet, J. J. and Kind, M., (2001), Methods for processing experimental drying kinetics data, *Drying Technology*, 19(1), 15-34.

Lancaster, P. A., Ingram, J. S., Lim, M. Y., & Coursey, D. G., (1982), Traditional Cassava-Based Foods: Survey of Processing Techniques, *Economic Botany*, 36(1), 12-45.

Madamba, P. S., Driscoll, R. H., & Buckle, K. A. (1996). The thin-layer drying characteristics of garlic slices. *Journal of food Engineering*, 29(1), 75-97.

Magoon, R. E., (1986), *Method and Apparatus for Drying Fruit Pulp and the Like*. US Patent 4,631,837.

Maskan, M., (2000), Microwave/Air and Microwave Finish Drying of Banana. *Journal of Food Engineering* 44(2), 71-78.

Ogunnaike, B. A. (2011), *Random Phenomena: Fundamentals of Probability and Statistics for Engineers*. CRC Press.

OHAUS Corporation, (2011), Instruction Manual MB45 Moisture Analyzer, OHAUS Corporation, 7 Campus Drive, Suite 310, Parsippany, NJ 07054 USA.

Page G. E., (1949), *Factors Influencing the Maximum Rates of Air Drying of Shelled Corn in Thin Layer*, M.Sc. Thesis, Purdue University, Lafayette, IN, USA.

Sanful, R. E., Addo, A., Oduro, I, Ellis, W. O. (2015). Air Drying Characteristics of Aerial Yam (Dioscorea bulbifera). *Scholars Journal of Engineering and Technology* (SJET) 2015; 3(8), 693-700.

Sharifian, F., Motlagh, A. M. and Nikbakht, A. M., (2012), Pulsed Microwave Drying Kinetics of Fig Fruit (*'Ficus carica'L.*). *Australian Journal of Crop Science*, 6(10), 1441.

Togrul, I. T. and Pehlivan, D., (2003), Modelling of Drying Kinetics of Single Apricot, *Journal of Food Engineering*, 58(1), 23-32.

Traub, D. A., (2002), The Drying Curve, Part 1. Process Heating, September 2002 Retrieved from https://www.process-heating.com/articles/86586-the-drying-curve-part-1.

Tzempelikos, D. A., Vouros, A. P., Bardakas, A. V., Filios, A. E., & Margaris, D. P. (2014). Case studies on the effect of the air drying conditions on the convective drying of quinces. *Case Studies in Thermal Engineering*, 3, 79-85.

United States Department of Agriculture (USDA), (2017), Agricultural Research Service USDA Food Composition Databases, Retrieved August 30, 2017, from https://ndb.nal.usda.gov/ndb/foods/show/3266?man=&lfacet=&count=&max=&qlookup=&offset=&sort=&format=Abridged&reportfmt=other&rptfrm=&ndbno=&nutrient1=&nutrient2=&nutrient3=&subset=&totCount=&measureby=&Qv=1&Q6170=1&Qv=21&Q6170=1

DEVELOPMENT AND CHARACTERISATION OF HIGHLY CRYSTALLINE BORON DOPED MULTI-WALLED CARBON NANOTUBES AS POTENTIAL ADSORBENT FOR REFINERY WASTEWATER TREATMENT

***Kariim I.[1,2], Abdulkareem A.S.[1,2], Tijani J.O.[2,3], Abubakre O.K.[2,4]**

[1]Chemical Engineering Department, Federal University of Technology, Minna, Nigeria
[2]Nanotechnology Research Group, Centre for Genetic Engineering and Nanotechnology, Federal University of Technology, Minna, Nigeria
[3]Chemistry Department, Federal University of Technology, Minna, Nigeria
[4]Department of Material and Metallurgy Engineering, Federal University of Technology, Minna, Nigeria
*Email of the Corresponding author: k.ishaq@futminna.edu.ng

ABSTRACT

The development of novel engineering materials for adsorption process has received numerous attentions from researchers around the globe following the discharge of harmful materials into the environment due to massive industrialization. In line of this challenge, this study focuses on the development and application of purified multi-walled carbon nanotubes (MWCNTs) and boron doped MWCNTs as novel adsorbents for the removal of phenol and cyanide. The boron doped MWCNTs was developed via impregnation method. The resulting boron-doped MWCNTs was characterized for its internal morphology, crystallinity, d-spacing, surface area and elemental composition using High-Resolution Transmission Electron Microscope (HR-TEM), X-Ray diffraction (XRD), Selected Area Diffraction (SAED), Braunner Emmett Teller (BET) and Energy Dispersion X-Ray (EDX) techniques respectively. The result of the simultaneous sorption of phenol and cyanide indicate that the optimum adsorption of 98.97 % and 96.84 % were observed at the residence time of 60 min, adsorbent dosage of 0.3 g and temperature of 60 ^oC for B-MWCNTs adsorbent respectively. The study revealed that the developed boron-doped MWCNTs possessed promising sorption properties suitable for phenol and cyanide removal from refinery wastewater.

***Keywords**: Carbon Nanotube; Characterization; Phenol; cyanide; Adsorption*

1. INTRODUCTION

The geometric progression in the area of urbanization and industrialization in some developed and developing countries have resulted to continuous discharge of harmful materials into the water bodies and the environment which poses serious health challenges to the ecosystem including man and animals. Such pollutants could either be mixed in the form of toxic liquid (phenol and cyanide), gases, viruses and bacterial. The need to develop an effective material for the removal of such pollutants from industrials effluents is paramount.

Carbon nanotube is one of the promising engineering materials that possesses active properties towards tailored applications and it's reported to be one of the most active fields of research (Ayala *et al*., 2010). On the properties and area of applications of pristine carbon nanotubes, several literatures have revealed the enormous progress in recent time with an observable interest geared towards the improvement and the controlling of their inherent properties via novel functionalization techniques (Ramanathan *et al.,* 2005; Francesca, 2009; Christopher and James, 2004). The remarkable technological changes are reportedly achieved on the properties of carbon nanotubes either by defect placing on the tubes sides or through doping with heteroatom (Tsang *et al.,* 2007). Carbon nanotubes doping with heteroatoms have a potential of improving the structural, chemical, and electronic properties towards some areas of applications such as catalysis, composites, adsorption, electrochemistry, organic solar and photovoltaics (Blackburn *et al*., 2006; Lin and Xing, 2008; Li *et al.,* 2002; Chen *et al.,* 2007; Gong *et al.,* 2000).

Refineries have been identified as one of the major producer of phenol and cyanide as one of the constituents of the discharged effluent which possess high risk to human and the aquatic habitat (Ilaboya et al., 2013). The concentration of phenol and cyanide over the allowable limit could be observed in other industries such as plastics, paints, agriculture. There is urgent need to device and develop an improved materials capable of treating wastewater containing cyanide and phenol from refinery wastewater before being discharged into the surrounding ecosystem.

Several researchers have worked extensively on numerous methods of wastewater removal. Such methods include reverse osmosis, nanofiltration,

membrane separation, coagulation and flocculation, extraction, and adsorption process (Cataldo et al., 2016). Though membrane based processes such as ultrafiltration, microfiltration, nanofiltraton, and reverse osmosis are pressure-induced and but are costly to operate and maintain. High technicalities are required for efficient and effective design and operation of membrane based techniques compared to adsorption process. Therefore, there is need to develop an efficient and effective method of phenol and cyanide sorption from refinery wastewater through adsorption process.

In this present study, boron-doped multi-walled carbon nanotube was produced via wet impregnation method. The developed boron-doped MWCNT was characterized via transmission electron microscope (TEM), Selected area electron diffraction (SAED), X-Ray diffraction (XRD) and Energy dispersion X-ray (EDX) and applied as adsorbent for the removal of phenol and cyanide from refinery wastewater. The effects of residence time, adsorbent dosage and temperature were also investigated on the percentage removal of phenol and cyanide in a batch adsorption process.

2. MATERIALS AND METHODS

All the chemicals (boric acid by Sigma Aldrich, Distilled water was obtained from the Centre for Genetic Engineering and Biotechnology, FUT Minna) used in this study were of analytical grades with 99.99 % percentage purity. The properties of the MWCNTs used in this study have been reported elsewhere (Kariim *et al.,* 2015). Wastewater was collected from Kaduna refinery and petrochemicals and the composition of phenol and cyanide were determined via titrimetric approach.

2.1 Development of boron doped MWCNTs Adsorbent

A known weight ratio of 80:20 wt % (g/g) of the MWCNTs to boric acid was mixed in 50 ml of distilled water in a beaker. The resulting mixture was stirred for a period of 24 hours and then dried at a temperature of 120 ^{o}C for 10 h. The dried boron-doped MWCNTs was grinded then sieved through a 150 micrometre sieve size then stored in an airtight container for further analysis. The obtained nano-adsorbent was characterized using TEM/EDX, XRD, SAED and BET for the morphology/elemental composition, crystallinity, d-spacing and surface area respectively.

2.2 Characterization of the developed boron-doped MWCNTs adsorbent

The developed boron-doped MWCNTs was analysed for the crystallinity via the use of the XRD (Bruker AXS D8 X-ray diffractometer system), internal morphology/crystallinity/elemental composition (Zeiss Auriga HRTEM/SAED/EDX operated at 3950 V) and surface area via BET (Nova-e series).

The crystallite size of the boron-doped MWCNTs was calculated from the XRD data using the Scherer Equation as shown in Equation (1) (Chen *et al*.,2006).

$$D = \frac{0.9\,\lambda}{\text{FWHM Cos}\theta} \qquad (1)$$

2.3 Adsorption Process

The percentage removal of phenol and cyanide onto the synthesized MWCNTs and B-MWCNTs adsorbent were determined in a batch reactor. The percentage removals of cyanide and phenol were determined using Equation 2.

$$\%\ Removal\ = \frac{(Co-Ce)}{Co} \times 100 \qquad (2)$$

Where C_o and C_e, V represent the initial concentration before the adsorption process (mg/L) and the final concentration after adsorption (mg/L respectively.

3 RESULTS AND DISCUSSION

The crystallinity of the produced boron doped MWCNTs is shown in Figure 1. In addition to the crystallinity extracted from the XRD result, the XRD spectral was also used to determine the average crystallite size, the lattice phase and the d-spacing of the atomic composition in the bulk of the boron doped MWCNTs.

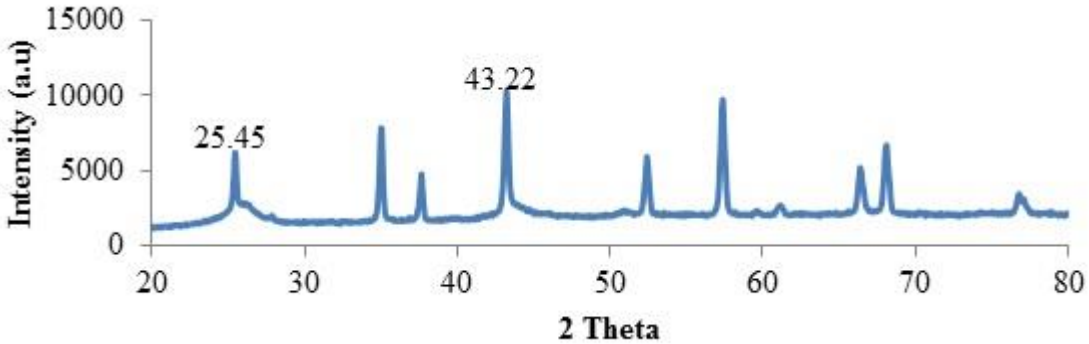

Figure 1: XRD Spectral of the Developed Boron Doped MWCNTS Adsorbent

From Figure 1, there are several identifiable peaks found in the spectra though the peaks at the 2 theta of 25.45 and 43.22 were assigned to the presence of graphitised carbon in the developed adsorbent. This observation of peaks formation is in agreement with the findings of Aliyu *et al.*, (2017) who worked on the development of MWCNTs using the developed Fe-Ni supported on kaolinite clay. The remaining peaks could be attributed to the phases inherent from the catalyst particles used during the MWCNTs synthesis.

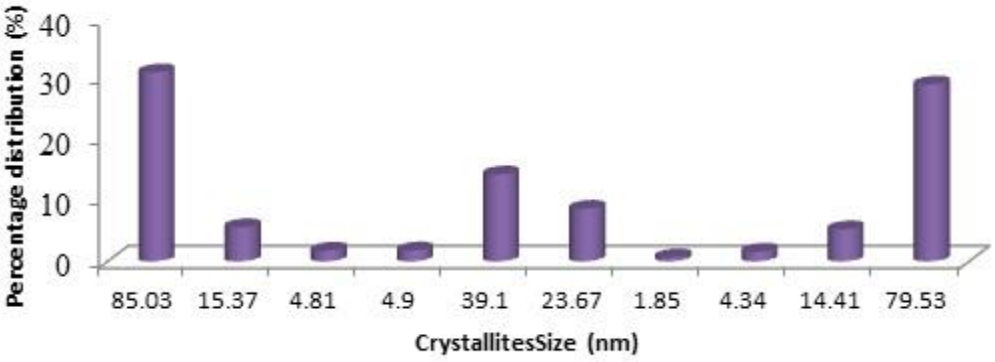

Figure 2: Crystallite Size Distribution of the Developed Boron Doped-MWCNTs Adsorbent

From Figure 2, the average crystallite size of the produced boron-doped MWCNTs was determined to be 22.75 nm using Scherer equation as illustrated in Equation 1. Furthermore, the crystallite particle sizes were found to exist within the ranges of 1.85 to 85.03 nm in the bulk of the boron doped MWCNTs adsorbent as depicted in Figure 2.

The result of the HR-TEM micrograph of the developed boron doped MWCNTs is shown in Figure 3.

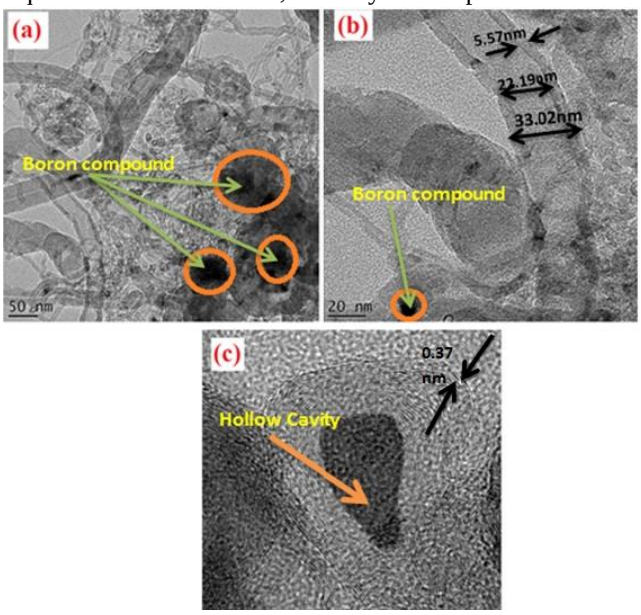

Figure 3: HR-TEM Micrograph of Boron Doped MWCNTS Adsorbent

The HR-TEM micrograph is as depicted in Figure 3(a-c). Figure 3a clearly shows the presence of long and continuous strands of MWCNTs formation. In addition to the noticeable observations on the Figure 3a, the presence of embedded boron compounds were associated with the darker part of the micrograph with oval shape indication. The wall thickness, internal and external diameter of the produced MWCNTs was estimated to be 5.57, 22.19 and 33.02 nm respectively as depicted on Figure 3b. The obtained values show that the produced nanocomposites formed have its dimension in nanoscale hence, the obtained material is nanomaterial. From Figure 3c, the hollow nature of the developed nanocomposite was shown with several walls making the cavity. The presence of the concentric walls was a direct indication for the multi-walled nature of the formed nanocomposites as observed on the starting MWCNTs material. The result as indicated in Figure 3c

further shows that the adopted doping process has no effect on the structural make-up of the starting material.

The crystals lattice as estimated from the Figure 3c was found to be 0.37 nm which was relatively higher than that of the staring as-synthesized and purified MWCNTS. The reason for this appreciable increases in the d-spacing could be linked to the contribution of the adsorption of physiosorbed water molecules into the pores of the MWCNTS and the penetration of boron containing compound used for doping process into the wider formation of inter-particle spacing.

The results of the energy band of the constituent elements and the elemental composition are shown in Figure 4 a and b respectively.

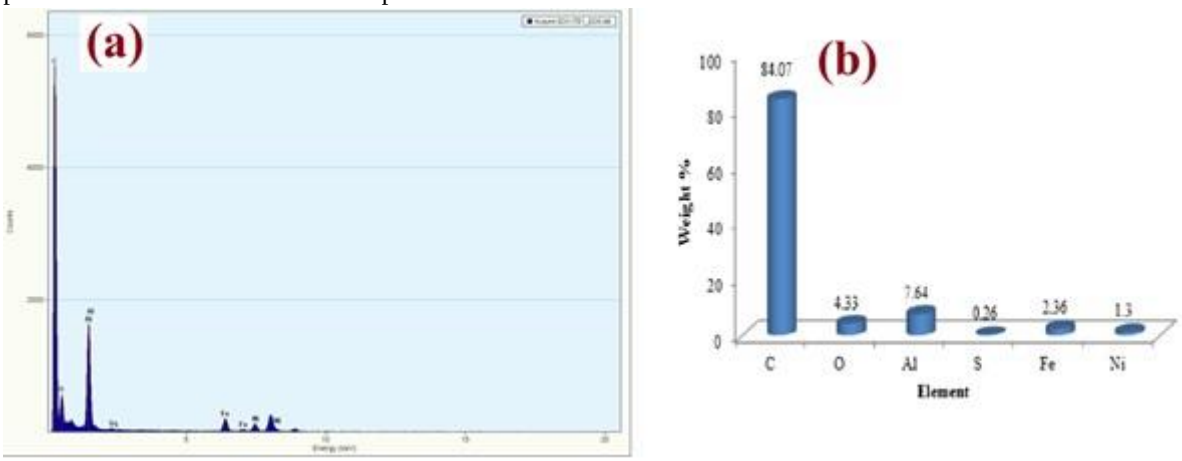

Figure 4: (a) EDX Spectra and (b) Elemental Composition of the Developed Boron Doped MWCNTs Adsorbent

The EDX spectrum of the developed boron doped MWCNTs is as presented in Figure 4a. The Figure 4a as presented shows the variable energy level of the constituent elements in the adsorbent mix. Primarily, C, O, Al, S, Fe and Ni were the observable elements composed in the developed boron doped MWCNTs adsorbent. The presence of both Fe and Ni at variable energy level is an indication of their unique properties one of which is the variable oxidation state; property exhibited by transition metals. At lower energy level, both the Fe and the Ni exist in the form of oxides although the occurrence of S in the bulk of the adsorbent could be associated with possible introduction of impurity during the course of sample preparation for the HR-TEM microscopy. On the other hand, the result in Figure 4b shows the presence of six distinctive elements present in the developed adsorbent. The elements include Carbon, Oxygen, Aluminium, Sulphur, Iron and Nickel with weight percentage of 84.07, 4.33, 7.64, 0.26, 2.36 and 1.30 respectively. From these elements present, Carbon was found to have the highest weight percentage in the adsorbent mix. The presence of the observable highest percent of carbon could be as a result of the carbon nanotubes used as the main component of the developed adsorbent and possible inclusion from the carbon grid used during the electron microscope analysis. Furthermore, the presence of Ni and Fe elements was linked to the remnant of the metallic catalyst unremoved during the purification process. The BET surface area was determined to be 330 m^2/g.

The result of the SAED Pattern of the developed boron doped MWCNTs is as presented in Figure 5.

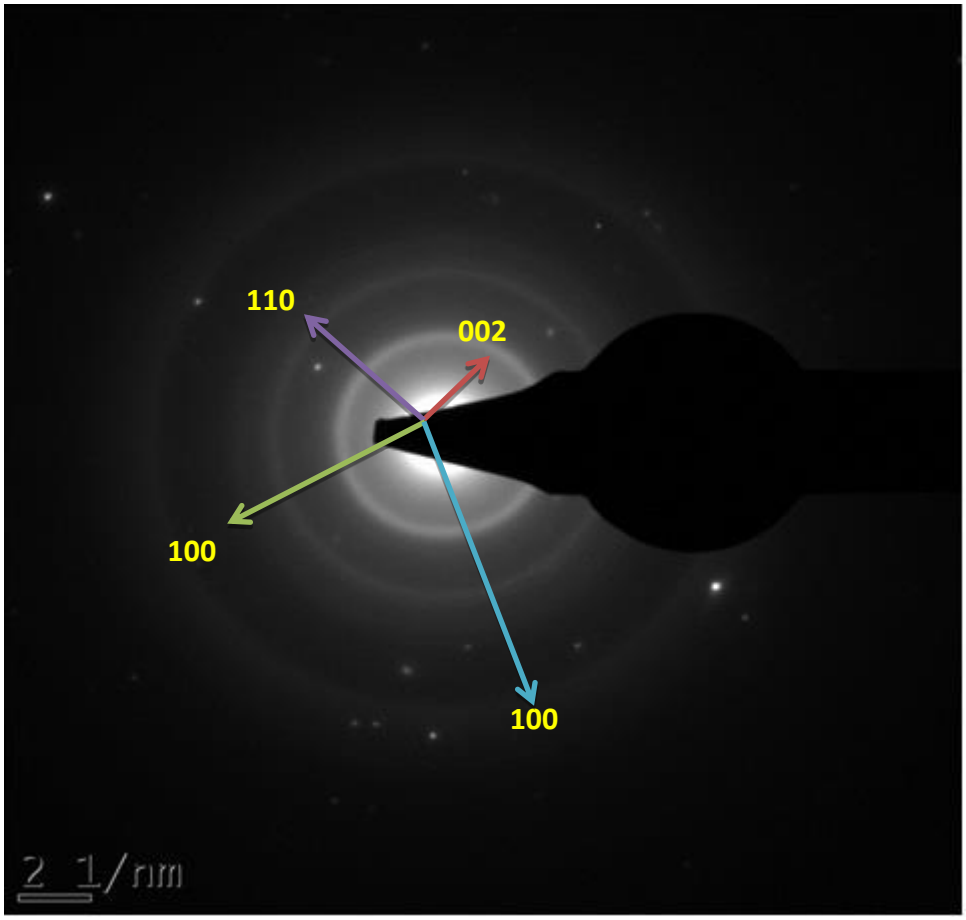

Figure 5: SAED Pattern of the Developed Boron Doped MWCNTS Adsorbent

The SAED pattern as shown in Figure 5 depicts several concentric rings representing different phases and respective d-spacing lattice in the crystals of the produced boron doped MWCNTs adsorbed. The crystallite sizes, the d-spacing and the lattice indexing is shown in Table 1.

Table 1: Crystallites Diameter and Phase Identification of Boron Doped MWCNTs Adsorbent

S/N	Ring Diameter (nm)	Ring radius (1/nm)	Radius (nm)	Ring Radius (Å)	hkl indexing
1.	4.988	2.493	0.401	4.010	002 (FCC)
2.	8.976	4.488	0.2228	2.228	110 (BCC)
3.	11.170	5.585	0.1790	1.790	100 (FCC)
4.	15.220	7.610	0.1314	1.314	100 (FCC)

From the Table 1, the graphitic nature of the MWCNTs was depicted with the crystallite lattice of FCC and corresponding hkl indexing of (002).

The results of the effect of contact time on the removal of phenol and cyanide onto the surfaces and the pores of the developed adsorbents are presented in Figure 6 (a-b).

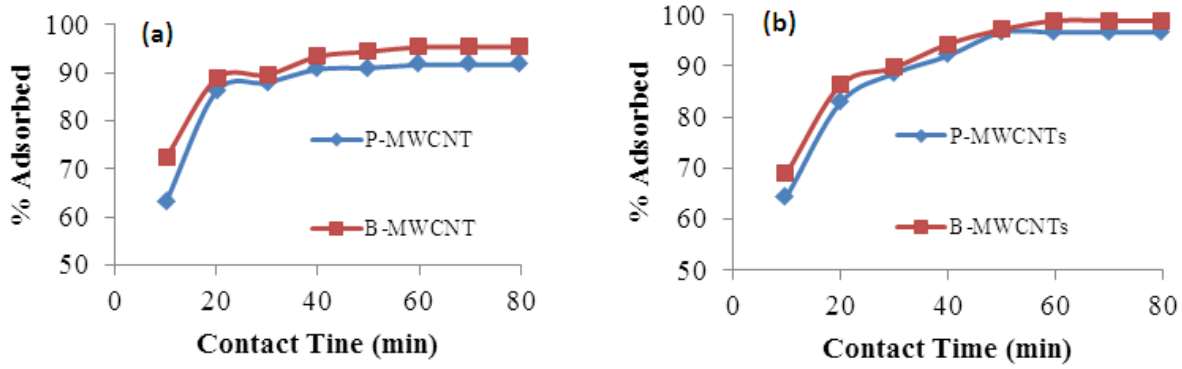

Figure 6: Effect of contact time on the percentage removal of (a) Cyanide and (b) Phenol onto MWCNTs and B-MWCNTs nanoadsorbent.

From Figure 6, the adsorption process was found to be swift at the initial stage. The rapid increase in the percentage adsorbed could be as a result of higher driving forces between the adsorbent and the sorbate. This was followed with a reduced adsorption percentage until equilibrium was attained at 60 minutes for the PMWCNTs and B-MWCNTs nanoadsorbents. At a period above the equilibrium point for both the cyanide and phenol adsorption, a smooth and nearly straight line curves were observed which indicates a saturation point. This finding is in agreement with the report of Saliihi *et al.*, (2015). Furthermore, the percentage adsorbed on to the MWCNTs adsorbent increases from 61.95 to 94.534 % and from 68.97 to 97.85 % for cyanide and phenol respectively as shown in Figure 6 (a-b). The variation in the percentage adsorbed for each pollutant could be linked to the variation in their diffusion efficiency. There was a noticeable improvement in the percentage cyanide and phenol adsorbed when the adsorbent was doped with boron. The percentage adsorbed was found to increase from 72.22 to 95.97 % and from 68.97 to 98.74 % for both the cyanide and phenol respectively.

The effect of adsorbent dosage on the phenol and cyanide sorption was determined and the result is as presented in Figure 7.

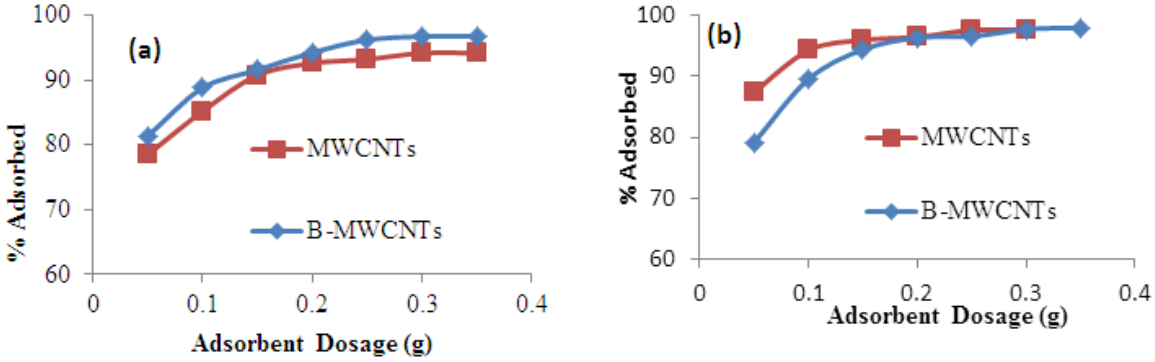

Figure 7: Effects of adsorbent dosage on the percentage removal of (a) Cyanide and (b) Phenol onto MWCNTs and B-MWCNTs nanoadsorbent.

From Figure 7 (a-b), the percentage removal of cyanide and phenol on to the purified MWCNTs increases from 78.49 to 94.15 % and from 76.75 to 97.57 % respectively while the adsorbent dosage was varied from 0.05 to 0.35 g. The appreciation in the percentage cyanide and phenol removal could be due to the present of increased active sites which aid adsorption process while the quantity of the adsorbent was increased. As the adsorbent dosage increases, the particles of the adsorbent available for adsorption process also increases due to provision of available exchangeable sites for more molecular attachment to the surfaces and the pores of the adsorbent. The same observations were noticeable when the adsorption was carried out with B-MWCNTs nanoadsorbent. Furthermore, at 0.35 g adsorbent dosage, the adsorption process attained a plateau; a point where the increment in the adsorbent dosage has no positive impact on the adsorption efficiency. At this point, the percentage adsorbed becomes constant this is in accordance with the report of Kilic *et al.*, (2011).

The effect of temperature on the removal efficiency of the developed adsorbents for the removal of cyanide and phenol were investigated and the result is as shown in Figure 8 (a-b).

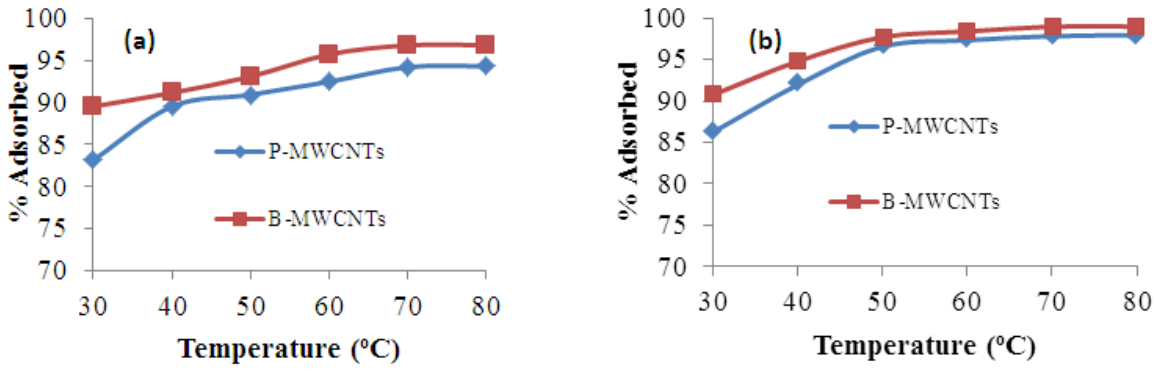

Figure 8: Effects of adsorbent dosage on the percentage removal of (a) Cyanide and (b) Phenol onto MWCNTs and B-MWCNTs nanoadsorbent.

As depicted in Figure 8 (a-b), an increase in temperature from 30 to 60 °C resulted to an increase in the percentage of cyanide and phenol removal for both the P-MWCNT and B-MWCNTs adsorbents. This could be attributed to a possible increase in the inner pores of the adsorbents to encompass more sorbates than it could have removed at room temperature. For cyanide, the percentage removal increases from 83.148 to 94.231 %, and 89.573 to 96.844 % for P-MWCNTs and B-MWCNTs nanoadsorbents respectively while that of phenol also increased from 86.207 to 97.816 % and 90.713 to 98.966 % for P-MWCNTs and B-MWCNTs nanoadsorbents respectively.

4 CONCLUSION

Aligned and concentric multi-walled carbon nanotubes doped with boron was successfully developed. The HR-TEM micrograph images revealed the nano-size nature of the developed material with the inner and outer diameters of 22.19 and 33.02 nm respectively. The result of the simultaneous sorption of phenol and cyanide indicate that the optimum adsorption of 98.97 % and 96.84 % were observed at the residence time of 60 min, adsorbent dosage of 0.3 g and temperature of 60 °C for B-MWCNTs adsorbent respectively. Thus, the developed boron doped MWCNTs nanoadsorbent depicts excellent sorption properties for the removal of phenol and cyanide from refinery wastewater.

ACKNOWLEDGEMENT

The financial support from the senate research based fund of Federal University of Technology, Minna with grant number (SENATE/FUTMINNA/2015/06) is much appreciated. Support received for the use of facilities at Centre for Genetic Engineering and Biotechnology, CGEB, Federal University of Technology, Minna, Nigeria is also acknowledged.

REFERENCES

Aliyu A, Abdulkareem A. S, Kovo A. S, Abubakre O. K, Tijani J. O and Kariim I. (2017). Synthesis of Multi-walled Carbon Nanotubes Via Catalystic Chemical Vapour Deposition Method on Fe-Ni Bimetallic Catalyst Supported on Kaolin. *Carbon letters*, 21, 33-50.

Ayala P., Arenal R., Ru¨mmeli M, Rubio A and Pitcler T. (2010). The doping of carbon nanotubes with nitrogen and their potential applications, *Carbon* 48, 575 – 586.

Blackburn J. L., Yan Y., Engtrakul C., Parilla P.A., Jone K., Gennett T., Dillion C and Heben M. (2006). Synthesis and characterization of Boron doped Single-Walled Carbon Nanotubes Produced by the Lesser Vaporization Technique. *Chemistry of Materials*, 18, 234-240.

Cataldo, S., Gianguzza, A., Milea, D., Muratore, N. and Pettignano, A., (2016). Pb(II) adsorption by a novel activated carbon- alginate composite material. A kinetic and equilibrium study, *International Journal of Biological Macromolecule*, 92, 769-778.

Chen W., Duan L. and Zhu D Q. (2007). Adsorption of polar and nonpolar organic chemicals to carbon nanotubes. *Environmental Science and Technology*, 41(24), 8295-8300.

Chen Y, Zhang, Y Q, Zhang T. H, Gan, C. H, Zheng C. Y, and Yu, G. (2006). Carbon Nanotube Reinforced Hydroxyapatite Composite Coatings Produced Through Laser Surface Alloying, *Carbon*, 44,37-45.

Christopher A D. and James M.T. (2004). Covalent functionalization of single-walled carbon nanotubes for materials applications. *The journal of physical chemistry* A, 108 (51), 11151-11159.

Francesca M T. (2009). Covalently functionalized carbon nanotubes and their biological applications, Thesis submitted for the degree of Doctor of Philosophy, Scuola Internazionale *Superiore di studi Avanzati, International School for Advanced studies*. 1-141.

Gong X., Liu J., Baskaran S., Voise R D. and Young J S. (2000). Surfactant-Assisted *Processing of Carbon Nanotube/Polymer Composites. Chem. Mater*. 12 (4), 1049-1052.

Ilaboya, I., Oti, E., Ekon, G. and Umukoro, L. (2013). Performance of Activated carbon from cassava peels for the treatment of effluent wastewater. *Iranica Journal of Energy and Environment* 4(4), 361-371.

Kariim I., Abdulkareem A S., Abubakre O K, Mohammed I A., Bankole M T. and Tijani J. O. (2015). Studies on the Suitability of Alumina as Bimetallic Catalyst Support for MWCNTs Growth in a CVD Reactor. *International Engineering Conference (IEC2015). Book of proceeding*, 296-305.

Kilic, M., Apaydin-Varol, E. and Putun, A.E. (2011). Adsorptive removal of phe¬nol from aqueous solutions on activated carbon prepared from tobacco residues: equilibrium, kinetics and thermodynamics. *J Hazard Mater*, 189(1-2), 397–403.

Klumpp C., Kostarelos K., Prato M. and Bianco A. (2006). Functionalized carbon nanotubes as emerging nanovectors for the delivery of therapeutics. Biochim. Biophys. Acta, (BBA) - *Biomembranes* 1758, (3), 404-412.

Saliihi, F., Mohammed, K.R., Mohammed, H.I., Nasiru, A. and Hammed, A. (2015). Biomass as low cost Adsorbents for removal of heavy metals from aqueous solution-*A review of some selected Biomass*, 2, 1-8.

ADDING VALUE TO SOLID MINERAL PROCESSING: THE ROLE OF CHEMICAL ENGINEERING

***Olanrewaju, O. F., Momoh, S.O., Okogun, O.J., Okeleye, A. T., Okesola, A., Madaki, M., Ayodele, B. E. and Folaranmi, F.**

National Agency for Science and Engineering Infrastructure (NASENI), Department of Engineering Infrastructure, Idu Industrial Area, Abuja, Nigeria.

*Corresponding Author: sonictreasure@gmail.com

ABSTRACT

Nigeria is richly endowed with solid minerals. Each of the states in the country is blessed with at least one mineral resource. However, the solid minerals of the country such as barite, iron ore and tin are not being fully exploited in spite of the fact that they are available in commercial deposits. This is largely due to the under developed state of the solid minerals sector of the nation. In order to achieve development in solid minerals and for value chain addition, Nigeria needs the expertise and professional intervention of chemical engineers. Chemical engineering is that branch of engineering that deals with the design, construction, installation, operation and maintenance of processes for the conversion of raw materials to the desired finished products. In the light of this definition, Chemical Engineering as a profession indubitably has indispensable roles to play in the development of the solid minerals sector of Nigeria. This paper focuses on the role of Chemical engineering in solid mineral development using iron ore processing as an example. Iron ore is the largest solid mineral that is processed in Nigeria so far.

***Keywords**: Solid minerals, Chemical engineering, beneficiation, process, development, exploitation, iron ore.*

1.0 INTRODUCTION

Chemical engineering is a branch of engineering that applies physical sciences (physics and chemistry) and life sciences (microbiology and biochemistry) together with applied mathematics and economics to produce, transform, transport and properly use chemicals, materials and energy. Essentially, chemical engineers design large-scale processes that convert chemicals, raw materials, living cells, microorganisms and energy into useful forms and products (Wikipedia, 2016). Among the raw materials that are converted into useful products by chemical engineering processes are mineral ores.

Generally, operations in the solid minerals sector of any country can be broadly classified into exploration, exploitation, and processing.

1.1 Exploration

Exploration encompasses all activities that are carried out in order to establish or ascertain the availability of solid minerals deposit in a particular location/region. This includes the quantity of the deposit, the precise location of the deposit underground as well as the geological characteristics of the site. Exploration is usually carried out by geologists and surveyors

.

1.2 Exploitation

This involves the use of the appropriate techniques to mine (bring out) the minerals from their deposits underground to the surface of the earth.

1.3 Processing

The processing stage involves the transportation of the minerals to temporary storage prior to processing via beneficiation or refining of the minerals and the conversion of the refined minerals to the desired finished products for the end-users.

Development in solid minerals is possible if and only if the value added chain is perfected such that the final products meet local and international specifications/standards; as the ultimate aim of any firm or nation is to market her products profitably both locally and internationally. The role of Chemical Engineering in solid minerals development includes the design of process machinery for the successful transportation of the raw minerals from the mines to the beneficiation facility, the beneficiation of the minerals and finally, the conversion of the minerals to the desired products. At this stage, the indispensable roles of

Chemical Engineering in solid mineral development can be appreciated.

2.0 SOLID MINERALS IN NIGERIA

Naturally, no solid mineral is found in its pure state. They are mined as ores because of the impurities they contain. These impurities must be separated from the minerals before they can be used. Hence, there is need for beneficiation/purification of the minerals after they are unearthed from their deposits. Figure 1 depicts the various solid minerals in Nigeria and their locations (Chinago *et al*., 2015) and Table 1 lists the minerals and the locations they are found in Nigeria (Malomo, 2007)

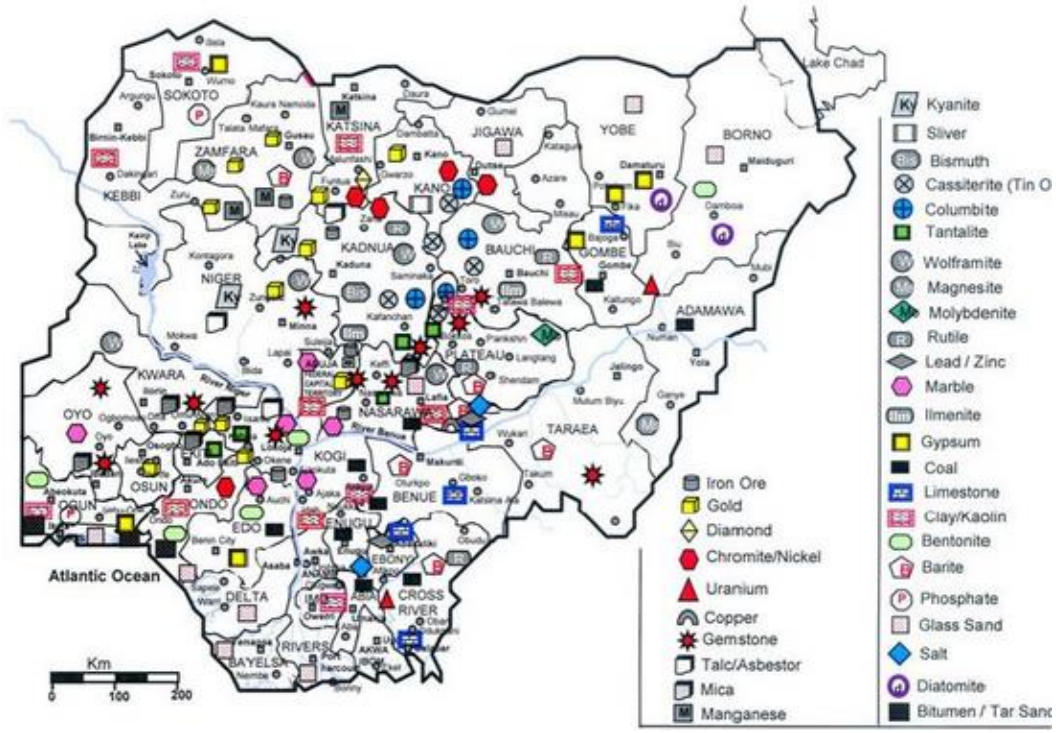

Figure 1: Solid Minerals in Nigeria (Chinago *et al*., 2015).

Table 1: Solid Minerals and their Locations (Malomo, 2007)

MINERAL	LOCATIONS
Kaolin	Katsina, Plateau, Ogun, Bauchi, Ekiti, Ondo, Edo Anambra, Cross River, Akwa Ibom, Abia, Kogi, Enugu, Imo, Benue, Nasarawa, Yobe, Delta, Niger, Kano, and Osun States
Diatomite	Yobe, Borno, and Gombe states
Glass Sand	Cross River, Akwa Ibom, Abia, Imo, Ondo, Lagos, Delta, Rivers, Bayelsa, Ogun, Niger, Nasarawa, Kaduna, Bauchi, Katsina, Kano, Zamfara, Taraba, Sokoto, Jigawa
Gypsum	Adamawa, Taraba, Benue, Edo, Yobe, Sokoto, Gombe, Ogun, Ebonyi, and Borno States
Coal	Benue, Enugu, Nasarawa, Gombe, Edo, Anambra, Abia, and Ondo States
Lignite	Anambra, Imo and Delta,
Kyanite	Kaduna, Niger, Ekiti, and Oyo States
Limestone	Enugu, Abia, Anambra, Cross River, Akwa Ibom, Ogun, Edo, Benue, Nasarawa, Borno, Gombe, Kebbi, Sokoto, Adamawa, Ebonyi, Imo and Yobe States
Salt	Nasarawa , Taraba, Kebbi, Cross Rivers, Bayelsa, Benue, Gombe, and Ebonyi States
Talc	Niger, Osun, Ekiti, Oyo, Ogun, Ondo, Plateau, Kogi, Kaduna, Cross River States and FCT
Marble	Oyo, Edo, Nasarawa, Kogi, Katsina, Niger and FCT
Phosphate	Ogun, Sokoto, Ondo, Kogi, Abia and Cross River states
Dolomite	Kogi, Oyo, Edo, Niger, Nasarawa, Kaduna States and FCT
Feldspar	Ekiti, Kogi, Kwara, Osun, Nasarawa, Ogun, Ondo, Plateau, Niger, Borno, Adamawa, Edo, Kebbi, Katsina, Taraba and Bauchi States

MINERAL	LOCATIONS
Clay (ball clay)	Widely located all over the country.
Bitumen	Ondo, Ogun, Delta and Edo States
Barite	Benue, Cross River, Ebonyi, Adamawa, Yobe, Nasarawa, Gombe, Plateau, Taraba States
Mica	Kogi, Kwara, Nasarawa, Niger, Plateau, Gombe, Bauchi, Borno, Katsina, Kebbi, Benue, Kaduna, Adamawa and Oyo States
Gemstones (topaz, emerald, garnet, sapphire, fluorspar, aquamarine, tourmaline, fluorspar, etc.)	Plateau, Bauchi, Yobe, Borno, Oyo, Ondo, Kwara, Kogi, Ekiti, Nasarawa, Kano, Kaduna, Zamfara and Niger states
Trona (Soda Ash)	Yobe, Adamawa, Bauchi, Borno and Taraba states
Bauxite	Taraba, Adamawa, Yobe, Kebbi, Sokoto, Borno Ekiti, Plateau, Benue, and Cross River States
Bentonite	Yobe, Abia, Anambra, Adamawa, Edo, Imo, Ebonyi, Akwa Ibom, Cross River, Gombe, Kebbi, Borno States
Copper Ores (Chalcopyrite, Malachite)	Bauchi, Kano and Nasarawa states
Graphite	Niger, Gombe, Katsina, Adamawa, Kaduna, Bauchi, and Taraba states
Ilmenite	Plateau, Nasarawa and Bauchi States
Manganese ore (Pyrolusite)	Plateau and Nasarawa Bayelsa and Cross River and Zamfara states
Monazite	Niger, Plateau and Nasarawa states
Quartz	Niger, Kogi, Katsina, Kebbi, Bauchi, Plateau, Ekiti and Ebonyi states
Rutile	Plateau, Nasarawa, and Kogi States
Tantalite	Niger, Osun, Kwara, Kogi, Kaduna, Bauchi states and FCT
Uranium	Cross River, Adamawa, Taraba, Plateau, Bauchi, and Kano States
Wolframite (Tungsten ore)	Kwara, Kogi and Plateau States
Zircon	Plateau, Bauchi, Taraba, Kaduna and Nasarawa states
Flourspar	Ebonyi, Benue and Taraba states
Columbite	Plateau, Kano, Kaduna, Bauchi, Kogi, Kwara, Nasarawa States
Gold	Cross Rivers, Edo, Kaduna, Katsina, Kebbi, Niger,, Osun, Zamfara States
Zircon	Nasarawa, Plateau, Kaduna, and Taraba states
Galena (Lead ore)	Nasarawa, Plateau, Taraba, Bauchi, Gombe, Ebonyi, Imo, Kano and Benue states; FCT
Sphalerite (Zinc ore)	Nasarawa, Plateau, Taraba, Bauchi, Gombe, Ebonyi, Imo, Kano and Benue states; FCT
Cassiterite (Tin ore)	Plateau, Bauchi, Kano, Cross Rivers, Ekiti, Kaduna, Nasarawa, Taraba States
Columbite	Bauchi, Plateau, Kaduna, Nasaraw, and Taraba states
Iron Ore	Kogi, Bauchi, Kaduna and Plateau states, Nasrawa

The solid mineral deposits are equivalent to wealth deposits which are potential sources of foreign exchange for the diversification of the economy of Nigeria. The proper exploitation of the minerals in the Table 1 above can fast-track the nation's recovery from economic recession.

2.1 A Case study of Iron ore

Iron ore is one of the most popular minerals found in Nigeria. Iron ores are rocks and minerals from which metallic iron can be economically extracted. The ores are usually rich in iron oxides and vary in colour from dark grey, bright yellow, deep purple, to rusty red. The iron itself is usually found in the form of magnetite (Fe_3O_4, 72.4% Fe), hematite (Fe_2O_3, 69.9% Fe), goethite (FeO(OH), 62.9% Fe), limonite (FeO(OH).n(H_2O)) or siderite (FeCO3, 48.2% Fe).

Ores c ontaining very high quantities of hematite or magnetite (greater than 60% iron) are known as "natural ore" or "direct shipping ore", meaning they can be fed directly into iron-making blast furnaces. Iron ore is the raw material used to make pig iron, which is one of the main raw materials for steel. 98% of the mined iron ore is used to make steel. Indeed, it has been argued that iron ore is "more integral to the global economy than any other commodity, except perhaps oil" (Wikipedia1, 2016).

In Nigeria, Iron ore is found in commercial quantity in Kogi, Bauchi, Plateau, Kaduna and Nassarawa States. The industrial applications of steel are numerous and it is one of the products of the beneficiation of solid minerals which can be exported if the steel mills of Nigeria are fully revived. The following sections focus on some of the unit operations involved in the beneficiation of iron ore as a case study.

Beneficiation of minerals, also called mineral processing, implies processing of mineral resources to enhance its potential value for the benefits of humankind. Therefore, the objective of the mineral processing is to render mineral resources beneficial to the modern life of humankind. Indeed, they occur as a textual intergrowth of various mineral components, and need further treatment before they can be used. Essentially the technology of mineral beneficiation resides in the separation of the mineral components by the least energy-intensive means (Inoune, n.d).

2.2 Iron ore beneficiation plant

The process flow for iron ore beneficiation can take different forms as illustrated in Figures 2A and 2B. Iron ore is collected from different plants and blended, and stored in a stockpile. These are then conveyed to a surge bin from where they are classified into particles of the size range of – 1mm.

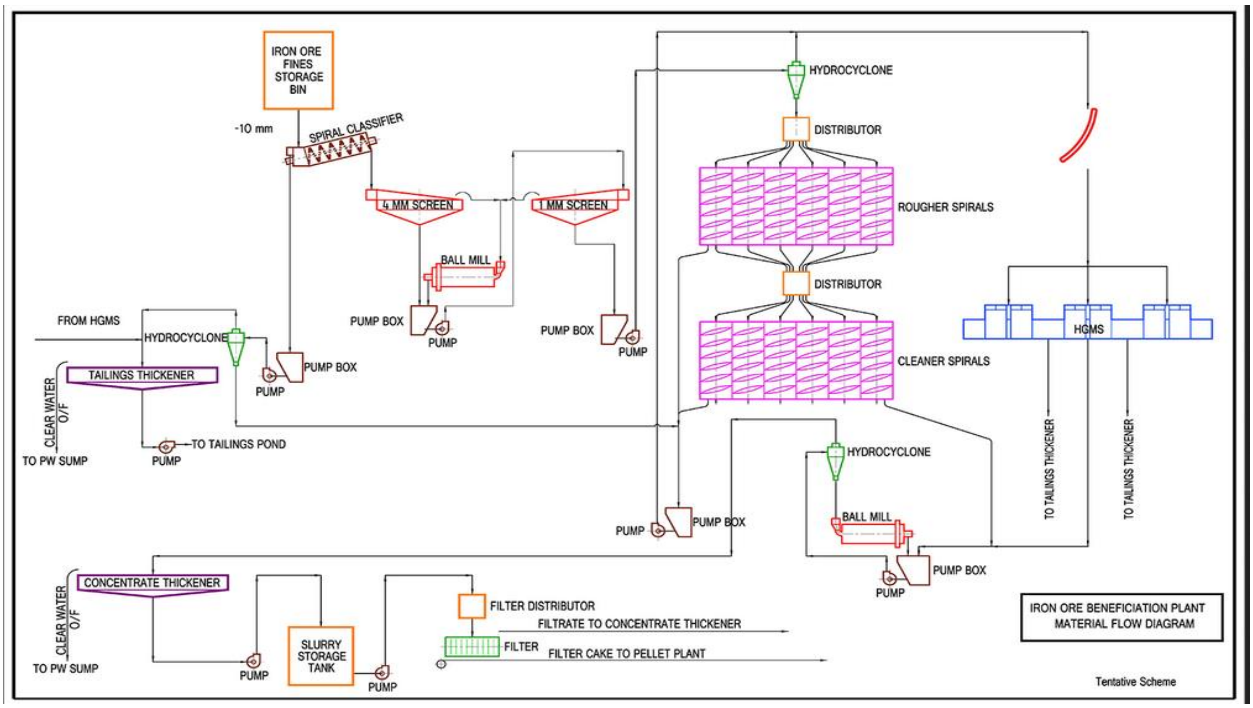

Figure 2A: Iron ore beneficiation process (*Iron Ore Beneficiation,* n.d)

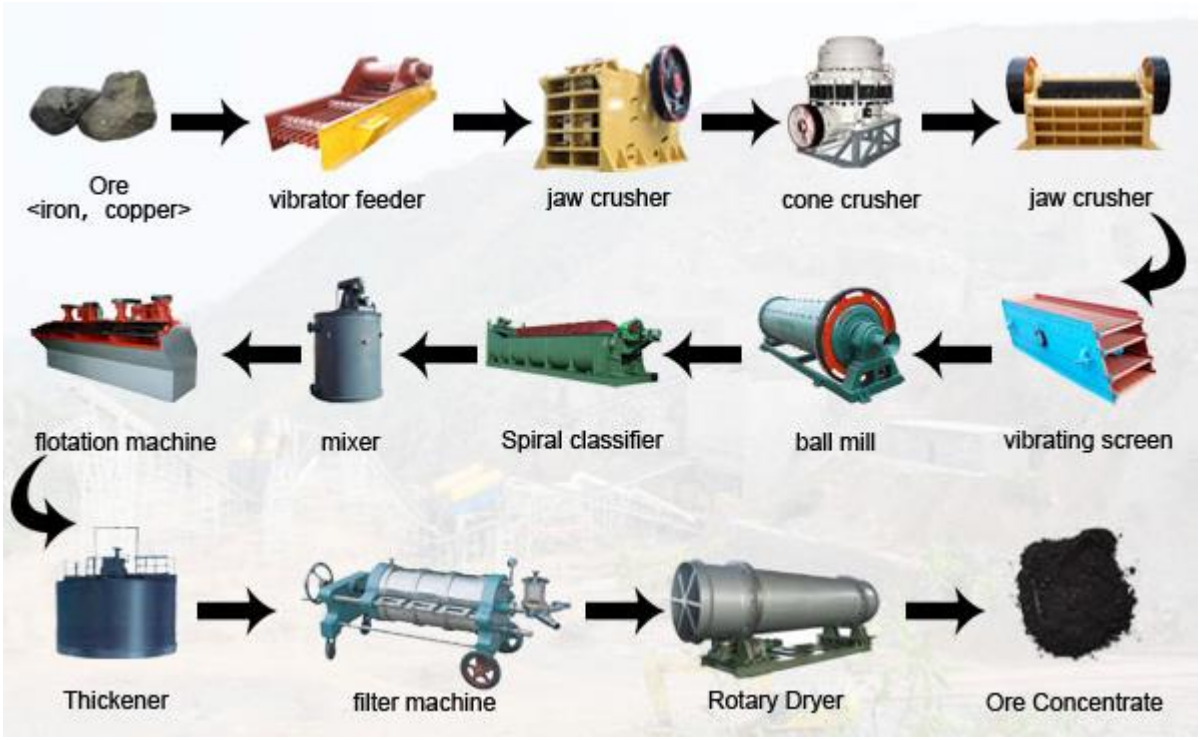

Figure 2B: Iron ore beneficiation process (Kefan Machinery, 2012)

2.3 Classification

Classification involves sorting the initial feed into different size ranges. The aim of classification is to obtain 100% -1mm particles, which is the suitable particle size for gravity separation. This is achieved by screening and milling. First the ore is screened for + 4mm and – 4mm particles. The undersize -4mm fraction is pumped to another screen, where the – 1mm fraction is screened off. The oversize + 4mm fraction and the + 1mm fraction from the second screen are ground together in a ball mill, in closed circuit with a screen, to obtain 100% – 1mm particles. The product is washed and then pumped to spirals for gravity separation. The concentrate from the spirals is then pumped to a concentrate thickener. The concentrate thickener product is then filtered to get a product of maximum 8% moisture. The filter cake is conveyed to a stockpile *(VT Corp*, 2016).

The major unit operations that are involved in the process depicted in Figures 2A and 2B are further discussed below.

2.3.1 Grinding mill

Size reduction (comminution) of the ore either from the mine, or at some intermediate stage takes place in the grinding mill, thereby, reducing the feed to powder. The product passes through a screen of say 40 mesh (where a mesh is the number of holes per inch of the screen). This occurs by the actions of compression, impact or attrition. Example is a hammer mill (Figure 3), which operates by impact (Gulin, 2013).

Figure 3: PF Impact crusher (Gulin, 2013)

In the hammer mill there is a horizontal, high speed rotor, turning in a horizontal cylindrical casing. The ore or material is fed in through the top of the casing, and the particles are broken by a set of swinging hammers pinned to a rotor disk. All the feed particles are impacted by the hammers. They break into pieces, and fly upon a stationary anvil plate inside the casing, which breaks them into smaller particles. Thereafter, they are rubbed

into powder by the hammers and pushed through a screen.

2.3.2 Screens

Screens are devices that separate particulate matter according to their sizes. In operation the solid particles are dropped on or thrown against the screen. The screen surfaces have to be agitated in some manner, such as gyrating or vibrating either mechanically or electrically. Particles that are smaller than the screen openings pass through it, while those particles that are larger than the screen openings are retained. To know the maximum and minimum sizes of the particles that pass through screen, the solid particles are often passed through a series of screens. Screening is sometimes done wet, but is often done dry. Screens are made from woven metal wires, silk or plastic cloth, example shown in Figure 4. They may consist of metal bars, or perforated metal plates. These metals are usually steel or stainless steel. Screens finer than 150 mesh are not normally used, because other methods of separating such fines are more economical. Specific types of screening equipment include: stationary screen, grizzly, gyrating screen, vibrating screen, centrifugal sifter (*Screening Machine, 2015).*

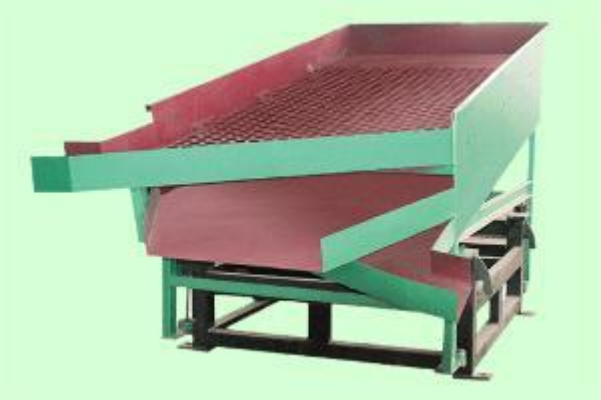

Figure 4: Screening Machine (*Screening Machine, 2015*).

2.3.3 The Spiral Separator.

The spiral separator shown in Figure 5 is a device for separating slurry components by density. The device consists of a tower around which a sluice is wound in a spiral configuration. At the base of the sluice, slots are installed to collect the separated particles. As larger and heavier particles travel faster and faster down the sluice, they experience more drag, and thus move towards the centre of the sluice and travel slower. Lighter particles move towards the edge of the sluice and travel faster. At the bottom of the sluice higher and lower density parts are separated by slots. Wash water inlets may be added along the length of the spiral to aid the separation of lighter materials (*Spiral Separator, 2016*).

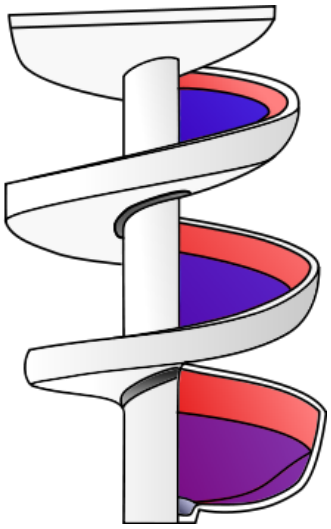

Figure 5: Spiral Separator. (*Spiral separator, 2016*)

2.3.4 The Cyclone Separator

The cyclone separator, as shown in Figure 6 is a device for separating particulates from gases or liquids by vortex separation, where rotational and gravitational forces are used to separate mixtures of particles and fluids. A cyclone that separates particulates from liquid is called a hydrocyclone. In the operation of the cyclone, a high speed rotating gas flow is established in a partly cylindrical and partly conical container. The air flow in the cyclone is helical, beginning at the top and ending at the bottom, where it exits the cyclone. Larger or denser particles have too much inertia and can't follow the tight curve of the flow. They move outward, and strike the walls of the container. Thereafter, they fall to the bottom of the cyclone where they are removed. At the conical part at the bottom of the cyclone, the radius of rotation of the flow gets smaller, thus separating smaller particles. The cut point of the cyclone is defined as the particle size that will be removed with 50% efficiency. Particles larger than the cut point will be removed with a greater efficiency and particles smaller than the cut point will be removed with smaller efficiency (*Cyclone Separator, 2016*)

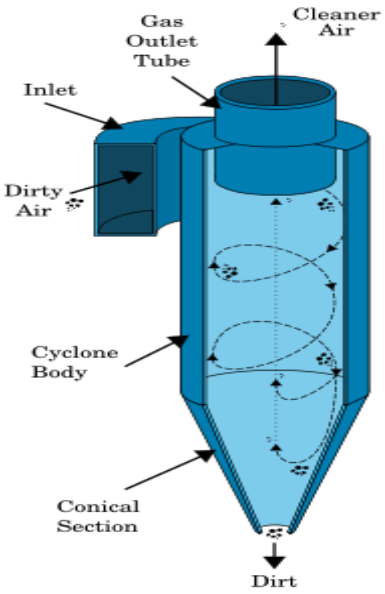

Figure

Figure 6: A Cyclone Separator (Cyclone Separator, 2016

2.3.5 Thickener

In a thickener, particles of solid heavier than the suspended liquid are removed in a large settling box or settling tank (Figure 7). Here the fluid velocity is low and the particles have ample time to settle out. In industrial separators provision is made for continuous removal of settled solids (Thickener, 2013)

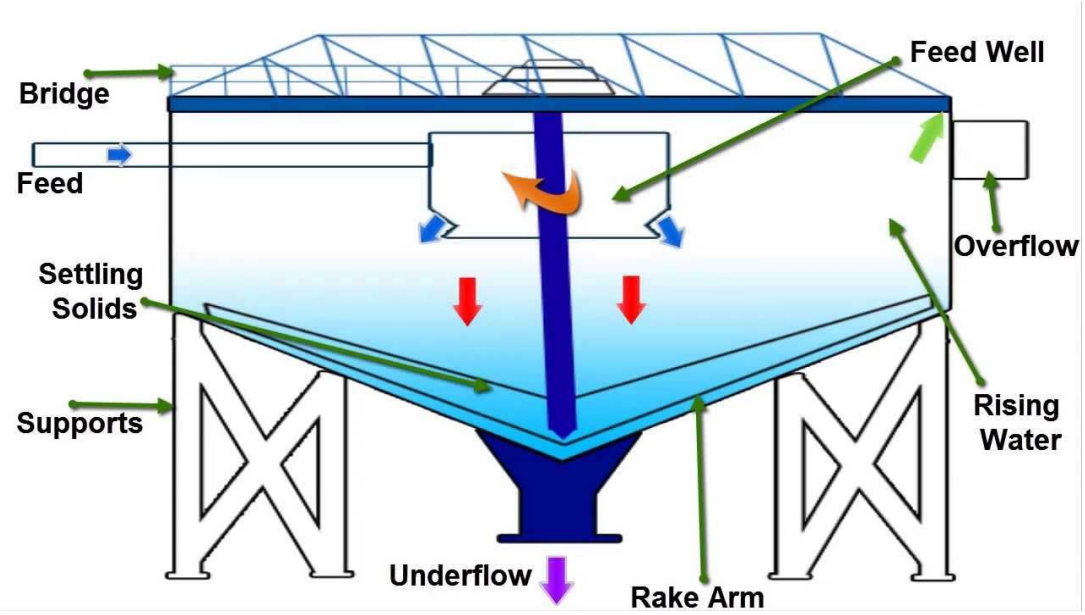

Figure 7: A Thickener (Thickener, 2013)

2.3.6 Froth floatation cells

Froth floatation is the process of separating hydrophobic and hydrophilic materials. In froth floatation minerals are separated from gangue. The hydrophobicity of valuable minerals and waste gangue are increased by application of surfactants or wetting agents. Before froth floatation can work the ore has to be reduced to fine grains of physically separate minerals, by crushing and grinding, i.e comminution. The ground ore is mixed with water to make a slurry, thereby making the desired mineral hydrophobic (if naturally not already hydrophobic). The slurry is mixed with an appropriate surfactant. The slurry of hydrophobic and hydrophilic

material, called a pulp, is pumped into tanks, known as floatation cells, Figure 8. The tanks are aerated to produce bubbles. The hydrophobic materials get attached to the bubbles, and float to the top as a froth. The froth of concentrated mineral is collected as a concentrate.

The pulp that does not float is known as floatation tailings, and may be floated again to recover minerals that did not float the first time. This is called scavenging.

Froth floatation efficiency depends on the probabilities of particle – bubble contact, particle-bubble attachment, transport between pulp and froth, and froth collection in the product. Floatation often takes place in stages in series, to increase particle residence time, and increase the probability of particle bubble contact (Wikipedia2, 2016).

Figure 8: Froth floatation cell (Wikipedia2, 2016)

2.3.7 Filters

Filtration involves the removal of solid particles from a fluid by passing it through a medium, where the solids are deposited. Due to pressure difference across the medium, the fluid flows across the medium. Cake filters separate quite large amounts of solid as a cake of crystals or sludge. They operate with pressure above atmospheric on the upstream side of the medium, or with a vacuum at the downstream side of the medium. An example of a cake filter (Figure 9) is the horizontal tank pressure shell and leaf filter (Andritz, 2014)

Figure 9: Filter Press (Andritz, 2014)

3.0 ROLE OF CHEMICAL ENGINEERING IN THE ABOVE PROCESSES

Figures 2A and B depict a typical process (beneficiation of iron ore). The process consists of various unit operations that are linked. The system also portrays the

value-added chain for iron ore. A critical look at the process in Figures 2A and B show that the unit operations involved are basically separation processes. With respect to the definition of chemical engineering profession and the beneficiation process described above (as a case study), the indispensable roles of chemical engineering in solid mineral development can be outlined as follows:

1. Preliminary design of economically feasible processes for the beneficiation and processing of the solid minerals in Nigeria.
2. Optimization and automation of the processes to meet international standards as well as to enhance profitability.
3. Construction and installation of process plant machinery at the production site.
4. Plant commissioning, operation and maintenance with a view to achieving design and production objectives/targets.
5. Quality control of the various end-products to ensure that international standards are met, as well as the end users.
6. Networking, design and implementation of marketing strategies to ensure sustainability of demand and supply (exportation) of end products thereby generating foreign exchange for the country.
7. In the area of research for innovations to meet with the global trend in processing of Nigeria solid minerals

4.0 CONCLUSION

No solid mineral exists in its pure state when it is mined. Solid minerals must undergo beneficiation to add value to them and convert them to a state that man can conveniently use to meet his needs. The role of chemical engineering in adding value to solid minerals has been highlighted in this paper using the beneficiation of iron ore as a case study. Beneficiation involves the application of appropriate technologies to optimally purify solid minerals. Development of these technologies (processes) calls for professional intervention of chemical engineers. This is because chemical engineering is the only branch of engineering that deals extensively and intensively with process design for raw material conversion. The principles of process plant design in chemical engineering can be applied by chemical engineers to develop efficient processes for the beneficiation and processing of Nigerian solid minerals towards diversifying the nation's economy and job creation.

REFERENCES

Andritz (2014). *Andritz Separators*. Retrieved October 24, 2016 from https://www.andritz.com/se-downloads-iron_ore.pdf

Chinago, A. B., Clinton, A. and Ameh, E. F. (2015). *Geographical Survey of Nigerian Mineral Resources: A Step toward Planned Development.* Journal of Culture, Society and Development, Vol.6, Pg 3.

Cyclone Separator, 2016. Retrieved October, 24, 2016 from http://www.bing.com/images/search?q=Cyclone+Separator+&view=detailv2&qpvt=Cyclone+Separator+&id=187E589BF48C1AC9374979A43D363F421952F920&selectedIndex=1&ccid=ldmsHKTm&simid=608031490438988910&thid=OIP.M95d9ac1ca4e6457d8165a8a17c8e71ebo0&ajaxhist=0

Kefan Machinery (2012). *Beneficiation plant process of iron ore and beneficiation equipment in India*. Retrieved October 18, 2016 from http://www.mineselect.com/news/beneficiation-plant-process-equipments-iron-ore.html

Gulin (2013). *Impact breakers crusher stone*. Retrieved October 24, 2016 from http://www.chinagrindingmill.net/products/impact/impact-breakers-crusher-stone.html

Malomo, S. (2007). *Nigeria Mineral Resources.* Paper Presented at the International Workshop on sustainable development of Nigeria's Mineral Potentials .Held at the International Conference Centre, Abuja, Nigeria, 22" - 29 th November, 2007.

Screening Machine (2015*). The factors influencing iron ore screening equipment*. Retrieved October 24, 2016 from http://www.iron-solution.com/news-4/iron-ore-screening-equipment.html 2015

Spiral Separator (2016). Retrieved October, 24, 2016 from http://www.bing.com/images/search?q=Spiral+separator+&id=1E000D8EA27208AC29678119FA931C695DF7CBBE&FORM=IQFRBA

Thickener (2013). *What are thickeners & how do they work - Mineral Processing* [video file] Retrieved October 19, 2016 from https://www.youtube.com/watch?v=qtScIThaKus.

Toshio Inoune, (n.d). Mineral Comminution and separation systems. Retrieved October 18, 2016 from *www.eolss.net/Sample-Chapters/C05/E6-37-06-05.pdf*

VT Corp (2016*). Iron Ore Beneficiation*. Retrieved October 17, 2016 from http://www.vtcorpindia.com/iron-ore-pellet-plant-division/

Wikipedia (2016). *Chemical Engineering*. Retrieved October 17, 2016 from http://en.wikipedia.org/wiki/chemical_engineering.

Wikipedia1. (2016). *Iron Ore*. Retrieved October 18, 2016 from https://en.wikipedia.org/wiki/Iron_ore

Wikipedia2, 2016. *Froth Floatation.* Retrieved October 24, 2016 from https://en.wikipedia.org/wiki/Froth_flotation

THE EFFECT OF TEMPERATURE AND CATALYST MODIFICATION ON THERMOCATALYTIC DEGRADATION OF LOW DENSITY POLYETHYLENE

***Osigbesan A. A.[1,2],Waziri, A.Y.[1], Dabai, F.N.[2], Fasanya, O.[1], Atta, A.Y.[2], AND Jibril, B.Y.[2]**

[1]Petrochemicals and Allied Department, National Research Institute of Chemical Technology, Zaria

[2]Chemical Engineering Department, Ahmadu Bello University, Zaria

Corresponding author's email address: aishatosigbesan2011@gmail.com

ABSTRACT

Low density polyethylene (LDPE), which is non biodegradable, is a major constituent of municipal solid waste and source of light hydrocarbons when recycled using thermo-catalytic processes. In this study, the effects of temperatures (400 and 500 ^oC) and catalysts (commercial and modified mordenite) on the reforming of the vapour obtained from the pyrolysis of LDPE were studied. Commercial mordenite was acid treated and impregnated with 0.3 wt% Iron; the catalysts thus prepared were A1: commercial mordenite, A2: acid treated mordenite and A3: 0.3 wt% Fe loaded on mordenite. The catalysts were characterized using X-Ray Diffractometer and Brunauer-Emmett-Teller techniques, and then used to reform the pyrolysed LDPE at reforming temperatures 400 and 500 ^oC. The reformed products obtained were liquid and gases. The liquid products were analysed using GCMS. The results showed paraffins were predominant in the samples obtained from the use of A1. While the samples obtained using A2 and A3 had olefins and aromatics present. The carbon atoms in the hydrocarbons ranged from $C_5 – C_{36}$ for A1, and reduced to $C_5 – C_{16}$ and $C_5 – C_{22}$ for A2 and A3 respectively. The results showed the ability of mordenite to reform the vapours of pyrolysis to products within fuel range.

Keywords: Catalysts. LDPE, Pyrolysis, Reforming, Temperature.

1.0 INTRODUCTION

Plastics have replaced to a large extent packaging materials; most of these packaging plastics are thermoplastic type of polymer which could be recycled. It is widely agreed that used and unwanted plastics become waste and are dumped at landfill site most often. Since most plastics are non - biodegradable, they constitute menace to the environment.

The most appropriate approach to eliminate or reduce the environmental problems created by waste plastics is recycling [Norena et al, 2012]. There are various kinds of recycling processes, of which the tertiary recycling process is an advanced and most desired. This is so because tertiary recycling process produces valuable chemicals and fuels [Puente et al, 2002].

Polyolefins such as polyethylene, polypropylene and polystyrene are produced and consumed massively due to their wide range of applications in recent time. Tertiary recycling of these polymers as they become waste has been studied under various approaches which include laboratory scale catalytic degradation whereby the polymer and the catalyst of choice are in contact in a reactor and enclosed; the set up is heated to a reaction temperature and allowed for a reaction time; then the products are collected and analyzed (Panda et al, 2008). On the other hand, thermal cracking otherwise known as pyrolysis has been the method in existence in which the polymers are heated at very high temperature in order to breakdown the macromolecules of the waste polymer to smaller or micro molecules. Usually, the products of pyrolysis are a mixture of gaseous, liquid and solid hydrocarbons (Buekens et al, 1998) which are however, crude but can be upgraded. An advanced method of tertiary recycling is the two stage process involving the pyrolysis as the first stage and catalytic reforming as the second stage. Mochamad Syamsiro et al. (2013) reported on passing the products of pyrolysis through a catalytic reforming unit. They obtained and analyse wide range of products. The catalysts tested for the two stage recycling process include synthesized mordenite from Malaysian clay and commercial mordenite. This method caters for the shortcomings encountered in either of the previous two method earlier described.

Ishira et al. (1998) established the effective reforming of products of pyrolysis using several catalystsThey include zeolites like ZSM – 5, mesoporous MCM-41, USY, SiO_2-Al_2O_3, natural zeolites and so on; other forms of catalysts are metal impregnated on zeolite support like Nickel on ZSM -5, Cobalt on mordenite, etc.

In our study, , two stage recycling processes of pyrolysis and reforming were investigated using a commercial mordenite and its modified forms which included acid treatment and 0.3 wt% Fe impregnated on the

mordenite. This is to enable comparative study of the performances of the catalysts.

2.0 MATERIALS AND METHODS

A description of the materials and procedures adopted are outlined in this section.

2.1 Materials

The materials used in the work included commercial ammonium mordenite, which was purchased from Zeolysts International, Iron III nitrate nanohydrate (Guangdong Guanghua Chemical Factory Co., Ltd), distilled frompetrochemical laboratory of National Research Institute for Chemical Technology, Zaria and waste water sachets (LDPE) collected from household wastes.

The equipment included X-Ray Difractometer, VSorb APP surface area and porosity analyzer and Agilent Gas Chromatography/Mass Spectroscopy.

2.2 Preparation of catalysts

The commercial mordenite was first dried in an oven at 120 ^{o}C for 5 hours, and then calcined for 3 hours at 500 ^{o}C in a muffle furnace; this was named A1. The second catalyst, A2 was prepared by treating the ammonium mordenite with 500ml of 1M HCl at atmospheric pressure by stirring for 1hr. then, it was filtered and washed with distilled water, dried at 120 ^{o}C for 5 hours and calcined in a muffle furnace for 3 hours at 500 ^{o}C. A3 was prepared by impregnating Fe precursor i.e the iron III nitrate nonahydrate in the mordenite. 0.3 w/w% Fe was loaded on a 20 g of the mordenite. The quantity of the precursor, correctly calculated for loading, was dissolved in distilled water and poured in a beaker containing the 20g mordenite, it was heated at 75 ^{o}C and stirred slowly for 5 hrs. A3 wass then dried in the oven at 120 ^{o}C for 5 hrs and calcined afterward in a muffle furnace at 500 ^{o}C for 3 hours.

2.3 Characterization of the catalysts

The crystal structures of the catalyst samples were determined using XRD; about 0.5 g of each sample was seeded on a ceramic substrate. The XRD patterns were captured using Rigaku MiniFlex 600 at 40 KV, 15 mA and; a scanning speed and step size of 10 degrees/min and 0.02^{o} respectively for 2 theta values from 10 – 90. N_2 adsorption – desorption measurements were conducted at 77 K (-196 ^{o}C) on a VSorb APP to obtain the BET specific surface area (S_{BET}) as well as pore sizes and volumes of all the three samples.

2.4 Preparation of the feedstock (LDPE)

- The waste plastics (LDPE) were gathered from houses,
- the plastic wastes are washed and sun dried,
- Size reduction of the waste plastics by shredding was done.

2.5 Experimental procedures:

The experimental set up comprised of a is a pilot scale pyrolysis/reforming reactor system which was designed and fabricated at National Research Institute for Chemical Technology, NARICT, Zaria. It is a two stage reaction set up for pyrolysis and reforming; the other components of the set up include the cooling and receiving sections. The schematic diagram of this set up is shown in Figure 1 with the component description. 10 g of the waste LDPE is weighed into the round bottom flask immersed in the heating mantle of heating rate of rate 5 ^{o}C /min, where the pyrolysis takes place. An external digital K type thermocouple as well as a nitrogen gas line was inserted into the flask.

Prior to the pyrolysis, the system is scrubbed with the nitrogen gas in order to create an inert system. The vapour produced from the pyrolysis stage is allowed to flow to the reformer where it was reformed by catalyst at varying temperatures. The reforming stage consists of the reformer which is a fixed bed reactor made of stainless steel and surrounded by heating element of heating rate of about 14 ^{o}C /min, the length of this reactor is 20.5 cm while the inner diameter is 2 cm. 1 g of catalyst was weighed and loaded in the reformer at every experimental run, the catalyst was guided by glass wool before and after in the fixed bed in order to maximise the gas phase contact and reaction. The reforming temperature was set at either 400 or 500 ^{o}C. The reformed vapours then were released into the separating flask immersed in an ice water bath that was continually chilled by the water circulating through a chiller. The vapours which consist of condensable and non condensable gases were separated; the condensable gases remained in the flask as the liquid product and the non condensable gases pass through a gas line into a gas bag.

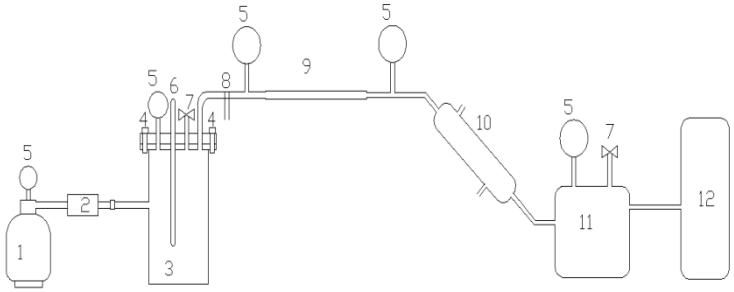

Figure 1: Schematic diagram of the experimental set up
Footnote: nitrogen tank (1), flowmeter (2), pyrolyser (3), pressure guage (5), temperature sensor (6), fixed catalytic bed (9), condenser (10), liquid collector (11) and gas collector (12).

2.6 Analysis Of Products

The chemical compositions of the liquid products were determined with Gas Chromatograph-Mass Spectrometer (GCMS) analyzer. The method described by Jin, Shen, Liu, & Xiao, (2016) was followed.

3.0 RESULTS AND DISCUSSION:

3.1 Characterization Of Catalysts:

The BET surface areas, pore volumes and pore sizes of the catalyst samples obtained from the N_2 adsorption-desorption isotherms and calculated using the BET and Langmuir methods are illustrated in Table 2. Sample A1 has the least surface area ($323mm^2/g$) and pore volume ($0.16cm^3/g$). Sample A2 has a higher surface area than A1, due to acid treatment and consequent dealumination of the mordenite which also indicate higher Si/Al ratio and more pore openings. The pore volume is also higher for A2 than A1. On iron impregnation, the surface area was smaller than that of the acid treated sample (A2), but still bigger than the initial mordenite sample (A1). The results on Table 1 also show that the pore size ranged from 2.0 – 2.7nm for all three catalysts (A1, A2 and A3). Hence, particles or molecules within the size range of 2.0 – 2.7 nm can have access to the pores of the catalysts, where the active sites are situated, so as to be broken down or reformed (Syamsiro et al, 2013).

Figure 2 shows the crystalline structure of the three catalysts (A1, A2 and A3) as analysed by X-ray diffractometer. The diffraction patterns show peaks at 2θ values from 10^o to 32^o, corresponding to the structural framework of mordenite as described by Trisunaryanti et al., (1996). These peaks remained present despite the acid treatment and metal impregnation, indicating the crystalline nature of the samples. Therefore, the XRD analysis shows that the zeolite structure of mordenite was not damaged even after acid treatment and metal

impregnation. The presence of iron oxide tends to be indicated by peaks around 2θ values of 33^o - 37^o (Calsavara & Lucano, 2008). However, the diffraction peaks of iron oxide were not visible in Figure 2. This is probably because the amount of iron oxide impregnated in the mordenite was very small compared to the detectable amount of at least 5 w/w% reported in literature (Aziz et al., 2016).

Table 1: BET report of the catalyst samples.

S/N	CODE	S_{BET} (m^2/g)	S_L (m^2/g)	Pore size range (nm)	Pore volume (cm^3/g)
1	A1	324	428	2.1 – 2.6	0.156821
2	A2	421	554	2.0 – 2.6	0.200430
3	A3	384	506	2.1 – 2.6	0.177825

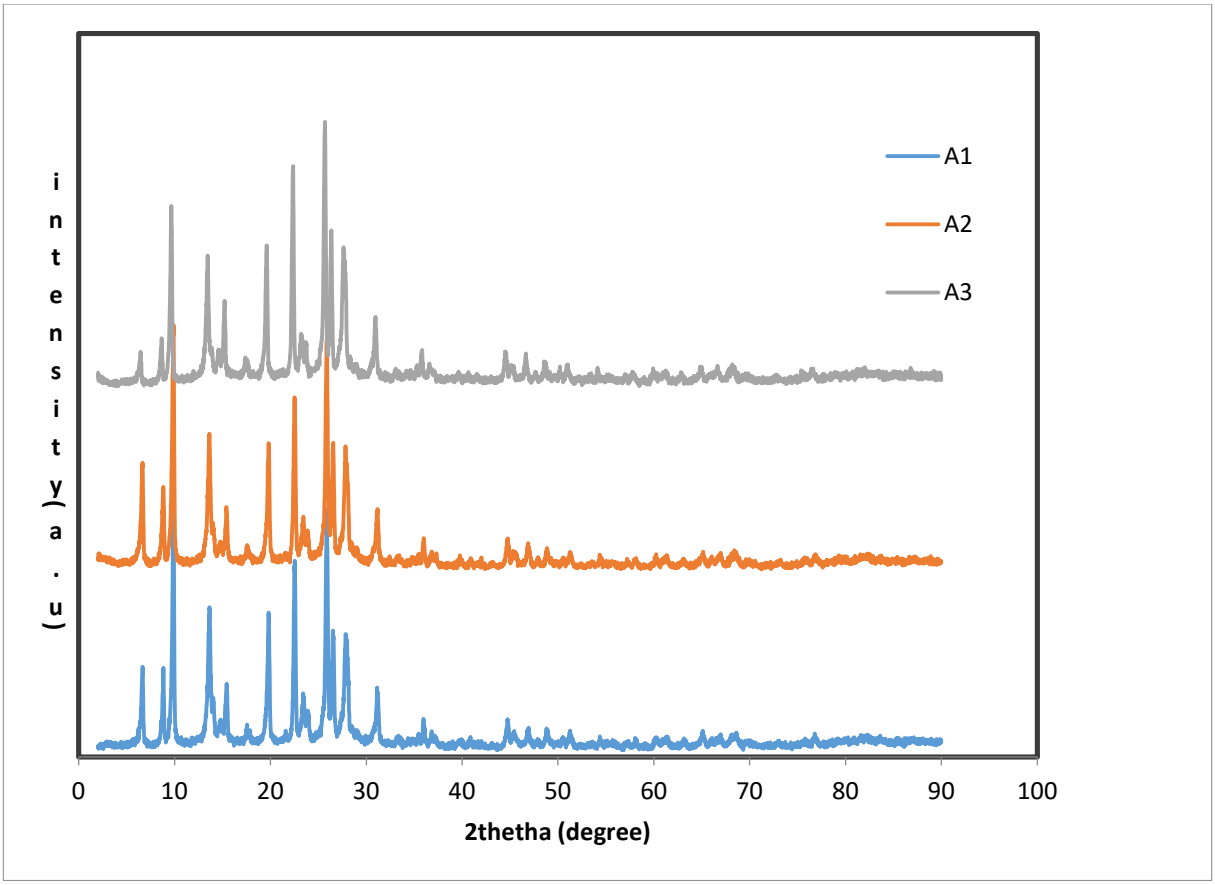

Figure 2: XRD patterns of: A1 (Commercial Mordenite); A2 (Acid Treated Mordenite) and A3 (0.3 w/w% Fe loading on Mordenite)

3.2 Product Analysis

Catalysts play significant roles in thermochemical reactions. They can improve the selectivity of desired products by driving the reaction towards a favourable reaction mechanism, which targets the desired product.

Tables 2 and 3 illustrate the chemical components of the liquid samples obtained from the GCMS analysis of the samples at 400 and 500 ^{o}C reforming temperatures respectively. Table 3 shows that the use of A1 results in a wide range of hydrocarbons from $C_6 - C_{36}$ identified to be majorly alkanes (paraffin). While the composition of the oil when A2 was used for reforming at 400 ^{o}C includes a number of olefinic compounds (C_5, C_6, C_7, C_{11}) and paraffinic compounds with the highest carbon atom of C_{26}. With the use of A3, a number of aromatic compounds (benzene), more olefins (C_7, C_{11}, C_{13}) and paraffins with the highest carbon atom C_{23} were obtained. This implies that as the reforming proceeds from no catalyst to A1 (without modification) to A2 (with acid treatment) to A3 (acid treatment and 0.3 wt% Fe), at the same temperature, cracking of the large hydrocarbons is enhanced progressively.

Table 2: The most abundant component of the GC-MS analysis of the reformed pyrolyzed oil samples of LDPE at 400 ^{o}C

Catalyst	Nomenclature	RT (min)	RA (%)	HC Type	No. of Carbon Atoms
A1	1,5-Heptadiene	8.85	0.28	Olefin	C_7
	Decane	9.01	0.28	Paraffin	C_{10}
	Undecane	10.89	0.93	Paraffin	C_{11}
	Cyclodecane	12.47	0.67	Cycloparaffin	C_{10}
	5-Dodecene	12.47	0.67	Olefin	C_{12}
	1,6-Octadiene	12.69	0.22	Olefin	C_{10}
	5-Tridecene	14.07	0.65	Olefin	C_{13}
	Tridecane	14.18	1.39	Paraffin	C_{13}

Catalyst	Nomenclature	RT (min)	RA (%)	HC Type	No. of Carbon Atoms
	1,5-Hexadiene	16.94	0.29	Olefin	C_6
	Pentadecane	17.04	2.36	Paraffin	C_{15}
	Hexatriacontane	25.82	2.97	Paraffin	C_{36}
A2	Decane	9.01	0.63	Paraffin	C_{10}
	4-Undecene	10.75	0.66	Olefin	C_{11}
	Undecane	10.89	1.96	Paraffin	C_{11}
	2,3-Hexadiene	12.08	0.28	Olefin	C_6
	4-Dodecene	12.46	0.96	Olefin	C_{12}
	Tridecane	12.61	4.74	Paraffin	C_{13}
	3-methyl-1,4-pentadiene	13.84	0.35	Olefin	C_5
	5-Tetradecene	15.55	1.18	Olefin	C_{14}
	Tetradecane	15.67	6.30	Paraffin	C_{14}
	1,5-Heptadiene	16.85	0.43	Olefin	C_7
	Pentadecane	17.05	6.87	Paraffin	C_{15}
	Octadecane	20.75	6.40	Paraffin	C_{18}
	Nonadecane	21.86	5.36	Paraffin	C_{19}
	Eicosane	22.91	4.73	Paraffin	C_{20}
	Heneicosane	23.92	3.98	Paraffin	C_{21}
	Docosane	24.88	2.96	Paraffin	C_{22}
	Hexacosane	25.81	2.60	Paraffin	C_{26}
A3	Nonane	6.95	0.40	Paraffin	C_9
	Decane	9.01	1.49	Paraffin	C_{10}
	2-ethyl-1,4-dimethylbenzene	10.61	0.42	Aromatic	C_9
	4-undecene	10.75	1.25	Olefin	C_{11}
	Undecane	10.89	2.99	Paraffin	C_{11}
	2-methyl-2,3-hexadiene	11.74	0.62	Olefin	C_7
	1-butylbenzene	11.92	0.65	Aromatic	C_{10}
	Cyclopropylbenzene	13.87	0.42	Aromatic	C_9
	1,5-Heptadiene	13.95	0.39	Olefin	C_7
	Tridecene	14.06	2.4	Olefin	C_{13}
	Hexadecane	18.35	6.70	Paraffin	C_{16}
	Heptadecane	19.58	5.63	Paraffin	C_{17}
	Octadecane	20.74	4.90	Paraffin	C_{18}
	Nonadecane	21.85	3.81	Paraffin	C_{19}
	Eicosane	22.89	3.35	Paraffin	C_{20}
	Heneicosane	23.91	2.67	Paraffin	C_{21}
	Triacosane	25.79	1.89	Paraffin	C_{23}

Table 3: The most abundant component of the GC-MS analysis of the reformed pyrolyzed oil samples of LDPE at 500 ^{o}C

Catalyst	Nomenclature	RT (min)	RA (%)	HC type	No. of Carbon Atoms
A1	1,5-Heptadiene	8.85	0.42	Olefin	C_7
	4-Undecene	10.75	1.27	Olefin	C_{11}
	Decane	10.89	1.23	Paraffin	C_{10}
	5-Dodecene	12.42	1.50	Olefin	C_{12}
	Cyclohexane	12.69	0.25	Cycloparaffin	C_6
	6-Tridecene	14.07	1.89	Olefin	C_{13}
	2,4,6-trimethyloctane	14.19	2.27	Paraffin	C_{11}
	3-methyl-1,6-Heptadiene	15.46	0.57	Olefin	C_7
	3-tetradecene	15.57	1.76	Olefin	C_{14}
	2-methyl-2,3-Hexadiene	15.90	0.25	Olefin	C_6
	Tetradecane	15.66	2.86	Paraffin	C_{14}
	1-Pentadecane	16.94	1.43	Paraffin	C_{15}
	Hexadecane	18.35	4.30	Paraffin	C_{16}
	Octadecane	20.75	4.45	Paraffin	C_{18}
	Nonadecane	21.86	4.48	Paraffin	C_{19}
	Eicosane	22.92	4.24	Paraffin	C_{20}
A2	Decane	9.01	0.82	Paraffin	C_{10}
	4-Undecene	10.76	1.07	Olefin	C_{11}
	4-Nonene	10.76	1.07	Olefin	C_9
	Undecane	10.91	2.02	Paraffin	C_{11}
	Benzene	11.95	0.64	Aromatic	C_6
	Benzene	13.842	0.55	Aromatic	C_6
	Benzene	14.70	0.43	Aromatic	C_6
	4-Dodecene	12.48	1.38	Olefin	C_{12}
	1,5-Heptadiene	12.72	0.33	Olefin	C_7
	2,3-Hexadiene	13.33	0.37	Olefin	C_6
	1-Tridecene	14.07	1.81	Olefin	C_{13}
	1-Pentadecene	16.95	0.91	Olefin	C_{15}
	Dodecane	12.63	5.19	Paraffin	C_{12}
	Tridecane	14.22	7.91	Paraffin	C_{13}
	Pentadecane	17.08	14.14	Paraffin	C_{15}
	Hexadecane	18.37	11.31	Paraffin	C_{16}
	Heptadecane	19.59	6.87	Paraffin	C_{17}
	Octadecane	20.76	3.33	Paraffin	C_{18}
	Nonadecane	21.86	2.05	Paraffin	C_{19}
	Eicosane	22.91	1.47	Paraffin	C_{20}
	Docosane	24.87	0.81	Paraffin	C_{22}
A3	Decane	8.99	0.25	Paraffin	C_{10}
	1,5-Heptadiene	10.74	0.5	Paraffin	C_7
	4-Dodecene	12.45	0.84	Olefin	C_{12}
	5-Dodecene	12.68	0.27	Olefin	C_{12}
	4,4-dimethyl-2-	13.31	0.21	Olefin	C_5

Catalyst	Nomenclature	RT (min)	RA (%)	HC type	No. of Carbon Atoms
	Pentene				
	5-tridecene	14.04	1.15	Olefin	C_{13}
	1-butyl-Benzene	13.94	0.62	Aromatic	C_6
	Dodecane	12.59	2.08	Paraffin	C_{12}
	Tridecane	14.17	3.02	Paraffin	C_{13}
	Pentadecane	17.02	2.43	Paraffin	C_{15}
	Hexadecane	18.32	1.79	Paraffin	C_{16}

Table 3 illustrates that at 500 ^oC, by using A1 the composition of the oil consists of hydrocarbons of majorly olefins ($C_7 – C_{14}$) and paraffin ($C_{10} – C_{20}$) while using A2 and A3 result in aromatic compounds (benzene, methylbenzene and butylbenzene) and more olefinic compounds. The results show that the highest carbon atom obtained when A2 was used is $C_{22,}$ while with A3, C_{16} was obtained; implying enhanced cracking in the presence of A2 and A3. Thus, the GC-MS analysis also confirms that increasing temperature from 400 to 500 ^oC played a key role in enhancing the cracking of the larger hydrocarbons.

Generally, the quality of the oil improved as catalyst was changed from A1 to A2 to A3 as well as increase in temperature from 400 to 500 ^oC. Also, the surface areas of A2 (421 m/g) and A3 (385 m/g) probably had accessible active sites where the reforming of the HCs took place. The aromatic compound present is mainly benzene, while the olefins are within the carbon number range of C_5 to C_{14}; the paraffin reduced to C_{10} - C_{16}. The oil obtained when A3 at 500 ^oC was used consists of gasoline range HC ($C_5 – C_{12}$), naphtha range HC ($C_8 – C_{12}$), kerosene range HC ($C_{11} – C_{14}$) and diesel and fuel oils HC ($C_{11} – C_{20}$).

4.0 CONCLUSIONS:

In this work, the performance of mordenite and Fe – mordenite on the reforming of pyrolysis vapours was investigated at varying temperatures. It can be concluded that the XRD results showed no structural deformation done to the mordenite despite the modification by acid treatment and iron loaded on the zeolite framework. The BET result showed the surface areas of the catalysts with the highest as 421 m^2/g (A2) and lowest is 384 m^2/g (A3); and pore sizes ranging from 2.0 – 2.7nm.

Two stage processes of pyrolysis and catalytic reforming was carried out on the waste LDPE. The composition of the liquid products analyzed by GCMS was largely paraffins of $C_6 – C_{40}$ for A1. The liquid products obtained for reforming over A2 and A3 contained some paraffin, olefin, diolefin and aromatic of $C_6 – C_{16}$ and $C_6 – C_{22}$ respectively. The aromatic compound present in the liquid is benzene.

ACKNOWLEDGMENT

This work was performed in the research laboratory of the National Research Institute for Chemical Technology, NARICT, Zaria as well as Ahmadu Bello University, Zaria. Utmost appreciations to Prof. B. Y. Jibril, Dr. A. Y Atta, Dr. F.N Dabai, Dr. Y. Alhassan and Engr. O.O Fasanya for their inestimable supervision and contributions to this research work.

REFERENCES

Aguado, J., Serrano, D. P., & Escola, J. M. (2008). Fuels from waste plastics by thermal and catalytic processes: A review. *Industrial and Engineering Chemistry Research*, *47*(21), 7982–7992. https://doi.org/10.1021/ie800393w

Aziz, A., Kim, S., & Kim, K. S. (2016). Fe/ZSM-5 zeolites for organic-pollutant removal in the gas phase: Effect of the iron source and loading. *Journal of Environmental Chemical Engineering*, *4*(3), 3033–3040. https://doi.org/10.1016/j.jece.2016.06.021

Buekens, A. G., & Huang, H. (1998). Catalytic plastics cracking for recovery of gasoline-range hydrocarbons from municipal plastic wastes. *Resources, Conservation and Recycling*, *23*(3), 163–181. https://doi.org/10.1016/S0921-3449(98)00025-1

Calsavara, V., & Luciano, M. (2008). Transformation of ethanol into hydrocarbons on ZSM-5 zeolites modified with iron in different ways, *87*, 1628–1636. https://doi.org/10.1016/j.fuel.2007.08.006

De la Puente, G., Klocker, C. and Serdan, U., (2002). Conversion of waste plastics into fuels recycling polyethylene in FCC. Applied Catalysis B: Environmental 36, 279- 285. Grieken, van R., Serrano. D. P., Aguado

Miguel G.S, Serrano D.P, Aguado J. Valorization of waste agricultural polyethylene film by sequential

pyrolysis and catalytic reforming. Industrial & Engineering Chemistry Research 2009; 48:8697-8703.

Ortega D., Noreña L., Aguilar J, Hernández I. and Ramírez V.(2006). Recycling of Plastic Materials Employing Zeolite and MCM-41 Materials. Revista Mexicana de Ingeniería Química Vol. 5, No.3 (2006) 189-195. Doi: http://www.redalyc.org/articulo.oa

Panda, A. K., Singh, R. K., & Mishra, D. K. (2010). Thermolysis of waste plastics to liquid fuel. A suitable method for plastic waste management and manufacture of value added products-A world prospective. *Renewable and Sustainable Energy Reviews*, *14*(1), 233–248. https://doi.org/10.1016/j.rser.2009.07.005

Syamsiro M, Hu W, Komoto S, Cheng S, Noviasri P, Prawisudha P, Yoshikawa K, Co-production of liquid and gaseous fuels from polyethylene and polystyrene in a continuous sequential pyrolysis and catalytic reforming system. Energy and Environment Research 2013; 3(2):90-106.

Syamsiro, M., Cheng, S., Hu, W., Saptoadi, H., Pratama, N.N., Trisunaryanti, W., Yoshikawa, K. (2014). Liquid and Gaseous Fuels from Waste Plastics by Sequential Pyrolysis and Catalytic Reforming Processes over Indonesian Natural Zeolite Catalysts. *Waste Technology*, *2*(2), 44-51. doi: http://dx.doi.org/10.12777/wastech.2.2..44-51].

MODELLING AND SIMULATION OF A CRUDE OIL TOPPING COLUMN USING THE LIEBMANN'S DECOMPOSITION MODEL

***Igbagara, P. W.[1], Akpa, J.[2], Alah, J.[3], and Okpanum, J.[4]**

[1,4]Department of Chemical Engineering, Federal University of Petroleum Resources, Effurun, Nigeria
[2]Department of Chemical Engineering, Rivers State University of Science and Technology, Port Harcourt, Nigeria
[3]Department of Chemical Engineering, Niger Delta University, Amassoma, Bayelsa State
*Email of the Corresponding author: igbagara.princewill@fupre.edu.ng

ABSTRACT

Crude Oil distillation commonly referred to as refining has dominated world energy supply, discourse, politics and economy for a better part of one and a half century. All components of Petroleum have found one useful application or the other in contemporary world economy. There is thus a huge volume of research work and technological advances in Petroleum refining using basic theories of distillation. An elementary method of determining the number of stages of a Crude Distillation Unit (CDU) is the McCaby - Thiele's method. However, it is only applicable for binary distillation. This work is an application of the McCaby - Thiele's graphical method for multicomponent distillation using the Decomposition Model of Liebmann. The study established usefulness of the Liebmann's decomposition model as a simple analytical tool for multicomponent distillation against complex and more rigorous models. Results of the Model were compared with rigorous and complex models from ASPEN HYSYS simulation software v8.6. The number of Theoretical Stages from the Model were twelve while the number of Actual Stages from the software were fifteen which shows good agreement between them.

***Keywords**: Modelling, Simulation, Topping Column, Decomposition*

1.0 INTRODUCTION

For many decades, fossil fuel has been the main source of world energy supply. Petroleum popularly referred to as Crude oil is a major source of fossil fuel complimented by Coal and Natural Gas (Chaudhuri, 2011). Today Crude Oil is refined all over the world with most of the oil industry's largest Refineries in Asia and South American. The World's largest Oil Refinery is the Paraguana Refinery in Venezuela which processes 940,000 barrels of Oil per day (Maples, 2000). The foregoing has created a compelling need for massive research and investment in multicomponent distillation for recovery of the innumerable products of Petroleum especially Gasoline, Kerosene, Diesel and other Fuel Oils such as the Vacuum Gas Oils (VGOs). Distillation as a means of separation of miscible liquids has been in existence since the early nineteenth century, although it was primarily used for the concentration of alcoholic beverages at the time. Its application gained swift acceleration in modern chemical industry on the discovery of its use as a means of separating Petroleum, a complex mixture of different components (Fair, 1983).

Design of Distillation Columns started with methods of determining the number of Stages and distillate reflux for binary mixtures by McCaby – Thiele and several others(Richardson et al., 2002). However, these methods were quickly extended to the design and analysis of multicomponent mixtures by Hengstebeck (1939), Jenny (1946) and others, thereby making separation of complex mixtures like Petroleum not only possible but relatively easy.

Petroleum distillation is complicated by the existence of different types and grades of Crude, whence its characterization to ascertain the distillability by a particular process becomes paramount in the sequence of refining operations. More recently, research efforts have been concentrated at predicting the quality and quantity of distillation products (Akpa and Umuze, 2013 and Yasin et al., 2013). Suffice to note however, that these parametres are dependent on Column sizing as was shown by McCaby – Thiele and later by the Fenske – Underwood – Gilliland (Kister, 1990). These models have been aggregated in simulation softwares which predominate contemporary design for accuracy of prediction (Shankar, 2015).

Design softwares for Petroleum processing are focused more on products specification (determination of product quality and quantity) as a general optimization problem. Little attention is given to basic sizing data which are often left for the designer to specify. The work therefore seeks to determine the size of a Topping Column (to process 12.5 bpd of Bonny Light Crude) by modification of the McCaby – Thiele's model using the decomposition theory of Liebmann (Kister, 1992) as a

way of bridging this gap. Specific objectives of the study included but not limited to;

i. Specification of Degree of Separation (i.e. Products' specification or determination of different fractions to be separated from the Crude.)
ii. Determination of the number of Stages
iii. Specification of reflux requirements and feed condition and
iv. Column sizing (height and diameter)

2.0 MATHEMATICAL EQUATIONS

The McCabe – Thiele's graphical method uses the popular MESH (Material Balance, Equilibrium, Summation and Heat Balance) equations given below in determination of the number of stages of distillation columns for binary mixtures. Extension of the method in the present work is based on the following assumptions;

i. The process operates at steady state
ii. The system is assumed to be ideal for both the liquid mixture and Stages
iii. There is constant molar overflow (i.e. the flow of liquid or vapour in each section of the column does not vary from tray to tray)
iv. The multicomponent Crude Oil mixture was assumed to be decomposed according to the scheme in Figure 4.

2.1 Material Balance Equation

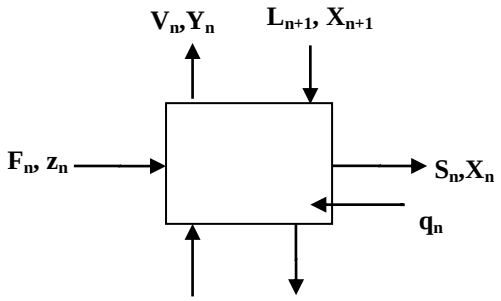

Figure 1: Material Balance on Stage (n)

The general material and component balances across Stage (n) depicted in Figure 1 above are given by Equation (1) and (2), Richardson et al. (2002):

$$F_n + V_{n-1} + L_{n+1} = V_n + L_n S_n \quad (1)$$

$$F_n Z_{i,n} + V_{n-1} Y_{i,n-1} + L_{n+1} X_{i,n+1} = V_n Y_{i,n} + L_n X_{i,n} + S_n X_{i,n} \quad (2)$$

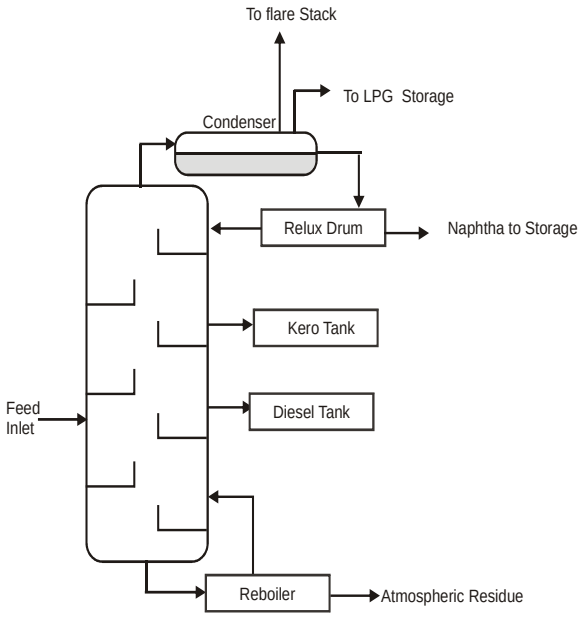

Figure 2: Schematic Diagram Distillation Column

Applying Equations (1) and (2) to the rectifying section of Figure 2 gives Equation (3) and (4) respectively;

$$V_n = L_{n+1} + D \quad (3)$$

$$V_n Y_n = L_{n+1} X_{n+1} + D X_d \quad (4)$$

But by assumption of molar overflow,

$$L_n = L_{n+1} \quad (5)$$

Equation (4) becomes;

$$Y_n = \frac{L_n}{V_n} X_{n+1} + \frac{D X_d}{V_n} \quad (6)$$

Similarly for the stripping section;

$$L_m = V_m + B \quad (7)$$

$$V_m Y_m = L_{m+1} X_{m+1} - B X_B \quad (8)$$

$$L_m = L_{m+1} \quad (9)$$

$$Y_m = \frac{L_m}{V_m} X_{m+1} - \frac{B X_B}{V_m} \quad (10)$$

Equations (6) and (10) are the top and bottom Operating Lines for construction of the McCaby – Thiele graph. However this is only possible with the help of an Equilibrium Curve which defines the vapour – liquid equilibrium of the system.

2.2 Equilibrium Equation

An ideal mixture maintains equilibrium between the liquid and vapour phases (Raoult's Law) as assumed in this process. Thus;

$$Y_n = K_n X_n \quad (11)$$

2.3 Summations Equation

$$\sum X_n = \sum Y_n = 1.0 \quad (12)$$

The Equilibrium Curve given in Equation (13) below results from algebraic manipulation of Equation (11) and (12), Kister (1990):

$$Y = \frac{\alpha X}{1 + (\alpha - 1)X} \qquad (13)$$

2.2 Heat Balance Equation

$$V_{\boldsymbol{n}}H_{i,n} + F_nH_{i,f} + Q_n = L_{n+1}H_{\boldsymbol{i},n+1} + S_nH_{i,n} \qquad (14)$$

The assumption of constant molar overflow eliminates the heat balance from the MESH equations.

3.0 SOLUTION METHODS

The relevance of this work lies in the solution method which decomposes the multicomponent Crude Oil mixture into binary systems for easy application of the McCabe – Thiele's graphical method. Two approaches are adopted here. First, the Crude is taken as a binary mixture of Naphtha and the rest fractions (as Residue) and second, is the Liebmann's decomposition model (Kister, 1992) which first 'binarilize' the Crude Oil into two components. Each of the two components are further separated thereby giving four products: Naphtha, Kerosene, Diesel and Atmospheric Residue.

i. **Naphtha and Rest Fractions (Model 1)**

The Crude Oil feed under Model 1 is assumed to be a binary mixture of Naphtha (component 1) and the rest fractions (component 2), thereby leading to a pure mono – product in Naphtha as shown in Figure 3.

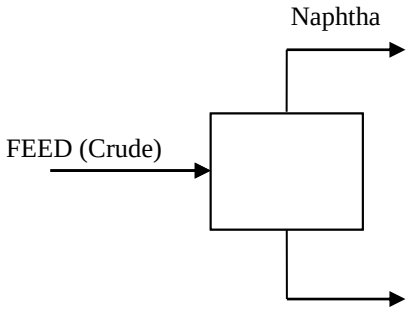

Figure 3: Block Flow Diagram of Naphtha as Mono-product

ii. **Decomposition into Two Binary System (Model 2)**

The second model assumes decomposition of the Crude Oil feed according to the scheme in Figure 4 below as proposed by Liebmann. The foregoing enables the application of the McCaby - Thiele's method to this multicomponent system. The number of Stages is the sum of the number of Stages of Column 2 and 3.

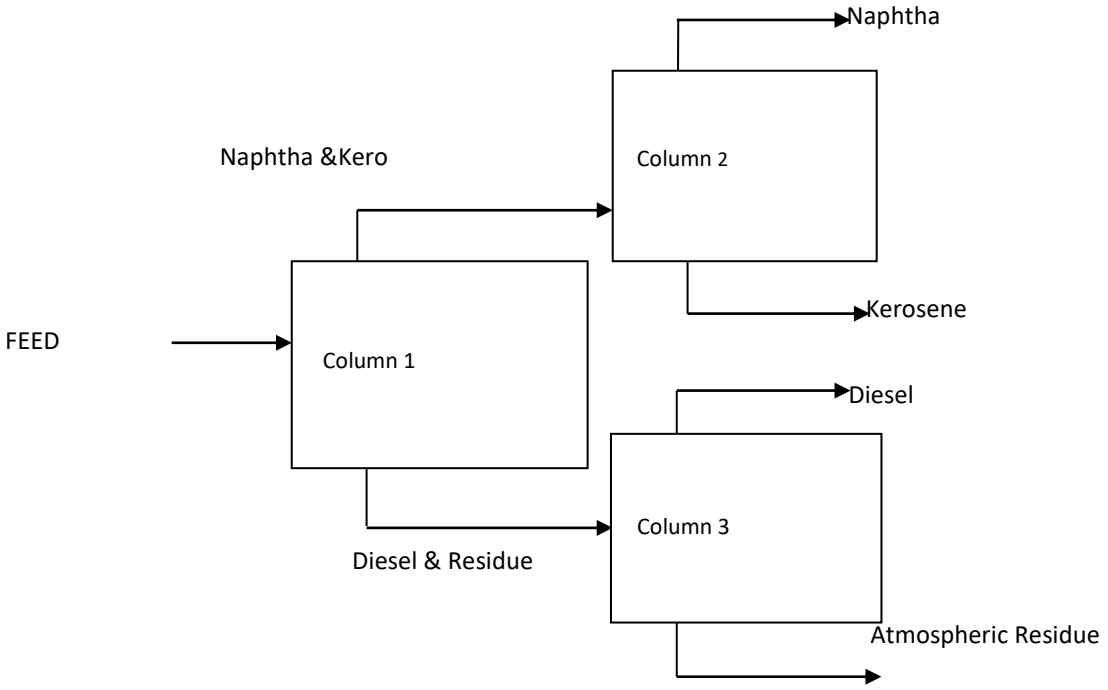

Figure 4: Block Flow Diagram for four Product

4.0 RESULTS AND DISCUSSION

Computations in the work were based on Crude Assay data from the Port Harcourt Refinery given in Table 1. as presented in the work of Akpa and Umuze (2013). A 90% product rate (or feed conversion) was assumed while Crude Oil fed into the Column was assumed to be at two conditions: either as vapour orliquid allat

Table 1: Feed Composition and Equilibrium Data for Computations

FEED COMPONENT	MOLE FRACTION	K-VALUES
Naphtha	0.26	1.4
Kerosene	0.139	0.44
Diesel	0.289	0.39
Residue	0.312	0.13

4.1 Number of Stages for CDU (Model 1)

Figure 5 shows the McCabe – Thiele's graph for Model 1 where Crude Oil is separated into only two fractions: Naphtha (as single product) and the Rest Fractions (as Residue). The separation is carried out at a reflux ratio (R = 1), with Crude fed into the Column as saturated vapour. From the graph, the top and bottom operating lines did not intersect within the equilibrium curve thereby making it impossible to determine the number of stages for CDU. This simply implies that separation of the Crude by Model 1 under the conditions specified is impossible.

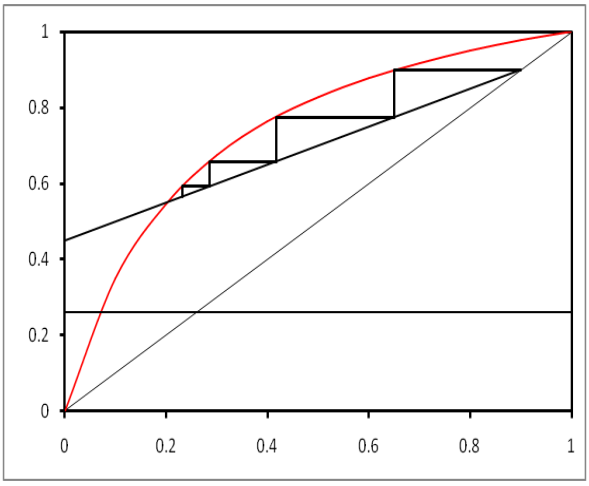

Figure 5: Number of Stages for Separation of Naphtha at q = 0 and R = 1

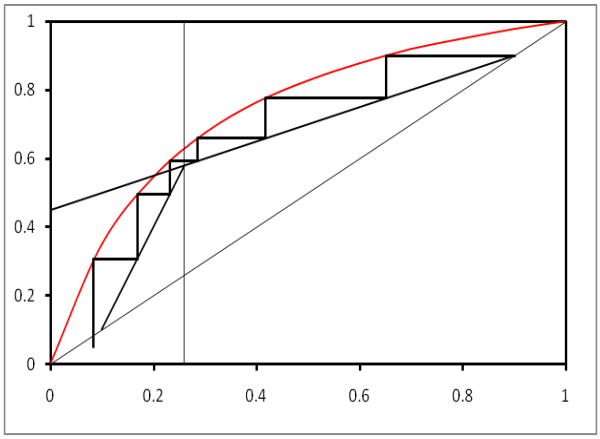

Figure 6: Number of Stages for Separation of Naphtha at q=1 and R=1

On the contrary, when Crude is fed as saturated liquid, Model 1 gives a perfect McCabe – Thiele's graph having a total of six (6) theoretical stages for separation of Naphtha as mono-product as shown in Figure 6.

4.2 Number of Stages for CDU (Model 2)

The decomposition model gives a total of six McCaby - Thiele's graphs for the two feed conditions (saturated vapour and saturated liquid) at reflux ratio (R = 1). The first Column (designated Column 1) separates the Crude into two bulk fractions: Naphtha and Kerosene (as one fraction) and Diesel and Residue (as another fraction). The second Column (Column 2) thereafter separates the top bulk fraction into Naphtha and Kerosene, while Column 3 separates the bottom bulk fraction into Diesel and Residue. Table 2 gives the number of theoretical stages required using the two Models at different feed conditions and a reflux ratio (R = 1).

Table 2: Number of theoretical Stages at Different Feed Conditions (R = 1)

Model Type		Model 2	
		Column 2	Column 3
q = 0	*Impossible	6	*Impossible
q = 1	6	5	7

**Impossible – represents impossible separation of fractions*

Results of the decomposition model (Model 2) show that Column 2 has six (6) Stages (see Figure 7) while intersection of the two Operating Lines is outside the

Equilibrium Curve in Column 3 (see Figure 8), therefore indicating impossible separation of the bottom bulk fraction into Diesel and Residue with feed as saturated vapour.

On the other hand, when feed is saturated liquid, five (5) and seven (7) Theoretical Stages are required to effect separation in Column 2 and Column 3 as shown in Figure 9 and Figure 10 respectively. The foregoing implies that a total of twelve (12) Theoretical Stages would be required for separation of the four products under these conditions using the decomposition model. This result is in good agreement with ASPEN HYSYS (version 8.6) simulation data for the same system which gave fifteen Actual Stages.

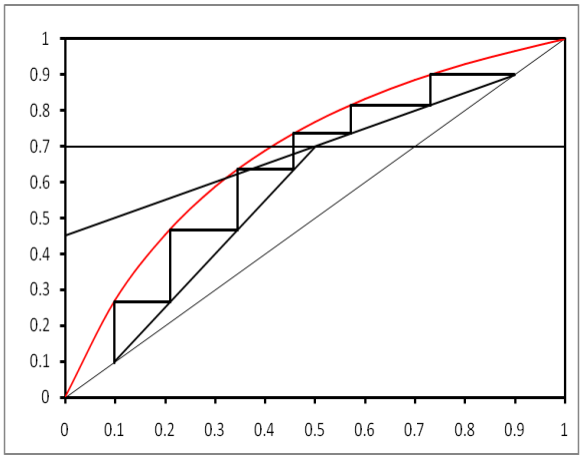

Figure 7: Number of Stages of Column 2 at saturated vapour for R=1

Important to note is the fact that at the reflux ratio (R = 1), separation of Crude Oil by Model 1 or Model 2 is not possible when the feed is saturated vapour. Feed therefore should be maintained at boiling point of Crude for successful operation. This result is in line with limitations of the McCaby - Thiele's graphical method which has better accuracy for simple mixtures such as binary mixtures and not multicomponent mixtures.

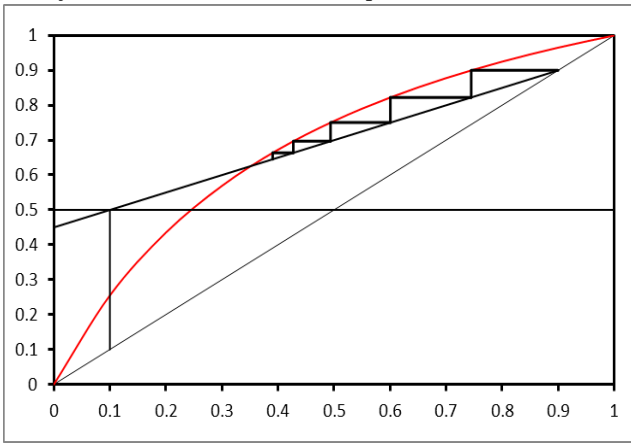

Figure 8: Number of Stages of Column 3 at saturated vapour for R=1

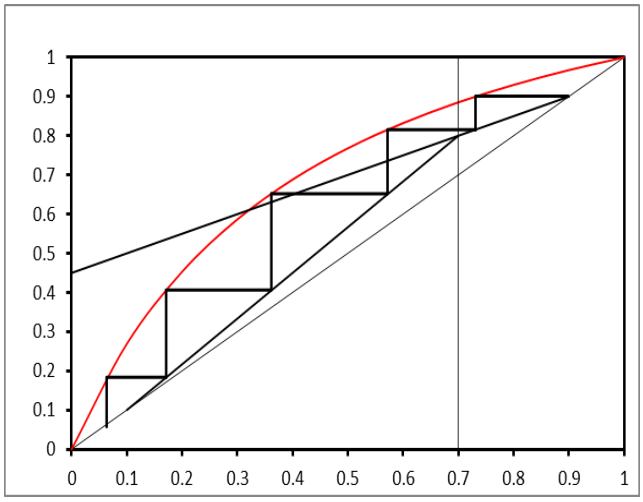

Figure 9: Number of Stages of column 2 at saturated liquid for R=1

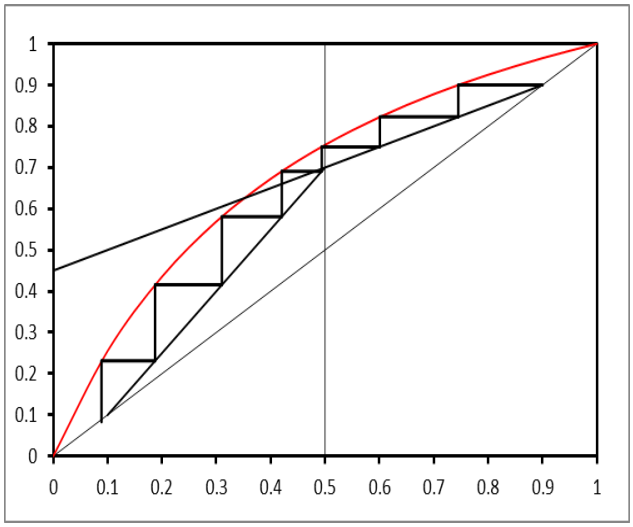

Figure 10: Number of Stages of Column 3 at saturated liquid for R=1

4.3 Effect of Reflux Ratio on the Number of Stages

Figure 11shows the relationship between reflux ratio and the number of Stages. Reflux (R) increases with decrease in the number of Stages for both the saturated vapour and saturated liquid conditions of the feed. This is consistent with theoretical principles of fractionation where at total reflux, the Column requires a minimum number of Stages to effect separation and vice versa Richardson et al. (2002).

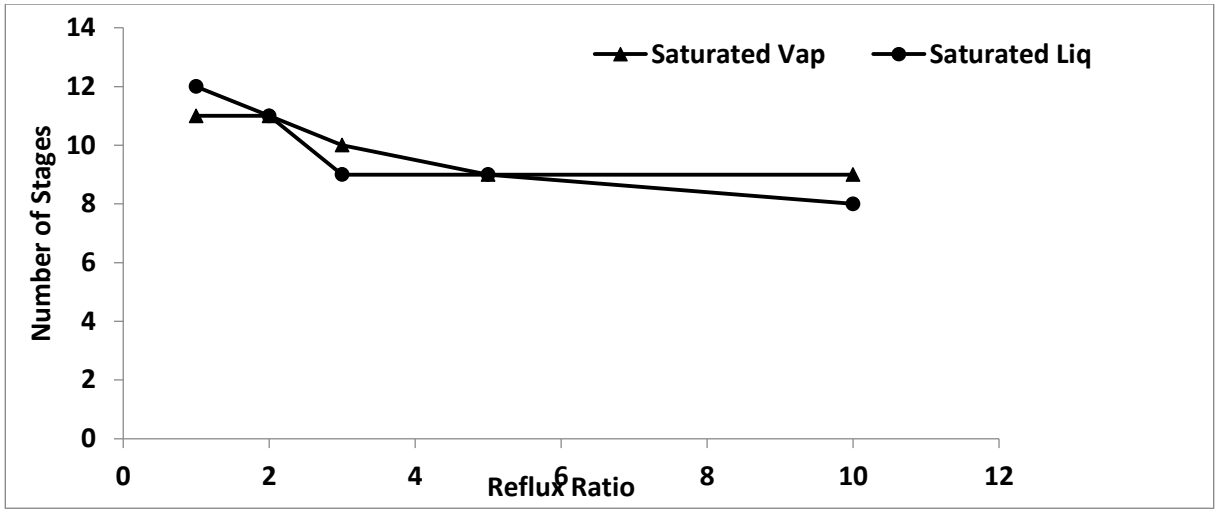

Figure 11: Effect of Reflux Ratio on Number of Stages

4.4 Column Diameter

Column performance largely depends on its diameter, thus proper sizing is central to effective distillation operations. At a vapour velocity of 0.09m/s, tray spacing was optimum at 0.25m and at Column diameter of 0.41m shown in Figure 12.

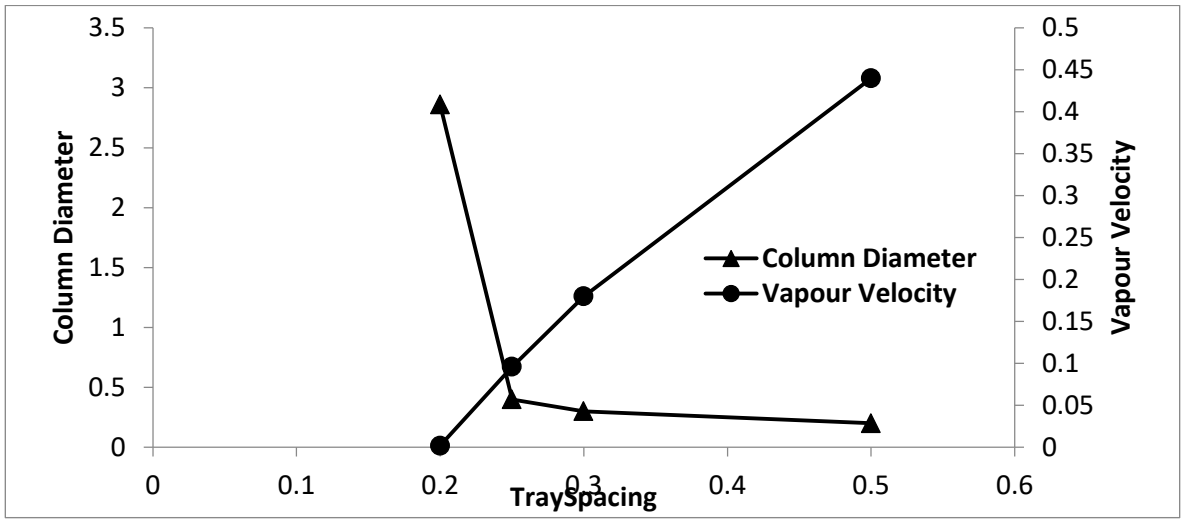

Figure 12: Effect of Tray Spacing on Column Diameter

5.0 CONCLUSION

The work demonstrated the utility of the decomposition model as an analytical tool for multicomponent distillation by application of the McCaby – Thiele's method as exemplified with Crude Oil distillation. The decomposition method thus presents a ready alternative with lesser computational time and effort as is the case with the rigorous models for distillation analysis and design.

Specifically, using the number of theoretical Stages as basis, the model compared quite well with the more exact solutions by computer simulation (ASPEN HYSYS, V.8.6). Also important to note from the work is the impossible separation of Naphtha from Crude Oil as a monoproduct when the feed is a saturated vapour for reflux ratio (R = 1). Similarly, it is generally observed that the decomposition model favours feed condition as saturated liquid at this reflux ratio.

Notations

R	**Re**flux ratio
V_n	Vapor flow rate from stage n
V_{n+1}	Vapor flow rate from stage n+1

$Z_{i,n}$	Mole fraction of component i in the feed stream at stage n
$Y_{i,n.}$	Mole fraction of component I in vapor at stage (n)
$Y_{i,n+1}$	Mole fraction of component i in vapor at stage n+1
$L_{n.}$	Liquid floe rate from stage n
$X_{i,n}$	Mole fraction of component i in liquid at stage (n)
S_n	Side stream from stage n
$X_{i,n-1}$	Mole fraction of component i in the liquid at stage n-1
L_{n-1}	Mole flow rate of liquid at stage n-1
$K_{i,n}$	K-value of component i
Σ	Summation
$H_{i,n-1}$	Enthalpy of component i at stage n-1
$H_{i,f}$	Enthalpy of component i in the feed
Q_n	Heat flow into or removed from stage n
$H_{i,}$	Enthalpy of component i at stage n
F	Feed flow rate
D	Distillate (top product) flow rate
B	Flow rate of bottom product
X_f	Mole fraction of feed
X_d	Mole fraction of distillate
X_b	Mole fraction of bottom product
V_m	Vapor mole flow rate in bottom section
L_m	Liquid mole flow rate at the bottom section
K_1	K-value of naphtha and kerosene
K_2	K-value of diesel and residue
K_3	K-value of kerosene and diesel
K_4	K-value of kerosene and diesel in column 3
K_{13}	K-value of kerosene, diesel and residue
K	K-value of residue only
α	Relative volatility
P	Pressure of gas
R	Gas rate constant
V	Volume of gas
T	Temperature of gas

REFERENCES

Akpa, J. G. and Umuze, O. D. (2013), Simulation of a Multicomponent Distillation Column, *American Journal of Scientific Research*© 2013, Science Huβ, http://www.scihub.org/AJSIR ISSN: 2153-649X, doi:10.5251/ajsir.2013.4.4.366.377, accessed February 10, 2019

Chaudhuri, U. R. (2011), *Fundamentals of Petroleum and Petrochemical Engineering*, CRC Press, Boca Baton, pp.9

Fair, J. R. (1983), *AIChE Symposium Series*, Vol. 79, pp. 239

Hengstebeck, R. J. (1939), *Transactions of American Institute of Chemical Engineers*, Vol. 35,pp. 635
Jenny, P. J. (1946), *Transactions of American Institute of Chemical Engineers*, Vol. 42, pp. 309

Kister, H. Z. (1990), *Distillation Operations*, McGraw Hill, New York

Kister, H. Z. (1992), *Distillation Design*,McGraw Hill, New York

Maples, R. E. (2000), *Petroleum Process Refining Economics*, PennWell Books,

Richardson, J. F., Harker, J. H., Backhurst, J. R. (2002),*Particle Technology and Separation Processes*, Vol.2, Sixth Edition, Coulson and Richardson's Chemical Engineering Series, Butterworth-Heinemann, Oxford, pp.540 – 570

Shankar, N., Aneesh, V. and Sivasubramanim, V. (2015), Aspen Hysys Based Simulation and Analysis of Crude Distillation Unit, *Department of Chemical Engineering, NIT Calicut*.

Yasin, G., Bhanger, M.I., Ansari, T.M Muhammad, S., Naqvi, S. R., Ashraf, M., Ahmad, K., and Farah NazTalpur, F.N. (2013), Quality and Chemistry of Crude Oils, *Journal of Petroleum Technology and Alternative Fuels* ,Vol. 4(3), pp.53 - 63

NONLINEAR RECYCLE COMPENSATOR

***Taiwo, O., Kolawole, K. and Bamimore, A.**
PSE Laboratory, Dept. of Chemical engineering, Obafemi Awolowo University, Ile-Ife, Nigeria.
*Email of the Corresponding author: ftaiwo@oauife.edu.ng, femtaiwo@yahoo.com

ABSTRACT

A nonlinear recycle compensator, which is applicable to both single-variable and multivariable nonlinear systems with recycle is derived. As opposed to the already formulated and widely used linear recycle compensator which involves linearizing the recycled state variable about nominal operating values, the nonlinear recycle compensator is derived from the nonlinear equations. Its implementation thus ensures exact compensation for detrimental recycle effects over the full operating window when compared to the linear recycle compensator, as has been borne out in simulations and experimental data emanating from this work.

***Keywords**: Nonlinear Recycle compensator; nonlinear systems.*

1. INTRODUCTION

The introduction of material and energy recycle is a common phenomenon in the process industries because steady state economics usually favour such operation, facilitating an efficient use of material and energy. The need to concentrate a desired product stream by purging a percentage to be recycled, or the need to save energy cost by recycling waste steam to be used in heat integration processes are all typical examples of common recycle operations. While this creates an avenue where more desired product is formed and obtained, yielding positive fiscal returns in monetary terms, it however, may result in poor process characteristics leading to difficulty in control.

The idea of a recycle compensator (RC) was proposed by Taiwo (1985, 1993) Taiwo and Krebs (1996) for the effective control of processes with recycle. It's effectiveness has been widely demonstrated by other researchers Armbrust and Shabaro (2010), Scali and Ferrari (1999), Mezaros, et al. (2005), Tremblay, et al. (2010), Lakshimarayan and Takada (2001).

However, for systems with nonlinear recycle dynamics, the linear recycle compensator will be most effective at and close to the nominal operating point and may not be particularly effective at operating conditions far from the nominal. Hence this work introduces the nonlinear recycle compensator which, due to its exact representation, removes the detrimental effects of recycle at all operating points.

The problem formulation is given in section 2, section 3 presents two illustrative examples. The work then ends with a discussion and conclusion section.

2. THE NONLINEAR RECYCLE COMPENSATOR

Consider the open loop block diagram of a nonlinear system with recycle as shown in Figure 1, where y, u and d are controlled, manipulated and disturbance variables respectively.

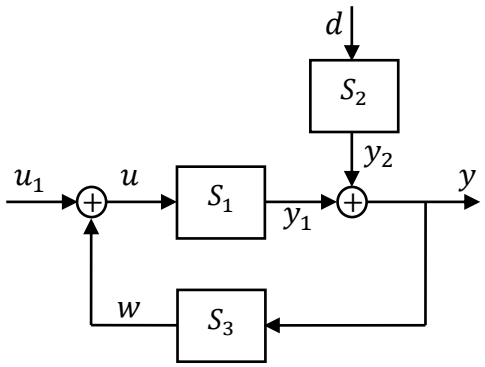

Figure 1: Open loop block diagram of a nonlinear plant with recycle

The forward path process (S_1) is given by:

$$\dot{x}(t) = f_p(x(t), u(t), t) \quad (1)$$

$$y_1 = g_p(x(t), u(t), t) \quad (2)$$

The disturbance process (S_2) is given by:

$$\dot{x}(t) = f_d(x(t), d(t), t) \quad (3)$$

$$y_2 = g_d(x(t), d(t), t) \quad (4)$$

The recycle process (S_3) is given by:

$$\dot{x}(t) = f_r(x(t), y(t), t) \quad (5)$$

$$w(t) = g_r(x(t), y(t), t) \quad (6)$$

where x, u and d are respectively the state, input and disturbance vectors, y is the output vector while f_p, g_p, f_d, g_d, f_r, g_r are nonlinear functions. We note that

$$y = y_1 + y_2 \quad (7)$$

while

$$u(t) = u_1(t) + w(t) \quad (8)$$

Without loss of generality, the recycle compensator may be specified as (5) and (6) which would make its output to be $w(t)$ as given in Figure 2. Hence $u_1(t)$ is given by $u_a(t) - w(t)$ and finally

$$u(t) = u_a(t) - w(t) + w(t) = u_a(t) \quad (9)$$

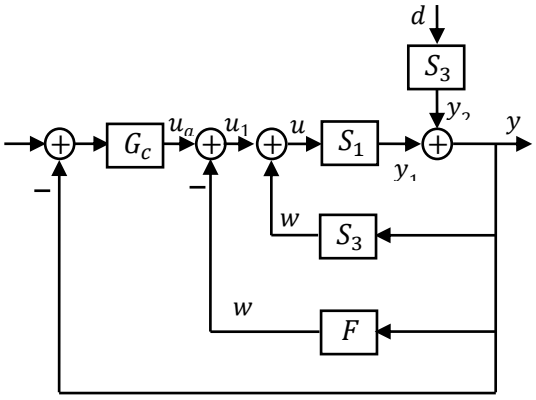

Figure 2: General structure of a nonlinear recycle system with nonlinear recycle compensator (*F*) and feedback controller $G_c(s)$

Consequently, this specification of $F = S_3$ produced an overall system which has perfectly compensated for the detrimental effects of recycle because the input to the plant is only the controller output just like the case of a process without recycle. Observe by looking at Figures 1 and 2 that without the compensator, the overall input to the forward process is given by $u(t) = u_1(t) + w(t)$ whereas with the introduction of the recycle compensator the input to the forward process $u(t)$ is given by $u_a(t)$, thus demonstrating that the recycle compensator has completely eliminated the detrimental effects of the recycle represented by $w(t)$ from the overall feedback system. Its superiority over the linear compensator is that it eliminates recycle effects at all operating points. Its implementation is straightforward, being only a programming effort. It is also assured to be implementable as S_3 is a physical system.

3. ILLUSTRATIVE EXAMPLES

3.1 Example 1: Three- tank system with recycle

Consider the three-tank system housed in the Process Laboratory of the Chemical Engineering Department, Obafemi Awolowo University, Ile-Ife. The details of the equipment can be found in (Amira, 2002) and (Bamimore, *et al*., 2012). The original system was modified to incorporate a recycle stream from tank 2 to tank1. The schematic diagram is shown in Figure 3. It is a two-input, tow-output process in which the controlled variables are the tank levels, and the manipulated variables are the volumetric flow rates delivered by the two pumps. The water level in tank 3 is observed but not controlled. The case with recycle ratio, $r = q_r/q_o = 0.5$ is considered.

$$\frac{dh_1}{dt} = \frac{1}{A_c}\left[q_1 + \mu_2.r.S_p.\sqrt{2gh_2} - \mu_1.S_p.sgn(h_1 - h_3).\sqrt{2g|h_1 - h_3|}\right] \quad (10)$$

$$\frac{dh_2}{dt} = \frac{1}{A_c}\left[q_2 + \mu_3.S_p.sgn(h_3 - h_2).\sqrt{2g|h_3 - h_2|} - \mu_2.(r+1).S_p.\sqrt{2gh_2}\right] \quad (11)$$

$$\frac{dh_3}{dt} = \frac{1}{A_c}\left[\mu_1.S_p.sgn(h_1 - h_3).\sqrt{2g|h_1 - h_3|} - \mu_3.S_p.sgn(h_3 - h_2).\sqrt{2g|h_3 - h_2|}\right] \quad (12)$$

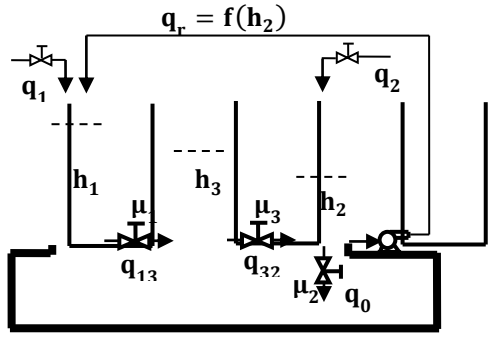

Figure 3: Experimental three tank system with recycle

The process parameters are given as:
A_c = 149 cm^2, S_p = 0.5 cm^2 , g = 981 cm^2/sec, μ_1 = 0.4926, μ_2 = 0.8452, μ_3= 04926, q_1 = 6 cm^3/sec, q_2 = 66.5 cm^3/sec.

Notice here that the recycle flowrate is given by

$$q_r(t) = \mu_2.r.S_p.\sqrt{2g} \times \sqrt{h_2} \quad (13)$$

Consequently

$$F(t) = \begin{bmatrix} 0 & \mu_2.r.S_p.\sqrt{2g} \\ 0 & 0 \end{bmatrix} \begin{bmatrix} \sqrt{h_1(t)} \\ \sqrt{h_2(t)} \end{bmatrix} \quad (14)$$

Equivalently, $F_1(t) = \mu_2 . r . S_p . \sqrt{2gh_2(t)}, F_2(t) = 0.$ This has been shown in Figure 2.

It is easily verifiable that $g_1(s)$ is diagonally dominant. Hence, designing feedback controllers using the principal diagonal elements would give a stable closed loop system (Rosenbrock, 1974). With filter parameter selected as 40, IMC-PI theory produced the following effective controllers:

$$G_C = \begin{bmatrix} 5.04 + \dfrac{0.0148}{s} & 0 \\ 0 & 7.699 + \dfrac{0.0906}{s} \end{bmatrix} \quad (15)$$

The responses of the recycle compensated feedback systems depict that the nonlinear recycle compensator produced an overall superior system than that of the linear recycle compensated system. The reader can consult our earlier work (Taiwo, *et al*. 2014) for details of the linear recycle compensator design. It should be noted that the simulation of the plant with both Linear and Nonlinear recycle compensators when the recycle ratio (r) is between $0.1 - 0.4$ gave similar responses. However, at $r = 0.5$, the model with the nonlinear recycle compensator gave a response with better set-point tracking and disturbance rejection as shown in Figure 4. As recycle ratio increases, nonlinearity in the overall plant dynamics increases as turbulence is greatly increased. The flow dynamics is more turbulent, hence the nonlinear recycle compensator is better able to control the system in this flow regime.

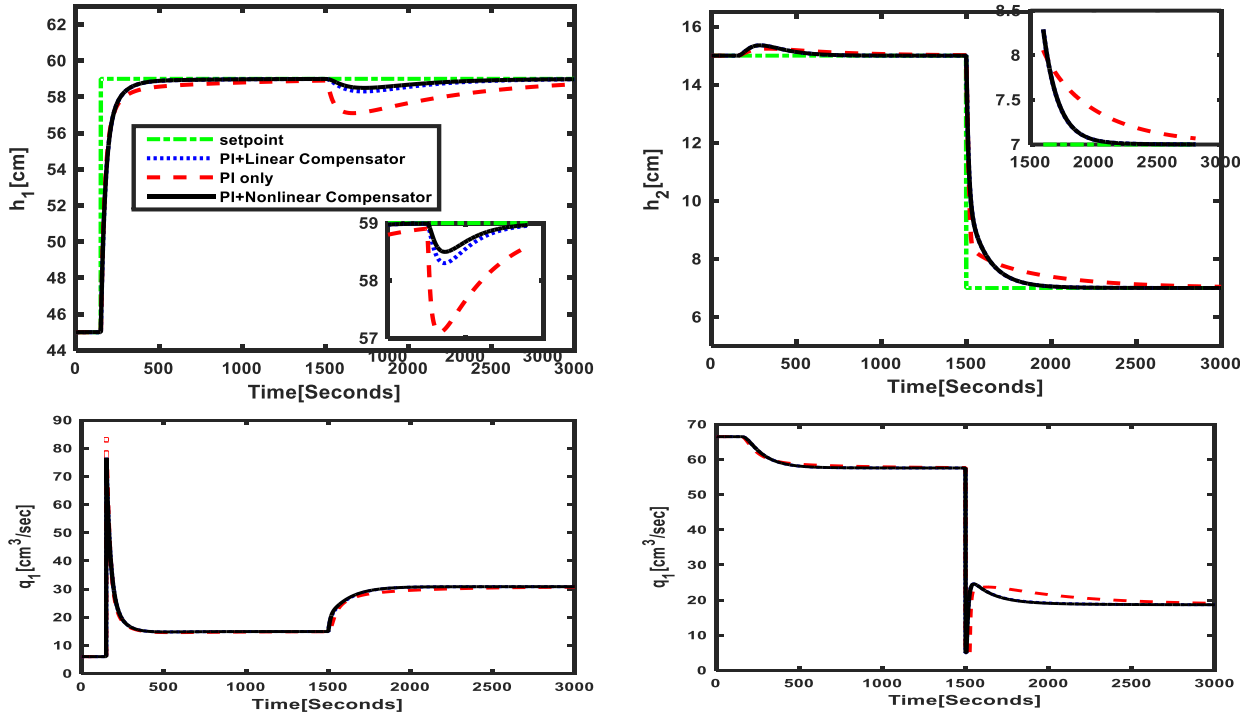

Figure 4: Comparison of closed loop response of tank 1 to a $+15$cm step at t=100s and tank 2 to a -10cm step at t=1500s.

3.2 Example 2: Heat Integrated Ammonia Production Plant

Morud and Skogestad (1998) in the analysis of instabiility of an industrial ammonia reactor reported an incident in an industrial fixed-bed reactor for the production of ammonia in Germany, whereby after a sudden decrease in reactor pressure, the reactor became unstable and the temperature oscillated with large amplitudes (limit cycles). The layout of the plant is shown in Figure 5 and a comparative analysis of the nonlinear compensated, linear compensated and uncompensated (original) system model is made.

3.2.1 Simplified model of heat integrated fixed-bed reactor (G_{rxn})

It consists of three beds in series with fresh feed quenching between each bed and preheating of the feed with the effluent. The reaction is as described below:

$$N_2 + 3H_2 = 2NH_3 \quad (16)$$

Ammonia and temperature distribution across the bed of reactor are modelled using partial differential equations:

$$w\frac{\partial c}{\partial z} = m_c r(T, c) \quad (17)$$

where c = Ammonia concentration (mass fraction), z = position in the reactor, m_c = catalyst mass in the bed, w= gas flow through the bed, r(T,c) = reaction rate,
The temperature distribution across the whole length of the fixed bed reactor is given by:

$$m_c C_{pc}\frac{\partial T}{\partial t} + wC_{pg}\frac{\partial T}{\partial z} = (-\Delta H_{rx})m_c r(T,c) + \Gamma m_c C_{pc}\frac{\partial^2 T}{\partial z^2} \quad (18)$$

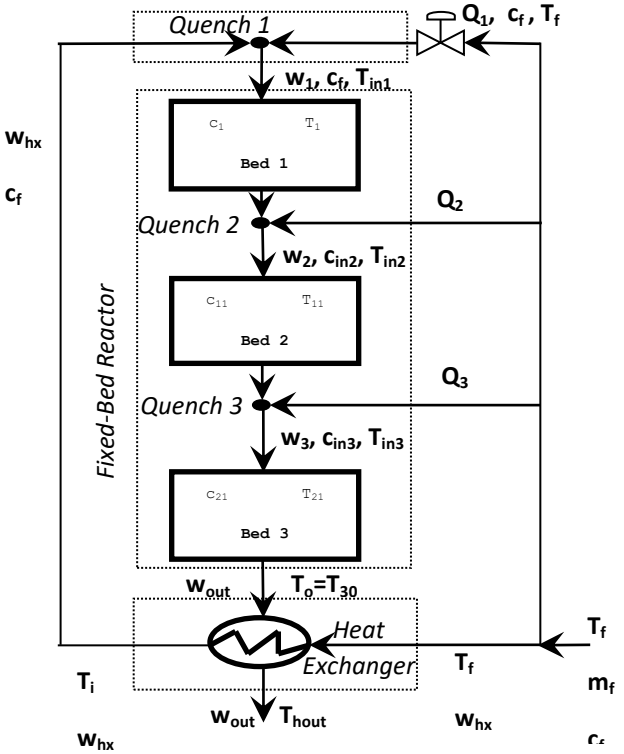

Figure 5: Fixed bed Reactor Diagrammatic representation

where t=Time, T = catalyst particle temperature, C_{pc} = heat capacity of catalyst, C_{pg} = heat capacity of gas, Γ = Dispersion coefficient. Detailed information about the process as well as list of assumptions made can be found in Bamimore and Taiwo (2017); Morud (1995). The solution approach to these models is to discretize using the finite difference method. By approximating the partial derivative $\frac{\partial c}{\partial z}$ by its finite difference approximation, we have:

$$\frac{\partial c}{\partial z} = \frac{c_j - c_{j-1}}{\Delta z} \quad (19)$$

where j is the grid point. Eqn. (17) can be written as (taking $\Delta z = 1$)

$$c_j = c_{j-1} + \frac{m_{c,j}}{w} r(T_j, c_j) \quad (20a)$$

However, for programming simplicity we approximate Eqn. (20a) further to:

$$c_j = c_{j-1} + \frac{m_{c,j}}{w} r(T_j, c_{j-1}) \quad (20b)$$

By also approximating the partial derivative $\frac{\partial T}{\partial z}$ by its finite difference approximation, we have:

$$\frac{\partial T}{\partial z} = \frac{T_j - T_{j-1}}{\Delta z} \quad (21)$$

By neglecting the diffusion term in Eqn. (18), we have:

$$m_{c,j} C_{pc}\frac{dT_j}{dt} = wC_{pg}(T_{j-1} - T_j) + m_{c,j} r(T_j, c_{j-1})(-\Delta H_{rx}) \quad (22)$$

The reaction rate is thus given by:
$r = r_{N_2}.(2 \times 17)/\rho_{cat}$
where:

$$r_{N_2} = (k_1 \frac{p_{N_2}.{p_{H_2}}^{1.5}}{p_{NH_3}} - k_{-1}\frac{p_{NH_3}}{{p_{H_2}}^{1.5}})$$

The p_i denotes the partial pressure of component I (in bar);

$p_{NH_3} = xP, p_{N_2} = (1-x) \times 0.25 \times P$

$p_{H_2} = (1-x) \times 0.75 \times P$

$x = \frac{n_{NH_3}}{(n_{NH_3}+n_{N_2}+n_{H_2})}$, $n_{NH_3} = \frac{m_{NH_3}}{17}$, $n_{N_2} = \frac{m_{N_2}}{28}$, $n_{H_2} = \frac{m_{H_2}}{2}$

$m_{NH_3} = c$, $m_{N_2} = (1-c) \times (28/34)$,

$m_{H_2} = (1-c) \times (6/34)$

$k_1{}^0 = 1.79 \times 10^4 \exp(-\frac{87090}{RT})$

$k_{-1}{}^0 = 2.57 \times 10^{16} \exp(-\frac{198464}{RT})$

In order to match the industrial data, the reaction kinetics were multiplied by a factor $f = 4.75$. Thus, $k_1 = f k_1{}^0$ and $k_{-1} = f k_{-1}{}^0$.
The mass of each bed is calculated as follows:

$$m_c(bed_i) = (Volume\ of\ bed\ i) \times \rho_c \quad (23)$$

3.2.2 Simplified model of preheater (G_{pre})

The preheater is modelled as a standard countercurrent heat exchanger (without dynamics for simplicity), which yields:

$$T_i = \epsilon T_0 + (1-\epsilon)T_f \quad (24)$$

where T_i is the preheater outlet (reactor inlet) temperature, T_0 is the reactor outlet temperature and $\epsilon \in [0\ 1]$ is a constant independent of temperature.

3.2.3 Mathematical model of quench points

The mixing of streams at the quench points were modelled as:

$$T_{mix} = \frac{w_F}{w_F + w_Q} T_F + \frac{w_Q}{w_F + w_Q} T_Q \quad (25)$$

$$c_{mix} = \frac{w_F}{w_F + w_Q} c_F + \frac{w_Q}{w_F + w_Q} c_Q \quad (26)$$

where w denotes the stream flow rate, subscripts F and Q denote the feed and quench points respectively. The equation for calculating the inlet temperature (T_{in1}) to the first reactor is obtained by taking energy balance at the mixing point before the first reactor (quench point 1), which is obtained as:

$$T_{in1}(t) = \frac{w_{hx}}{w_{hx} + Q_1} T_1(t) + \frac{Q}{w_{hx} + Q_1} T_f(t) \quad (27)$$

Table1. Process Nominal Operating Parameters

Feed flow rate	w_f	70 kg/s
Feed temperature	T_f	250^0C
Feed mass fraction	c_f	0.08
Mass flow rate through preheater	w_{hx}	35.28 kg/s
Quench bed 1	Q_1	16.11 kg/s
Quench bed 2	Q_2	9.72 kg/s
Quench bed 3	Q_3	8.89 kg/s
Reactor Pressure	P	200

3.2.4 Nonlinear Recycle Compensator

The implementation of the proposed recycle compensator is shown in Figure 6.

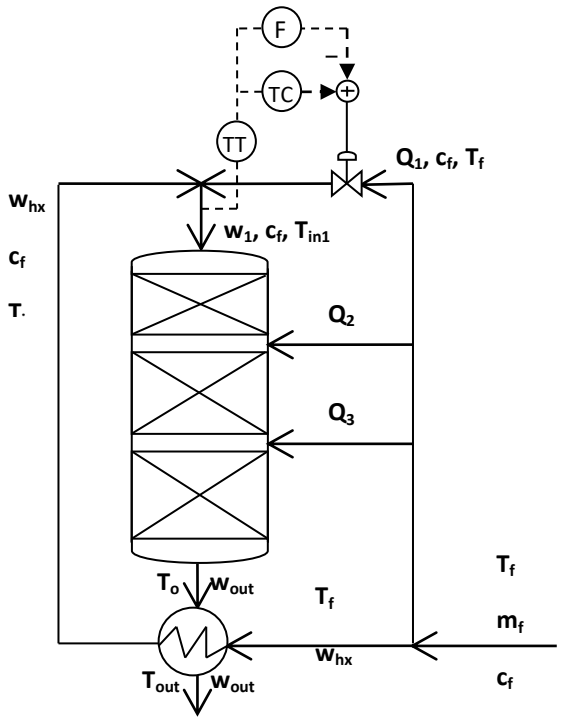

Figure 6: Nonlinear Recycle compensator scheme forr the control of Heat integrated Catalytic Reactor

The heat exchanger (preheater) and the reactor are all in the recycle path, while the energy balance around quench bed 1 is the forward path dynamic. The nonlinear recycle compensator that will restore the dynamically unfavourable recycle system to a heat integrated system appearing without recycle is thus given as:

$$F = S_3\big(T(t), T_{in1}(t), T_f(t), t\big) \quad (28)$$

where S_3 comprises all differential equations in the recycle path. This includes the heat exchanger (preheater), mixing point and the reactor.

3.2.5 Feedback controller design for the Uncompensated system

The uncompensated system is modelled by a complex quasi-rational transfer function. An integral only controller is able to stabilize the closed loop system, which is tuned as:

$$g_{c,uncomp} = -\frac{0.01}{s} \quad (29)$$

3.2.6 Feedback controller design for the Compensated system

Upon application of the recycle compensator, the system model becomes the model of the plant in the forward path only. This is given by $\frac{T_{in1}(s)}{Q_1(s)} = -2.2$. An integral only controller is able to stabilize the closed loop system. It is tuned as:

$$g_{c,comp} = -\frac{0.1}{s} \quad (30)$$

3.2.7 Simulation Result

The dynamic behaviours of both the open-loop and closed-loop systems were considered.

Figure 7 gives the open-loop response of the process variables to multiple step changes in the feed temperature T_f with both linear and nonlinear recycle compensators as well as without recycle compensator.

$$T_f(t) = \begin{Bmatrix} 250\,^0C; & 0 < t < 1000\ seconds \\ 230\,^0C; & 1000 < t < 4000\ seconds \\ 260\,^0C; & 4000 < t < 7000\ seconds \end{Bmatrix}$$

Figure 8 gives the open-loop response of the process variables to multiple step changes in the operating Pressure P with both linear and nonlinear recycle compensators as well as without recycle compensator.

$$P(t) = \begin{Bmatrix} 170\ bar; & 0 < t < 1200\ seconds \\ 150\ bar; & 1200 < t < 7200\ seconds \\ 220\ bar; & 7200 < t < 9000\ seconds \end{Bmatrix}$$

The closed loop response of the system with multiple step changes in feed temperature T_f and operating pressure P can be seen on Figure 9 and Figure10 respectively.

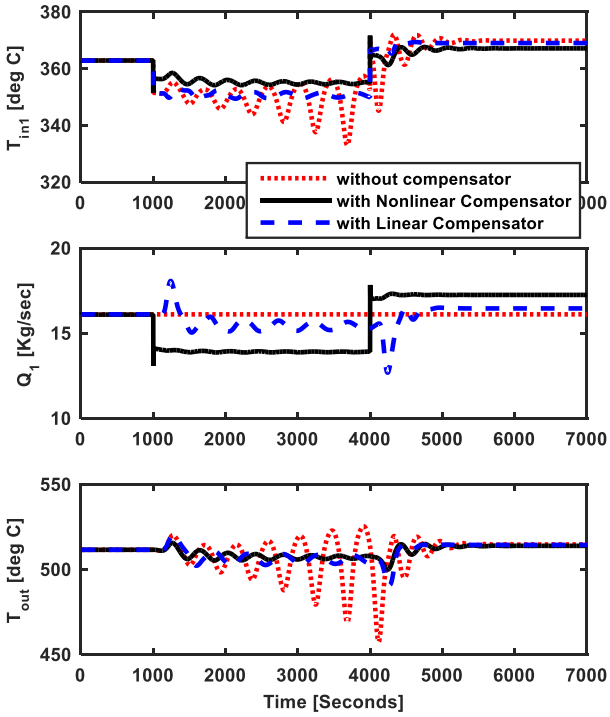

Figure 7: Open loop step response to multiple step changes in T_f [Legend: Thick line: With Nonlinear Compensator, dashed line: With Linear Compensator, dotted line: Without compensator]

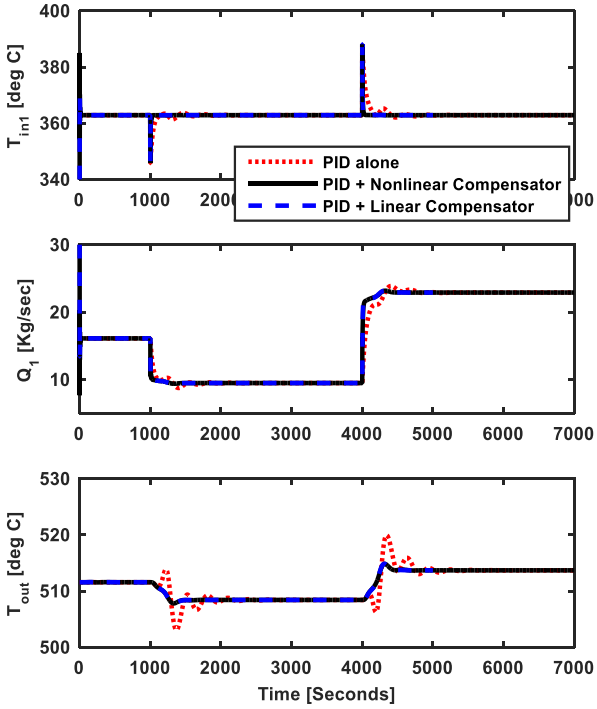

Figure 9: Closed loop step response to multiple step changes in T_f [Legend: Thick line: With Nonlinear Compensator, dashed line: With Linear Compensator, dotted line: Without compensator]

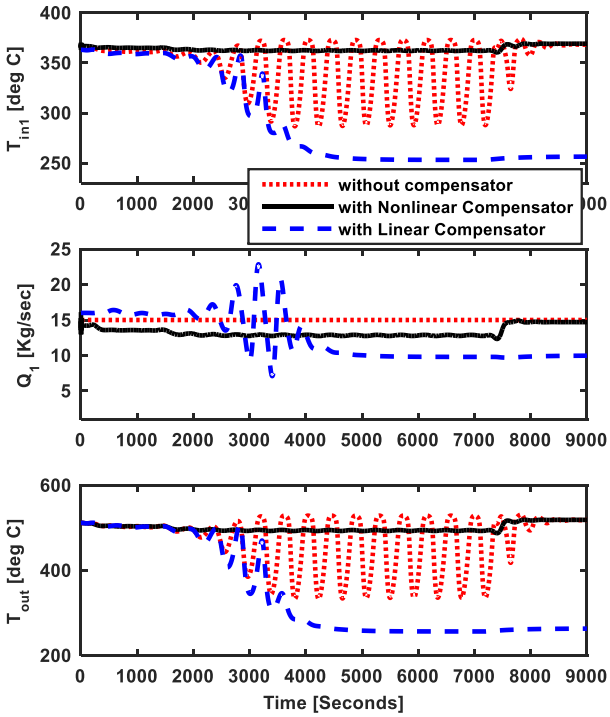

Figure 8: Open loop step response to multiple step changes in Pressure [Legend: Thick line: With Nonlinear Compensator, dashed line: With Linear Compensator, dotted line: Without compensator]

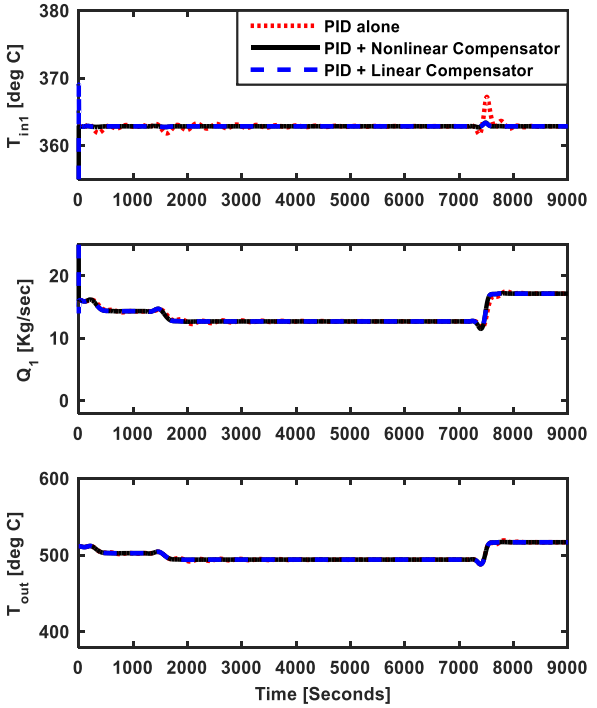

Figure 10: Closed loop step response to multiple step changes in Pressure [Legend: Thick line: With Nonlinear Compensator, dashed line: With Linear Compensator, dotted line: Without compensator]

It can be observed that while the uncompensated system model gave a response with lots of oscillations, both compensation techniques gave better response. With the linear recycle compensator giving minimal oscillations in some cases while the nonlinear recycle compensator gave a much less oscillation and no oscillations for many of the responses.

Hence, it can be concluded that the use of recycle compensator plus feedback controller was able to stabilize the plant with minimal oscillations. While the nonlinear recycle compensator is more suitable owing to the profound nonlinearity in the dynamics of the plant.

4 DISCUSSION AND CONCLUSION

This work has shown in great detail the design of the proposed nonlinear compensator, which makes use of the differential equation model of the recycle process, as opposed to its approximate Laplace domain transform expression. The result of this is a nonlinear recycle compensator that is able to better compensate for the effects of recycle at every operating point whether close or far from the nominal.

The work compared the simulation results of previous nonlinear systems compensated by the linear scheme to the ones simulated with the nonlinear recycle compensator.

As expected, results from processes using the nonlinear compensator compare favourably with those deploying the linear one.

5 REFERENCES

Amira. (2002). Laboratory setup three-tank system. Amira GmbH.

Armbrust, N., and Sbarbaro, O. (2010). On the Robust Tuning of Controllers with Recycle Compensators. *IFAC Symp. Syst. Struct. Control*, 211-217.

Bamimore, A., and Taiwo, O. (2015). Recycle Compensator facilitates rapid parameterization of proportional Integral/Derivative (PI/D) controllers for open-loop unstable recycle processes. *Industrial and Engineering chemistry research*, 5115-5127.

Bamimore, A. and Taiwo, O. (2017). Application of Taiwo's Recycle Compensator to an Heat Integrated Ammonia Production Plant. *Proceedings of the 1st Control Conference Africa*, 7–8 December, Liliesleaf Farm, Johannesburg, South Africa, IFAC PapersOnline 50-2, 77-82.

Bamimore, A., Ogunba, K., Ogunleye, M., Taiwo, O., Osunleke, A. and King, R. (2012). Implementation of advanced control laws on a laboratory-scale Three tank system. *Ife Journal of Technology*, 49-54.

Lakshminarayan, S., & Takada, H. (2001). Empirical modelling and control of processes with recycle: some insights via case studies. *Chem. Eng. Sci*., 3327-3340.

Meszaros, A., Sperka, L., and Burian, P. (2005). Adaptive Conrol of Processes with Recycle. In J. Mikkles, M. Fikar, and J. Dvoran (Ed.), 15th International Conference on Process Coontrol '05.

Morud, J. (1995). Studies of the dynamics and operations of Integrated plants. Dr. Ing Thesis, Nowegian University of Science and Technology, Trondheim.

Morud, J., and Skogestad, S. (1998). Analysis of Instabiility in an industrial ammonia reactor. *AICHE Journal* (44), 888-895.

Scali, C., and Ferrari, F. (1999). Performance of control systems based on recycle compensators in integrated plants. *J. Process Control*, 425-437.

Taiwo, O., Bamimore, A., Adeyemo, A. and King, R. (2014). On Robust Control System Design for Plants with Recycle. *IFAC World Congress*, Cape Town South Africa, 6pp

Taiwo, O. (1985). The dynamics and control of plants with recycle. *Journal of the Nigerian Society of Chemical Engineers*, 4, 96-107

Taiwo, O. (1986). The design of robust control systems for plants with recycle. *International Journal of Control*, 671-678.

Taiwo, O. (1993). Controlling Plants with recycle. *Proceeding of the 2nd European Conference*. Gronigen, The Neitherlands, 7-12

Taiwo, O., and Krebs, V. (1996). Robust Control system design for plants with recycle. *Chem. Eng. J*.

Tremblay, E., Desbiens, A., and Pomeleau, A. (2010). On theRobust Tuning of controllers with Recycle compensators. *IFAC Symp. Syst. Struct. Control*, 211-217.

CHEMICAL SECURITY IN NIGERIA: A CASE STUDY OF SELECTED UPSTREAM OIL AND GAS FACILITIES

Konee, N. D. and *Kuye, A.
Department of Chemical Engineering,
University of Port Harcourt,
Port Harcourt, Nigeria
*Email of the Corresponding author: ayo.kuye@uniport.edu.ng

ABSTRACT

This study evaluated the chemical security risks associated with chemical facilities in the upstream oil and gas sector in Nigeria concerning the chemicals they possess, their prevailing security measures, susceptibilities, malicious use and sabotage. The facilities were grouped into various categories such as, very low, low, moderate, high and very high risks using the chemical security risk self-assessment model (CHEM-SAM). Of the seven facilities that were investigated; findings indicated that Facilities II and VII pose low risks, Facilities I and IV pose moderate risks, whereas Facilities III, V and VI pose high risks. Also, there were variations in the security configurations of these facilities. Some had perimeter fences with installed intrusion detection systems, such as, alarms with well-trained onsite guards/mobile policemen as well as chemical cabinets/buildings housing chemicals with electronic access controls. Others had a few of these security components. From these findings, it would appear that there are no standardized chemical security regulations and/or policies in Nigeria for the upstream oil and gas facilities.

***Keywords**: chemical security; risk self-assessment; chemical facility; likelihood; consequence*

1. INTRODUCTION

Chemical Plants play a vital role in the economy and the public welfare. However, some of the chemicals produced or used by these plants are sublime and soluble solids, volatile liquids and gases, industrial feedstock and oilfield chemicals which can trigger fire or explosion. These properties can be exploited by people with malicious intent either to cause harm as in the case of terrorists, fight for a cause (sabotage) and/or for personal financial benefits (theft). In fact, chemicals have been deployed in attacks by various terrorist organizations such as; Hamas, Aum Shinrikho, Al-Qaeda and ISIS (Sweijs and Kooroshy, 2010; Nyberg et al., 2011; Forest, 2012; Hoette, 2012). In 2016, several upstream oil and gas infrastructure faced severe threats from militants, where major crude oil pipeline networks (mostly in the delta region of Nigeria) were vandalized (Kachikwu, 2017). It is, therefore, pertinent to have an active physical protection system around critical infrastructures to safeguard them against acts of sabotage, terrorism and natural disaster (Oyeyinka et al., 2014).

Relatively, terrorist attacks on chemical facilities have been few and far between. Nonetheless, the use of chemicals in more than half of the terrorist attacks worldwide further emphasizes the importance of security assessment and the management of chemical plants (Khakzad et al., 2018). Several studies have shown that chemical facilities and their highly valued products remain attractive to terrorists and criminals worldwide. In Nigeria, numerous bombings have been carried out by terrorist organizations where improvised explosive devices were utilized, and the trend appears not to have abated. Unfortunately, the precursors used for these devices are either obtained or obtainable from chemical facilities or somewhere along the chemical supply chain. The 2016 global terrorism index rating placed Nigeria as the third most terrorized nation with the seventh worst economic impact of 4.5% of GDP globally (GTI, 2016). Clearly, this indicates that the impact of terrorist organizations in Nigeria has extended far beyond political and religious boundaries.

As noted earlier, certain chemicals are precursors for improvised explosive devices. They can also be precursors for drug and may have dual use. There is need to protect such chemicals from people with malicious intent. This is the focus of chemical security. Chemical security is the prevention and protection against the intentional misuse of chemicals, people, or equipment for non-peaceful purposes. Thus, the present work evaluates the chemical security risk posture of seven selected chemical facilities in the upstream oil and gas sector of the Nigerian economy based on the chemicals they possess, their existing (onsite) security measures and vulnerabilities. For security reasons, the names of the facilities or the chemicals they handle would not be mentioned.

2. METHODOLOGY

This study employed the non-experimental descriptive survey technique. The instrument used was the questionnaire. The questionnaire, designed as part of the Chemical Risk Security Management Self-Assessment Model (Chem-SAM, 2017), consisted of 87 questions which were divided into 11 sections namely: (a) demography (Name, Gender etc.); (b) chemical asset and the likelihood of a chemical being targeted; (c) the effect of the release of the chemicals on human health; (d) the socio-economic impact of release of the chemicals; (e) chemical receiving; (f) materials control and accountability; (g) physical security of the chemicals at the facility; (h) personnel reliability; (i) information security; (j) the sales, distribution and disposal of chemicals and (k) chemical security management program. Further details about the questionnaires are given by Konee (2018). The questionnaires were administered to 400 employees from the seven selected chemical facilities designated as Facility I, II, III, IV, V, VI and VII respectively. Three of the facilities either produce or supply chemicals while the remaining ones are chemical users A brief description of each facility and the distribution of the questionnaires are shown in Table 1.

The responses were analyzed using the Chem-SAM. The Chem-SAM was developed by Sandia National Laboratories' International Chemical Threat Reduction Department in partnership with the U.S. Department of State's Chemical Security Engagement Program. (Chem-SAM, 2017). Chem-SAM model consists of four steps: 1. Administer the questionnaire and code the responses with the value between 0 and 4; 2. Define the potential adversaries; 3. Calculate the chemical security risk (the chemical security risk is viewable as a relative number between 0 and 4 or as a graph) and 4. Determine the risk acceptability (based upon the relative risks that were provided: the facility/laboratory must determine this risk) (Karimi Zeverdegani et al., 2016). In the Chem-SAM, the results are shown graphically for insiders and outsiders about theft risk, sabotage risk near populated area and sabotage risk near industrial areas in 5 ranges namely: very low, low, moderate, high and very high.

3. RESULTS AND DISCUSSION

Table 1 shows that out of the 400 questionnaires administered, 200 were fully completed and were used for the analysis. The number of responses ranged from 22 to 35 representing a response rate of 44% to 58.3% respectively. We are not aware of any standard for response rate. However, our values fall within the range suggested by Baruch and Holtom (2008).

Table 1: Facilities description, number of questionnaires administered and retrieved

Facility	Brief description	No. of Questionnaires Administered	No. of Questionnaires Returned	Response Rate (%)
I	Producer and supplier of diverse oilfield chemicals for drilling, completion, production and treating.	60	35	58.3
II	Exploits oilfield chemicals for drilling, completion, production and treating. Provides drilling and well services, directional drilling, mud logging and reservoir services.	60	31	51.7
III	Supplier of oilfield chemicals and services.	60	30	50
IV	Producer and supplier of diverse oilfield chemicals such as, drilling, completion, production and treating chemicals.	60	28	46.7
V	Spans the full – cycle of exploration, appraisal and development through production.	60	27	45
VI	Exploits drilling and completion chemicals.	50	27	54
VII	Conducts drilling and well services, directional drilling mud logging and reservoir services.	50	22	44
Total		400	200	

The results of the chemical security risk evaluation using the Chem-SAM software version 1.0 for each of the seven chemical facilities are shown in Table 2 and graphically in Figures 1 to 3. The risk evaluations were done for theft, sabotage near populated areas (SNPA) and sabotage near industrial areas (SNIA) for two scenarios namely outsider (external adversary) and insider (internal adversary). In Table 2 and Figures 1 to 3, the likelihood of success is a measure of the attractiveness of the chemical for misuse in the case of sabotage or potential for successful theft/diversion of the chemical based upon facility characteristics while consequences of malicious use is a measure of the impact to human health and/or facility of misuse of the chemical. The risk will, therefore, be very low if both the consequence and likelihood are very low (below 0.5). As Table 2 indicates, none of the facilities have very low risk; although the likelihood of success for Facility II is very low, its consequence is high especially near the industrial area.

Figure 1 indicates that for the outsider risks for theft are moderate for Facilities 1, III to VII while they are low for Facility II. For the insider, the corresponding risks for theft are low for Facility II, moderate for Facility I and III and high for the remaining Facilities. Figure 2 indicates that the risk levels are moderate for Facilities I, III, IV, V and VII while that for II is low and that for VI is high for the outsiders; the insider levels are the same or at the higher level. Similar deductions can be made from Figure. 3.

Table 2: Risks Values for Each Facility for External and Internal Adversaries

Facilities	External Adversaries	Likelihood of Success	Consequence of Malicious Use	Internal Adversaries	Likelihood of Success	Consequence of Malicious Use
I	Theft	2.23	2.86	Theft	2.15	2.80
	SNPA	2.30	2.32	SNPA	2.21	2.27
	SNIA	2.38	3.87	SNIA	2.31	3.85
II	Theft	0.53	2.91	Theft	1.00	3.79
	SNPA	0.53	2.54	SNPA	0.95	3.61
	SNIA	0.55	3.88	SNIA	1.12	3.81
III	Theft	2.22	2.75	Theft	2.85	2.75
	SNPA	2.37	2.31	SNPA	3.02	2.92
	SNIA	2.40	3.90	SNIA	3.17	3.83
IV	Theft	1.94	2.81	Theft	2.09	2.71
	SNPA	2.01	2.56	SNPA	2.21	2.50
	SNIA	2.11	3.87	SNIA	2.33	3.91
V	Theft	1.79	2.80	Theft	2.98	2.90
	SNPA	1.84	2.60	SNPA	3.00	2.53
	SNIA	1.98	3.89	SNIA	3.09	3.87
VI	Theft	2.49	2.48	Theft	2.89	2.79
	SNPA	2.52	2.77	SNPA	2.97	2.56
	SNIA	2.53	2.86	SNIA	3.00	2.90
VII	Theft	1.56	2.60	Theft	1.21	2.52
	SNPA	1.61	2.90	SNPA	1.24	2.87
	SNIA	1.72	3.85	SNIA	1.36	3.93

These results also indicate that Facilities II and VII have comparable risk levels which are generally lower than those for the other facilities. These low-risk levels are probably because the two facilities have similar security configuration. Facilities II and VII have perimeter fences with installed intrusion detection systems such as alarms with well-trained onsite guards/mobile policemen. Chemical cabinets/buildings housing chemicals have electronic access controls and are well-alarmed. They uphold proper chemical transportation as well as information policies, and all chemical incidences are tracked, reported, with follow-up actions. They also conduct regular vetting, safety and security drills amongst others. Facilities I and IV have perimeter fences with no intrusion detection systems, except alarms at the main entry and exit points. Chemical cabinets/buildings housing chemicals have manual access controls, but no alarms. They uphold proper chemical transportation policies, and all chemical incidences are tracked and reported. They also conduct periodic vetting, safety and security drills amongst others. In Facilities III, V and VI, chemical cabinets have no well-defined perimeters, no formal vetting for personnel, but there exist safety drills amongst others.

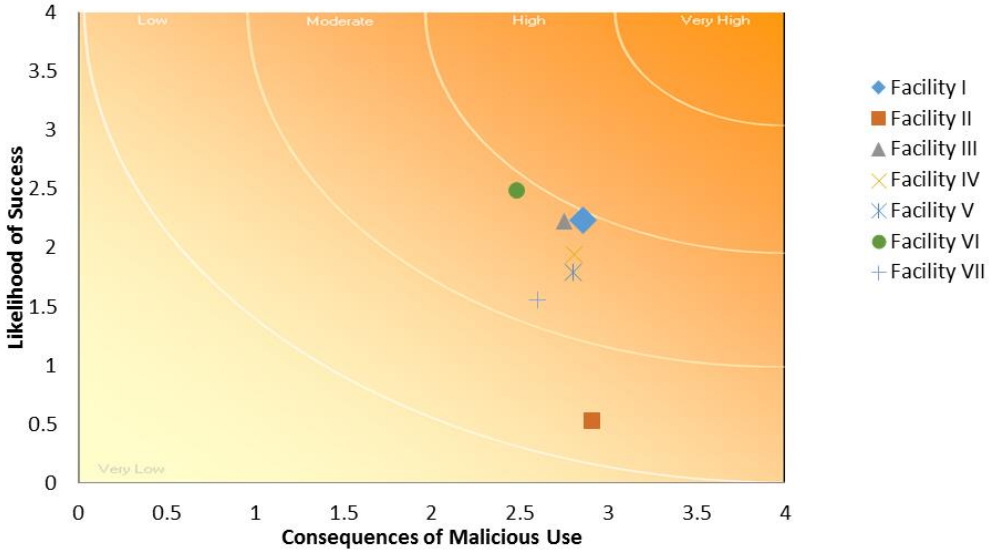

(a) Outsider

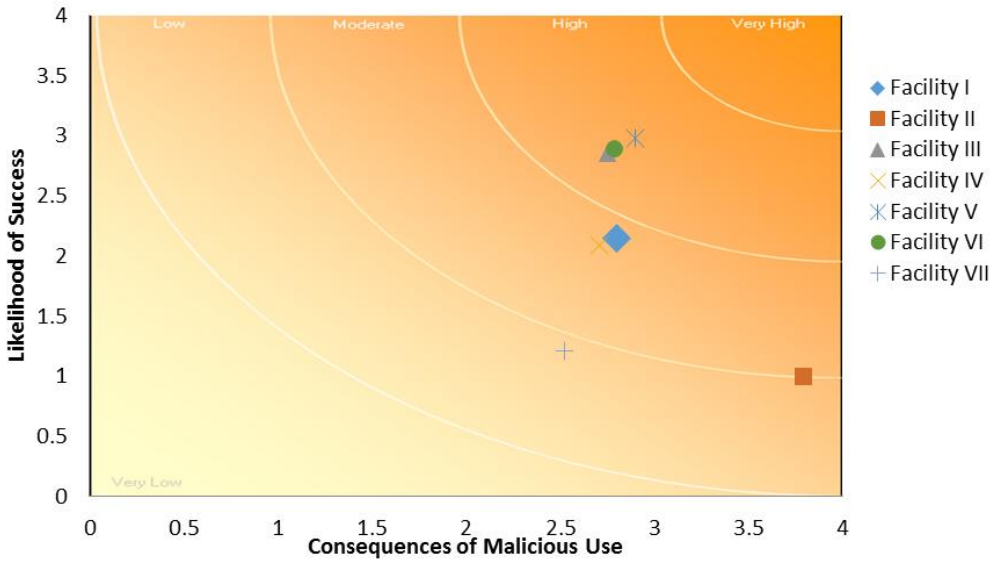

(b) Insiders

Figure 1: Facility Chemical Security Theft Risk

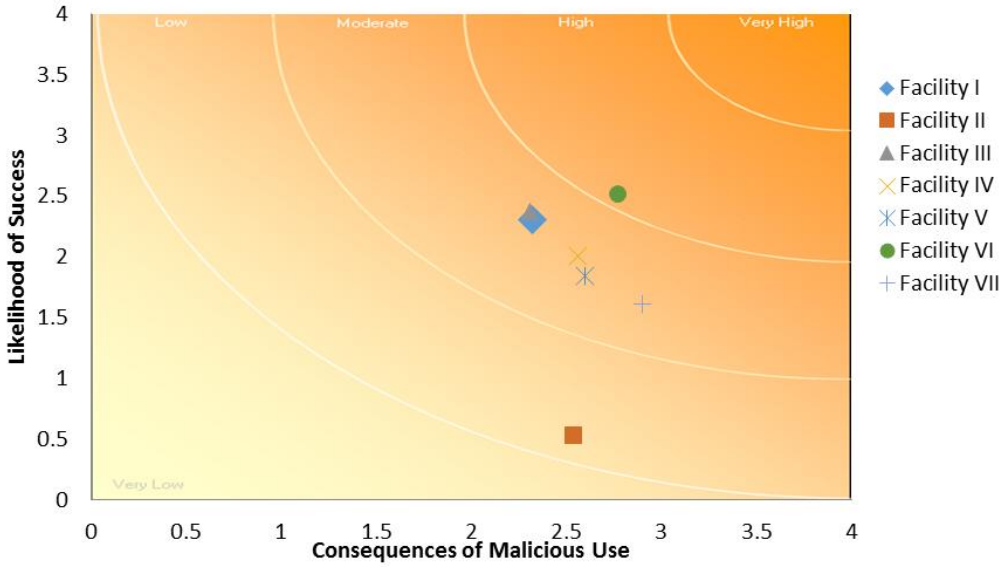

(a) Outsider

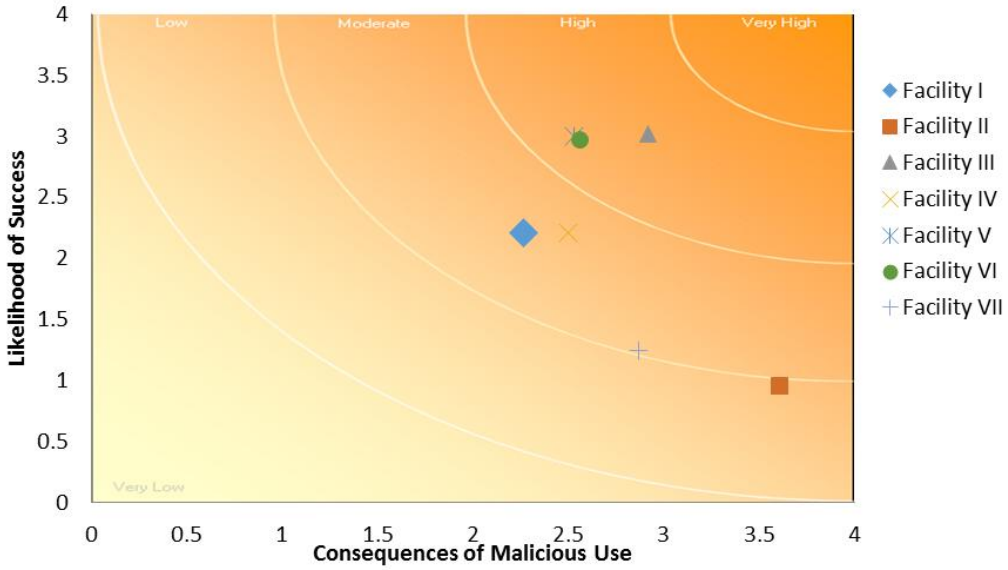

(b) Insiders

Figure 2: Facility Chemical Security Sabotage (NPA) Risk

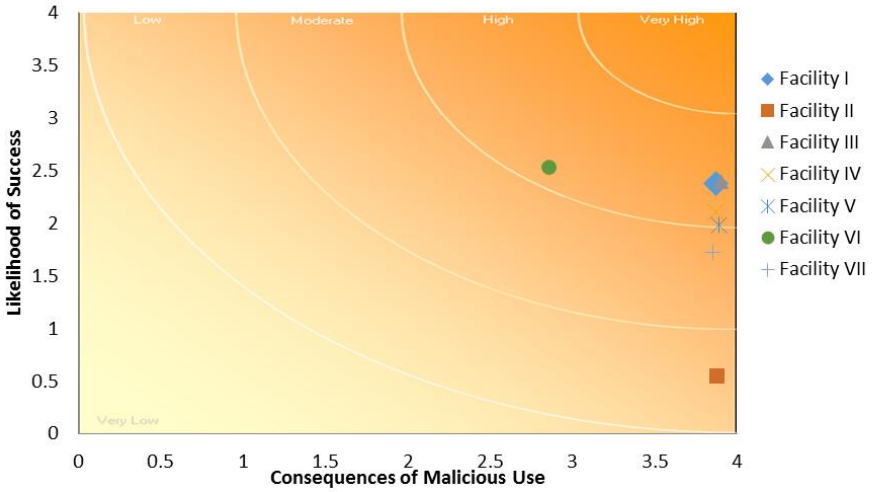

(a) Outsider

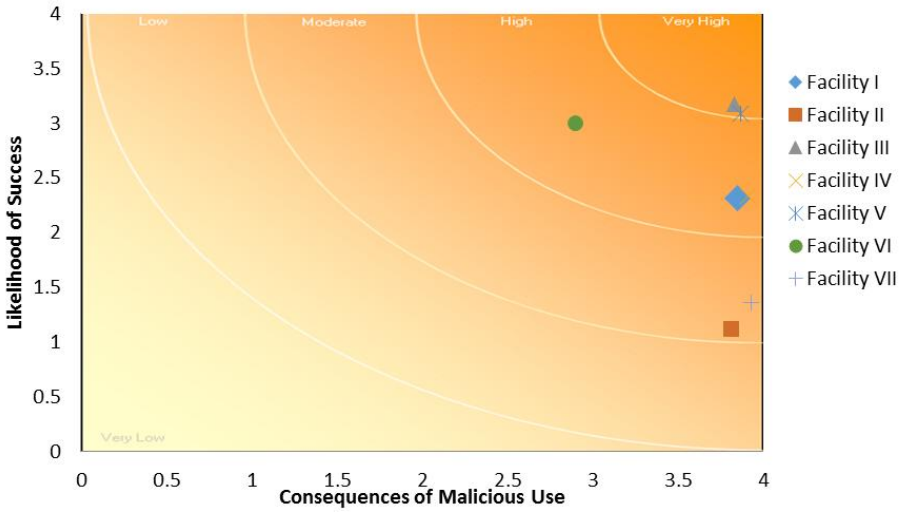

(b) Insiders

Figure 3: Facility Chemical Security Sabotage Near Industrial Area Risk

4. CONCLUSION

The assessment and evaluation of the chemical security risks (insider and outsider) associated with the seven selected chemical facilities were carried out. The findings indicate that facilities II and VII pose low risks, facilities I and IV pose moderate risks, whereas facilities III, V and VI pose high risks. The differences in the risk levels may be attributed to the different security configurations put in place at the various facilities examined. This observation tends to suggest the need for a regulation on the minimum security configuration requirement for chemical facilities in Nigeria.

5. REFERENCES

Baruch, Y. and B. C. Holtom (2008): *Survey response rate levels and trends in organizational research*, Human Relations, 61(8), 1139 – 1160.

Chem-SAM (2017): *Chemical Risk Management Self-Assessment Model*. International Chemical Threat Reduction Department, Sandia National Laboratories, Albuquerque, NM. Available online at: http://www.cspstate.net/ resources/chem sam (accessed March 14, 2017).

Forest, J. F (2012): *Framework for Analyzing the Future Threat of WMD Terrorism*. Journal of Strategic Security, 5(4), 51 – 68.

GTI (2016): *Global Terrorism Index: Measuring and Understanding the Impact of Terrorism*. Institute for Economics and Peace, New York.

Hoette, T. M, (2012): *Systems Analysis of Past, Present, and Future Chemical Terrorism Scenarios.* Sandia National Laboratories, California 94550.

Kachikwu, I. E. (2017): *Reforming and Repositioning the Oil and Gas Industry in Nigeria*. Keynote Address at the Nigeria Oil and Gas Conference and Exhibition, Feb. 28: Federal Ministry of Petroleum Resources.

Karimi Zeverdegani S, Barakat S, Yazdi M, (2016): *Chemical risk assessment in a chemical laboratory based on three different techniques*, Journal of Occupational Health and Epidemiology, Summer; 5 (3), 168 - 175

Khakzad, N., I. S. Martinez, H. Kwon, C. S. R. Perera and G. Reniers (2018): *Security Risk Assessment and Management in Chemical Plants: Challenges and New Trends*, Process Safety Progress, 37(2), 211-220,

Konee, N. D. (2018): *Chemical Security In Nigeria: A Case Study Of Some Selected Upstream Oil And Gas Facilities*, MEng Dissertation, University of Port Harcourt, Port Harcourt, Nigeria.

Nyberg, A. G, Stricklin D. and Sellstrom A. (2011): *Mass Casualties and Health Care Following the Release of Toxic Chemicals or Radioactive Material – Contribution of Modern Biotechnology*. International Journal of Environmental Research and Public Health, 8, 4521 – 4549.

Oyeyinka, O. D, Dim L. A, Echeta M. C, Kuye A. O (2014): *Determination of System Effectiveness for Physical Protection Systems of a Nuclear Energy Centre.* Journal of Science and Technology, 4(2), 9 16

Sweijs, T. and Kooroshy J. (2010): *The Future of CBRN*. The Hague Centre for Strategic Studies. Available at: http://www.hcss.nl/reports/thefutureofcbrn/18/. Accessed on 10/09/2017.

INITIATING LNG-FUEL TECHNOLOGY IN THE NIGERIA TRANSPORTATION SECTOR: A FUNCTION OF BETTER ENGINE EFFICIENCY

Nwosi H., Dulu A., Boma K. and Okocha S.

[a] Department of Petroleum & Gas Engineering, World Bank African Centre for Excellence (ACE), University of Port Harcourt, Nigeria

Corresponding authors: hezekiahandrews@yahoo.com, dulu.appa@uniport.edu.ng, boma.kinigoma@uniport.edu.ng steveokocha26@gmail.com

ABSTRACT

The transport sector fuel in Nigeria is dominated by two fossil fuels (PMS and diesel) which are products of Petroleum refinery. With the moribund state of Nigeria refineries and the challenges faced with the facet of fuel importation, the demand for transportation fuel has tripled in a geometric progression. The need to seek for other alternatives to bolster the country's transport sector cannot be overemphasized. Natural Gas has been researched as one of the most energy sources and fortunately, there is a profuse deposit in Nigeria, with total proven reserves of >187tcf. Thus, the initiative of employing Liquefied natural gas (LNG) will be systematically established. This paper is aimed at integrating LNG-fuel technology in transport sector to accelerate the transportation sector by looking into the exergy energy of using the boil-off gases from LNG into conventional vehicle engines. The analysis shows 24% exergy efficiency compared to conventional engines.

Keywords: LNG-fuel; Boil-off Gases; Exergy; Efficiency

1. INTRODUCTION

In Nigeria, in line with the report of the **National Bureau of Statistics, Nigeria** within the first quarter of 2017 spent $2.49 billion (N761 billion) on import of refined petroleum products of which 70% is consumed by the transport sector. Before this time, the main purpose of Natural gas liquefaction has been for its transport by vessel over stretched distances. In order to get it ready for additional transport by pipelines it has to be reduced again to a gaseous state, usually by upgrading the temperature through the use of sea water. Hence research has shown that LNG can be stored in small thermo-cooled bottles and utilized as fuel for vehicle transport. With the amount of money Nigeria spend on import of petroleum product, after much painstaking investigation it is clear that the country can build LNG refuelling stations and setup small scale plant for conversion of PMS cars to LNG cars across the country due to better engine performance. The transportation structure is principally made up of roads, rail transport, sea ports, internal waterways and airport via aviation respectively, of which road, air transport make up the major ones. The process will need the alteration LNG from a liquid phase to a gas phase for additional use authorize the use of exergy of LNG to various applications, which most times for electricity generation but here for car engine combustion. Energy access in transportation in the country lies below 50% as shown on the (NBS, 2017) report despite a rising trend in GDP and overall energy access. The rise in the global demand for natural gas is due to the high volume of reserves discovered in the world and it is straightforward to process and its multiple applications in different sectors. The production and processing of LNG in its vaporization state as Boil-off gases (BOG) attracted more research in different sectors of the energy usage value chain.

Figure 1 LNG Value Chain Modified

Conventionally, LNG is basically used as a carrier gas in vessels solely for the basis of exportation. During exploration and production, Natural Gas exists as an associated state in most wells and sometimes as a non-associated gas. Its treatment is vital due to the other constituents of hydrocarbons present in it. These other constituents like the Liquefied Natural Gas (LPG) are separated from Natural Gas and sent to homes leaving pure LNG (methane). This purified natural gas is then Liquefied into Liquid to accommodate for larger sizes in vessel and then exported to countries for usage in several sectors. The job of receiving LNG terminal is to receive the cargo of LNG from peak-shaving plant, in line with the operation plan – to process liquid LNG in the gas phase and at a particular pressure to introduce gas into the transmission system. Strategically, the LNG regasification facility begins playing a critical role. Notwithstanding the advancement of liquefaction methods and the technical know-hows concerned with the dropping of the energy consumption, liquefaction remains a very energy-consuming process at the place where it is performed (Remeljej, 2006). Based on several researches conducted by different scientist on the usefulness of LNG,in developed technologies the LNG can be used as a cold source in the direct production of electric energy (Liu & You, 1999). (Hisazumi*et al.* 1998) studied the possibilities of utilizing waste heat from A-gas-operated power facility for LNG evaporation. The cause of warmness in the Rankine cycle is condensation enthalpy from a steam turbine and heat of waste gases in the waste boiler. (Olivetti *et al.* 2012) investigated the problem of optimum thermodynamic use of cold sources, exemplified by LNG, to the electric energy production. The efficiency of thermodynamic process has been recently investigated by several others. (Dobrota, *et al.* 2013), investigated the "Problem of Boil - off in LNG Supply Chain," and the module regasification with ethane or ethylene for generating electric energy and energy transport within the established range of temperatures. (Liu and Guo 2011) initiated a process of thermal energy recapturing from LNG regasification with the use of two-component mixtures (tetrafluoromethane and propane) connected with steam absorption processes. Therefore, LNG as a cold energy source seems to be advantageous in any case when thermal energy waste is generated to the environment (Hang & Lior, 2006).The proposed configuration of LNG cryogenic tank installation will be based on the analysis of engine combustion performance to improve its efficiency as far as the produced energy and also thermodynamic efficiency.

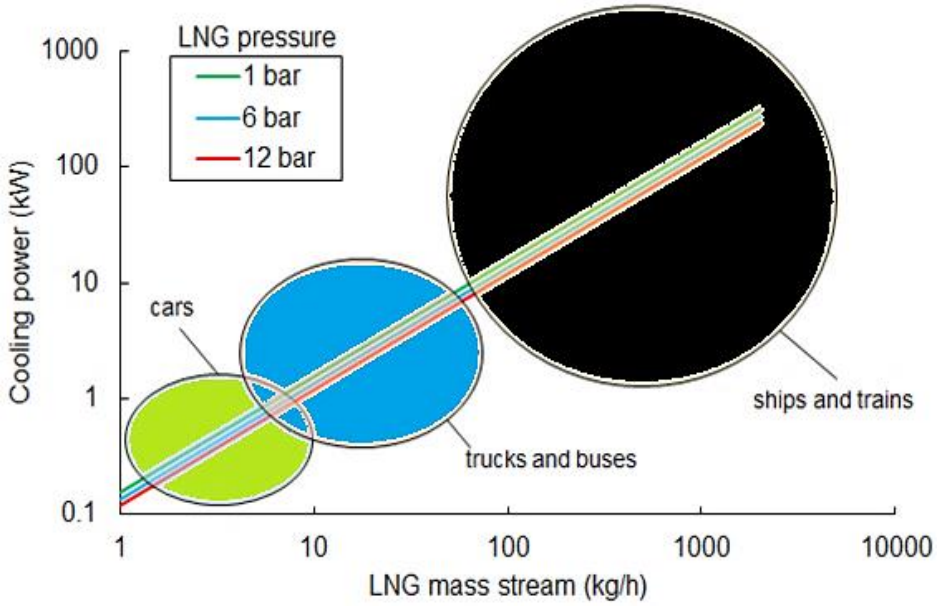

Fig 2- Cooling power systems for different LNG vehicle applications

From the figure 2, which is the cooling power system for different LNG transport applications, the allowable LNG mass stream (kg/h) shows the different mass flow rate into different vehicle engine rates. It can be seen that for small car engines, a mass flow rate arising from the boil-off rate from the cryogenic tank is between 1-10 kg/h. The range for buses and ship are at 10-100 kg/h and 100-10,000 kg/h respectively. These boil-off LNG are regulated by exchanging a coolant heat with the cryogenic tank with the surrounding. It can be seen that a cooling power of 0.1-1KW is necessary to maintain the boil-off rate from the cryogenic rank. The same can be seen for trucks and ships ranging from 0.5-10KW and 1-1000KW respectively. Different cryogenic tank pressures were tested for the fed tanks from 1bar -12 bars and it was noted that the pressures had little influences on the boil-off rates and the cooling power needed as shown in Figure 2. Although one the downside is that LNG boil-off can be a source of risky pressure increase in LNG tanks. There is therefore the need to research into other ways of controlling boil off buildup and reducing pressure of the boil-off gas and to avoid emitting of the boil-off natural gas in stored tank. The LNG business contributes to the country's economy, by creating employment through the construction and installation of new gas stations and plants respectively.Nwosi.*et al.*(2018). Using liquefied natural gas has numerous significance to our every living, especially in a developing nation like Nigeria where oil and gas companies even the host government is making effort to trim down gas flaring as a result, diversifying the usage of conventional fuel to gas is of major importance to the increasing the economy, because LNG is of less noise, cheap and pollution free due to its ability to absorb CO_2, thereby curtailing the emission of Carbon dioxide into the air that causes pollution which result in a terminal ailments. The gas utilization is done through the application of gas characterization technology, to characterize the gas either for industrial or domestic usage or external usage as air-conditioner in football stadium and offices that requires it through a condenser technology.

The aim of BOG liquefaction and utilization is lowering energy consumption. In the re-condenser both phases mixes: ca. 3 kg of cooled LNG per ca. 0.5 kg gaseous vapors, under a pressure of 4 to 6 bar. Gas liquefies through isobaric cooling process from the temperature gas has before the liquefaction to the temperature of boiling. Then in the course of Isobaric-isothermal transformations, condensation heat is recuperated. Liquefied gas exchanges heat with cooled LNG. Thermodynamic processes of LNG vaporization have been visualized in figure. 7. The course of plots illustrating the pathway of LNG starts from the inlet to the pump in the storing collector (point A), through the outlet of pump 1° (point B), inlet of LNG to re-condenser (point C – of the same enthalpy as point B), outlet of the evaporator (point D) and outlet of pump 2° (point E). Engine conversion is necessary to determine the suitability and ease of accommodating the newly introduced gas as fuel, the engine conversion will give rise to liquefied natural gas application in both transport sector and other usage in form of air-conditioner, energy to cars, engines and aeroplane. The liquefies natural gas(LNG) will use fuel engine consisting of natural gas

that will be of less noise, cheap and anti-pollutants to human activities. One major advantages of liquefied natural gas (LNG) is that, it can be operated in compression ratio.

2. MATERIALS AND METHOD

2.1 Description of the Boil-off production from Car's cooling system

The materials consist of an LNG tank, LNG sample; a car and the process. The method will be conducted in line with a sequence of data collection, natural gas laboratory analysis. The method followed all thermodynamic processes connecting LNG at the LNG receiving terminals environment of the LNG Boil-off Gas production process flow, the LNG is fed into the cryogenic tank via stream one tagged LNG, the atmospheric heat flux to the tank system is supplied through stream two while the outlet streams consist of metering element and the produced Boil-off Gas. A non-return valve is installed to control volume to the control volume tank to supply the gas to the engine for combustion. Liquid evaporation on vapor-liquid interface is: the temperature in the vapor phase space, the thermal stratification region and the main body area are all uniform. Vapor phase space is filled with the overheating vapor. Besides, the main body area is occupied by the super-cooled liquid. Furthermore the temperature in thermal stratification region is higher than the main body area.

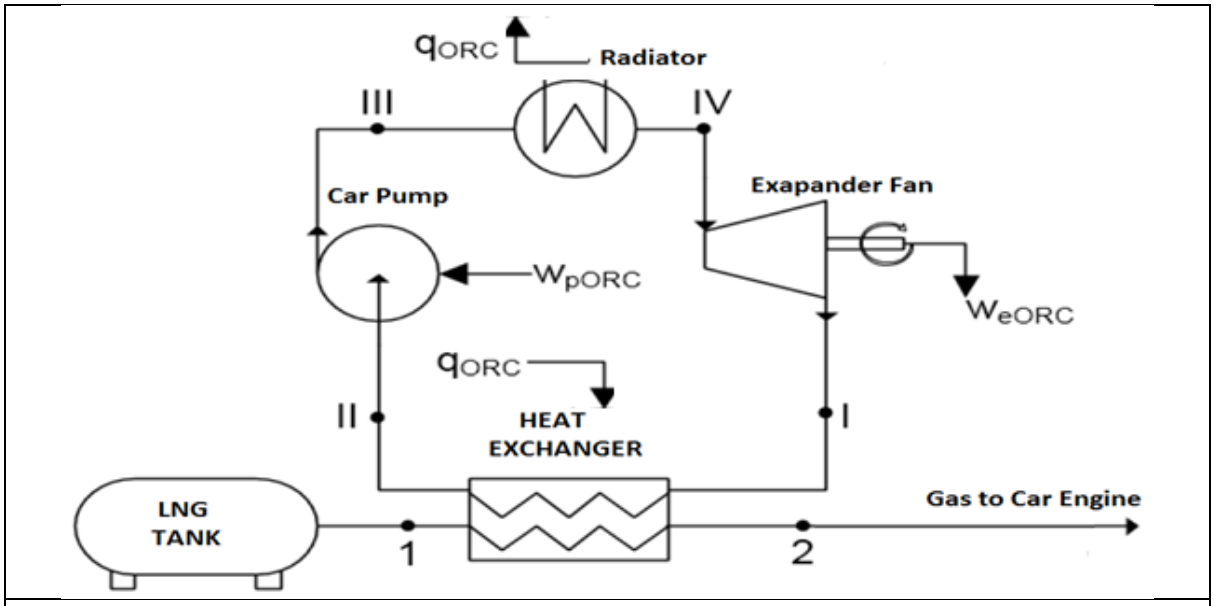

Figure .3 Description of the LNG Tank's Boil-off production process flow diagram

The re-gasification process from the cryogenic tank can be abetted more efficiently as shown in Figure 3. A heat exchanger can be used to exchange heat to the cryogenic tank to enhance the production of the boil-off gas by using the heat from the car's radiator. This heat raises the temperature of the circulating water and exchanges it with the LNG delivery stream to the car's engine. This gradually enhances the production of boil-off gases within its stream while the car's pump pushes the water back to the radiator to enhance its cooling efficiency. This process is made achievable due to the high vapor pressure of the LNG due to the methane constituents present within. Table 1 shows the vapor pressures of the different constituents of the Natural Gas according to Raoult's law.

Table 1. LNG AND BOG Composition (Łaciak, 2013)

Composition	Liquid Phase Mole Frac. [%] LNG	Vapor Phase Mole Frac. [%] BOG
Methane	89.87	94.011
Ethane	6.65	0.011753
Propane	2.30	0.00 (4.264×10^{-5})
n – Butan	0.57	0.00 (1.556×10^{-7})
i – Butane	0.41	0.00 (2.29×10^{-7})
n – Pentane	0.00	0.00
i – Pentane	0.01	0.00 (2.61×10^{-10})
Nitrogen	0.19	5.977

LNG density at temperature of -162°C (at pressure of 1 Bar) is 459.8 kg/m^3 and has calorific value equal to about 50 MJ/kg (21.5 GJ/m^3). In normal conditions, one cubic meter of re-gasified LNG has density about 0.79 kg/m^3, and its calorific value is about 34 MJ/m^3. If the whole change of enthalpy connected with LNG regasification from 112 K to ambient temperature is used, then the corresponding energy is about 724 kJ per 1 kg of LNG. Owing to the isobaric heating effect (from 112 K to ambient temperature), LNG undergoes the phase change and overheating.

2.2 Energy Consideration

Exergy E_x of heat Q given away to the environment is calculated as maximal work which the Carnot engine can perform at a given level of temperature

$$E_x = Q\left(\frac{T_n}{T}\right) \quad (1)$$

Where T-temperature of substance giving off heat and T_n is ambient temperature.

Thermal exergy connection with a difference of temperature

$$E_{x,t} = E_x\,(p, T_o) - E_x\,(p\ T_o) \quad (2)$$

$$E_{x,t} = \left(\frac{T_n}{T_s} - I\right) r + \int_{T_n}^{T_s} cp \left(I - \frac{T_n}{T_s}\right) \mathrm{dT} \quad (3)$$

Where r is the enthalpy of evaporation, being the enthalpy difference between gaseous and liquid phase,

Exergy coming from a difference of pressures (in constant temperature)

$$E_{x,t} = E_x\,(p,T) - E_x\,(pT_o) \quad (4)$$

$$\mathrm{Ex}, p = \int_{pn,T_n}^{p,T_S} v dp \quad (5)$$

Total exergy is a sum of both terms;

$$E_x\,(p, T) = E_{x,t} + \mathrm{Ex}, \quad (6)$$

3. RESULTS AND DISCUSSION

The Psychometric chart of the LNG was studied at the pressure - enthalpy relationship. Heat is being added as a result of the temperature from the ambient condition as well as from the heat from the radiator. This causes pressure build-up within the cryogenic tank still at the liquid phase and slightly some vapor components. The tank comes pressurized at an isobaric condition causing a drastic change in the phase of the LNG producing boil-off gases. These Boil-off gases still acquire heat addition and then are sent out to the engine for the car for fueling. Figure 4 shows the psychometric chart of the relationships of the LNG stream at different enthalpy and pressure conditions. The critical point is most best suited for the operating condition of the tank to sustain constant supply to the engine of the vehicle and the production of more boil-off gases to keep the process cycle in equilibrium. A deviation from the equilibrium will cause more pressure build-up as a result of less LNG mass stream to the engine or a drastic pressure drop as a result of more feed than boil-off production to the engine.

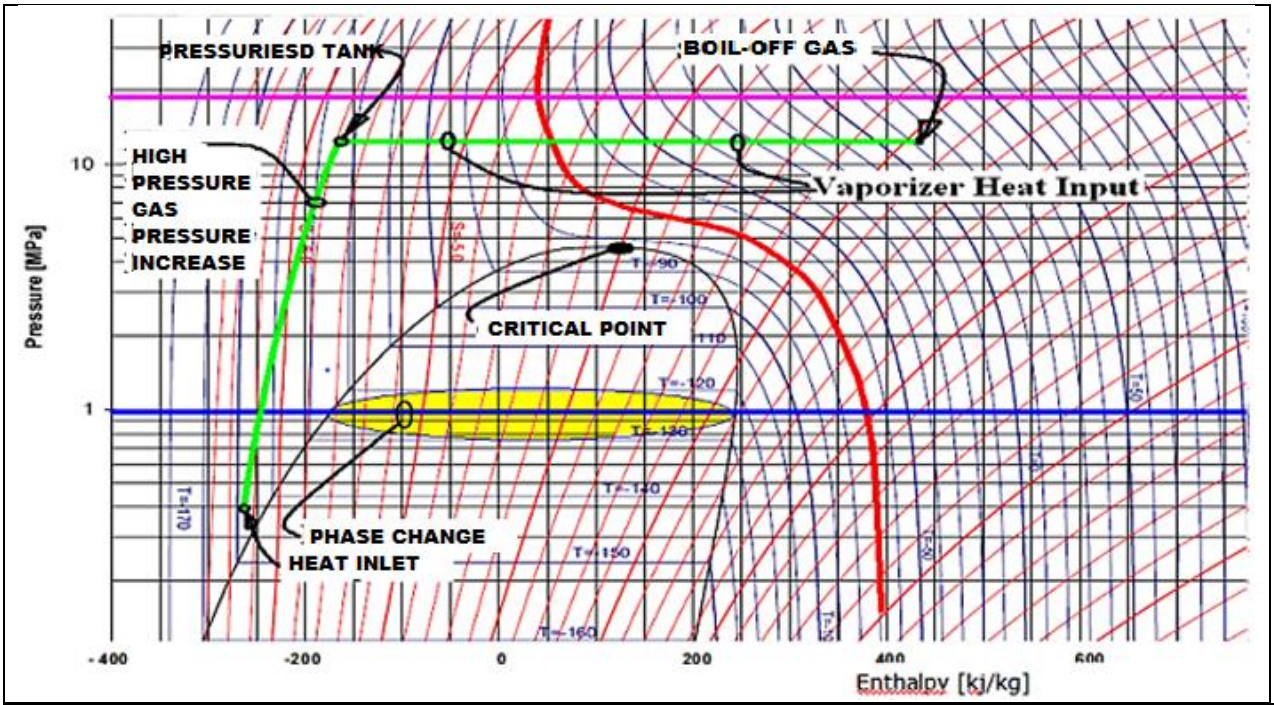

Fig 4. LNG Boil-off Pressure- Enthalpy process

Using the exergy analysis to determine the engine performance, it was deduced that the heat exchange creating the boil-off gas being fed to the energy is as a function of the expander work and the pump work of the cycle.

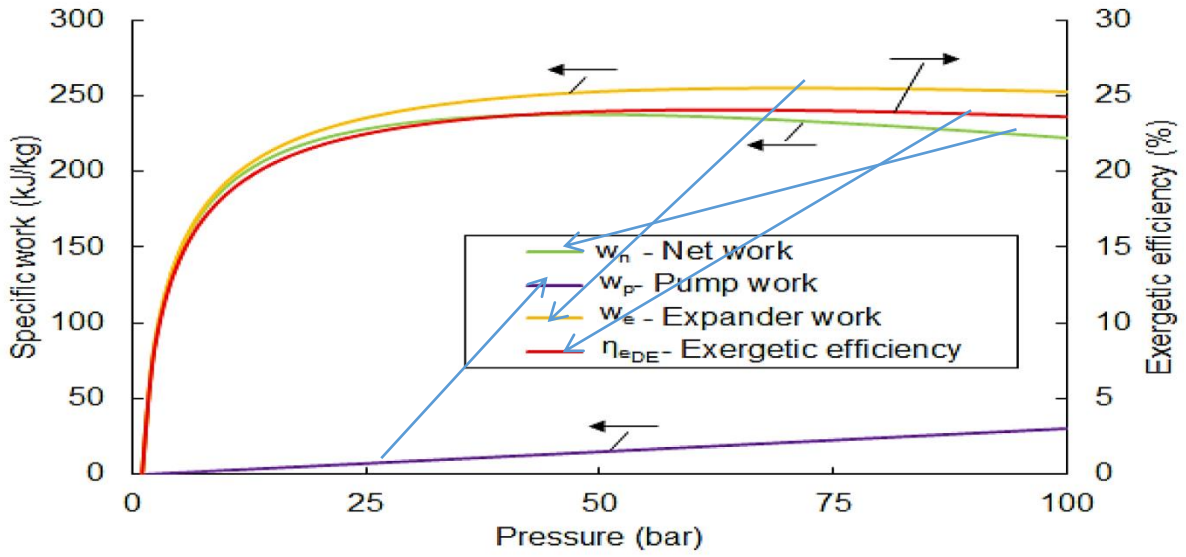

Fig 5. Network and Exergy efficiency of the Boil-off gas production inside the engine

The difference between the expender work and the pump work produces the net work of the gas in the engine. This is denoted by the area covered from the expander curve and the pump curve which equates to the net work curves from the base of the graph. This is stipulated at 22% efficiency. When considering the exergy of the system, which describes the useful work involved in the engine, the exergy efficiency amount to about 24% efficiency. This occurs at 230KJ/Kg.

4. CONCLUSION

In conclusion, the transport sector in Nigeria holds great business potentials and initiating LNG-fuel technology in the transportation sector which is a function of better engine efficiency. This new innovation will alleviate the hash economic challenges in the sector. The boil- off gas production from the build-up pressure in the cryogenic tank illustrates the LNG feed stream that is to be sent to the retrofitted car engine as a fuel.

5. REFERENCES

Applied *LNG Technologies*, http://www.altlngusa.com/ngf_lng.htm

Bahadori, A. (2014), *Thermal Insulation Handbook for the oil, gas and petrochemical Industries*, Elsevier.

BG Group, http://www.bg-group.com/group/LNG_2001.htm.

Chen, Q.S., Wegrzyn, J., and Prasad, V. (2004), *"Analysis of temperature and pressure changes in liquefied natural gas (LNG) cryogenic tanks," Cryogenics (Guildf)*, vol. 44, pp. 701–709

CH-IV, http://www.ch-iv.com/lng/lngfact.htm
Chive Fuels, http://www.lng-cng.com/chivefuels/liquefiednaturalgas.htm

Dobrota, D., Lalic, B., and Komar, I. (2013), *"Problem of Boil - off in LNG Supply Chain,"Trans. Marit. Sci.*, vol. 02, pp. 91–100.

Environmental Information Agency (EIA, 2016)
Hisazumi Y., Yamasaki Y., Sugiyama S., (1998). *Proposal for a high efficiency LNG power-generation system utilizing waste heat from the combined cycle*Applied Energy, 60

Liu H., You L., (1999). *Characteristics and applications of the cold heat exergy of liquefied natural gas Energy Conversion & Management*, 40

Liu Y., Guo K., (2011). *A novel cryogenic power cycle for LNG cold energy recovery Energy*, 36

*Łaciak M., (2012).Properties of Artificial Gaseous Mixtures for Their Safe Use and Support the Natural Gas Supply Networks.*Arch. Min. Sci., Vol. 57. No. 2, p. 351-362.

Łaciak* M., (2013).*Thermodynamic Processes Involving Liquefied Natural Gas at The LNG Receiving Terminals,* Arch. Min. Sci., Vol. 58, No 2, p. 349–359, DOI 10.2478/amsc-2013-0024

Olivetti G., Arcuri N., Bruno R., Simone M., (2012). *A rational thermodynamic use of liquefied natural gas in a waste incinerator plant*Applied Thermal Engineering, 35

Qiang W., Yanzhong L., Jiang W., (2004).*Analysis of power cycle based on cold energy of liquefied natural gas and lowgrade heat source.A*pplied Thermal Engineering, 24

Remeljej C.W., Hoadley A.F.A., (2006). *An exergy analysis of small-scale liquefied natural gas (LNG) liquefaction processes.* Energy, 31.

Shi X., Che D. (2009). *A combined power cycle utilizing low-temperature waste heat and LNG cold energy.* Energy Conversion & Management, 50

Siemek J., Nagy S., (2012). *Energy Carriers Use in the World: Natural Gas – Conventional and Unconventional Gas Resources.* Arch. Min. Sci., Vol. 57. No 2, p. 283-312.

Szargut J., Szczygieł I., (2009).*Utilization of the cryogenic exergy of liquid natural gas (LNG) for the production of electricity* Energy, 34

Vitale S.A., 2012. *LNG and Gas Thermodynamics Vol. II.GTI.*

Yang C.C., Huang Z., (2004).*Lower Emission LNG Vaporization.* LNG Journal Nov./Dec. 2004.

Zhang N., Lior N., 2006. *A novel near-zero CO2 emission thermal cycle with LNG cryogenic exergy utilization. E*nergy,

MARIUSZ Łaciak *Thermodynamic Processes Involving Liquefied Natural Gas At The Lng Receiving Terminals* Arch. Min. Sci., Vol. 58 (2013), No 2, P. 349–359

Mokhatab, S., Mak, J. Y., Valappil, J. V. and Wood, D. A. (2014), *Handbook of Liquefied Natural Gas, Elsevier.*

National Bureau of Statistics (NBS) 2017 *technical report.*

Nwosi, H. A., Appah, D., & Kinigoma, B. (2018,).*The New-Dawn for Liquefied Natural Gas Utilization: Empowering the Transportation Sector in Nigeria*. Society of Petroleum Engineers doi:10.2118/193437-MS

Yao Shouguang, Liang Ning, Ye Yong, Xiao Min and JiaXinwang (2014) *Experimental and Theory Study of the Lossless Storage Law for MarineLNG Storage Tank Based on Modified Three-District Model*.The Open Petroleum Engineering Journal,7, 104-108

Zakaria, M.S., Osman, A., and Musa, M.N. (2012), *"Boil-Off Gas Formation inside Large Scale Liquefied Natural Gas (LNG) Tank Based on Specific Parameters,"*Appl. Mech. Mater., vol. 229–231, pp. 690–694.

HIERARCHICAL ZEOLITES AS A NEW FRONTIER IN FCC CATALYSIS: A SHORT REVIEW

Nakakana, S.[1], Atta, A. Y.[1], *El-Yakubu, B. J.[1], Ahmed, A.S.[1] and Adefila, S. S.[2]

[1]Department of Chemical Engineering, Ahmadu Bello University Zaria, Nigeria

Engineering and Environmental Management Services Limited, Abuja, Nigeria

*Email address of the corresponding author: byjibril@gmail.com

ABSTRACT

Zeolites Y and ZSM-5 has been used extensively as part of Fluid Catalytic Cracking (FCC) catalyst blend. Owing to the dwindling global light oil reserves and large volume of heavy feedstock, it is important to optimize such catalysts and design new ones. One approach for improving the performances of zeolite catalyst is to develop its hierarchical structure. In the present review, various strategies employed for developing hierarchical structures are considered, with emphasis on the Top-Down and Bottom-Up approaches. These involved operations such as Dealumination, Desilication, Irridation, Mixed approach, Soft templating, Zeolitization and Hard templating strategies. Hierarchical ZSM-5 has currently being used along with USY in Vacuum Gas Oil (VGO) and Heavy Gas Oil (HGO) processing for possible use in the FCC. While top-down approaches (Dealumination, Desilication, Irradiation, Mixed approach), with specific emphasis on demetallation, are currently being employed on an industrial scale due to their facile nature, more specialized methods i.e. the bottom-up methods are currently being harnessed to become facile, and are generally more efficient in producing ordered hierarchical structures, with hard templating using carbonaceous materials showing the most promise, and therefore given particular attention. Our current approach on hierarchical zeolite Y for FCC catalysis is going to be emphasized.

***Keywords**: ZSM-5, Hierarchical, FCC, Top-down, Bottom-up, Carbonaceous*

1.0 INTRODUCTION

Zeolites are a family of aluminosilicate crystalline mineral, which are also synthesized, whose intrinsic structure, composing of a regular array of uniform micropores, framework stability and acidity make it a prime candidate of choice in a vast array of applications including as molecular sieves for adsorption, separation and catalysis. Zeolites enjoy wide use as solid catalysts in oil refining, petrochemical processing and organic synthesis (Zeolites occupy more than 40% of the entire solid catalysts in the current chemical industry (Na *et al*, 2013). New applications are under research and consideration in drug delivery, sensing and opto-electronics (Na *et al*, 2013). Among the different properties of zeolites, the shape, size and interconnectivity of its pores have a dominant impact on their functionality across all applications, by imparting the zeolites with unique and important capabilities such as shape and size selectivity, but also preventing the diffusion or movement of large molecules of feed into them: that is, the pore size distribution is in the micropore range (<2nm). This restriction of fluid movement into and out of its pores limits the application of the zeolites when bulky molecules are to be processed, via imposing severe mass transfer constraints, resulting in poor catalytic performance. This diffusion limitation also results in coking which deactivates the catalysts, thereby shortening the catalyst's life (Zhang and Ostraat, 2016). This diffusion conundrum has been the subject of intensive research since the early days of utilizing zeolites in catalytic processes.

Increasing the pores of the zeolites has been considered as a solution to this problem. But, with time, it was discovered that this also comes along with its own problems such as reducing the framework stability and acidity/activity of zeolites. This led to the understanding that a scheme had to be developed which, while increasing the accessibility of the active sites of the zeolites, hence its diffusion characteristics, would also maintain the framework stability and acidity/activity of the zeolites (Zhu *et al*, 2013). This culminated in the production of modern hierarchical zeolites. Different methods/approaches have been outlined in attempting to install the property of hierarchy within zeolites (Na and

Somorjai, 2015). There are generally two broad schemes by which it was sought viz.: top down and bottom up approaches. Hierarchical zeolites have been used in a wide variety of applications, most prominent of which is in oil refining (Zhu *et al*, 2013). They have been found to improve yield of more desired fractions obtained during Fluid Catalytic Cracking (FCC), Alkylation, Isomerization, Hydrogenation and Hydrodesulphurization (Zhu *et al*, 2013).

The earliest attempts at hierarchicalizing zeolites for FCC use were approached by steam treatment (Pavol, 2011) leading to the production of USY. This was later followed by chemical treatment, hard templating and soft templating. In the continuing search for better conversion of FCC feed stock (VGO), with an ever-increasing demand of gasoline and other light end fractions worldwide, the need for improved yield from the FCC unit, which gives the gasoline its required octane number, cannot be over emphasized. Thus, from ultra-stable zeolite Y to the experimental ITQ-39, the various frameworks and combinations of hierarchical zeolites produced by various routes for this use, have been tested (Vogt and Weckhuysen, 2015). Of important note is hierarchical ZSM-5 which has developed much interest due to its worldwide application in catalytic cracking (Ishihara *et al*, 2012). This work is designed to propound or attenuate the viability of hierarchical ZSM-5 use as FCC catalyst.

2.0 HIERARCHICAL ZEOLITES

For a material to be termed hierarchical, it must fulfil two basic criteria:

(i). It's structural elements have to be characterized by more than one length scale.

(ii). Each of these structural elements must have a very distinct, but complementary function (Schweiger *et al*, 2015).

Hierarchical materials have been known to outperform their individual entities by far e.g. the exceptional physical properties of natural materials (i.e. bones, wood) are typically ensured by a hierarchical arrangement of entities of either the same material having different dimensions, or of entities of different materials (Schweiger *et al*, 2015).

Leading from the above explanation, hierarchical zeolites are usually used in reference to zeolites materials having bi, tri or tetra modal (or more) porosities (Serrano *et al*, 2013). Typically, a hierarchical zeolite would have a minimum of one secondary porosity, in addition to it's primary porosity (micro porosity). More frequently than not, the secondary porosity would be in the mesopore range; the pore size depending on the synthesis strategy used in its processing (Serrano *et al*, 2013).

In comparison with conventional zeolite catalysts, hierarchical zeolites have shown a remarkable increase in performance in most cases. This is ever so prominent when dealing with bulky substrates feed. This is premised on the following advantages noticed during their use:

i. (Reduction of steric limitations in converting bulky substrates: The active sites located on the secondary pore surface of the hierarchical zeolite are not sterically hindered, i.e. not restricted due to their position and thus may catalyse reactions involving bulky substrates, making it possible to see the use of these zeolites in other fields e.g. fine chemicals synthesis

ii. .Increase in the rate of intracrystalline diffusion: Due to slow diffusion characteristics when molecular size of diffusion species approaches the dimensions of zeolite channels, intracrystalline transports determine the rate of many adsorption and catalytic processes when using them. Hierarchical zeolites attenuate this problem by decreasing the diffusion pathway followed by the substrates, leading to an increase in diffusional rate and thus the rate of the processes under consideration.

iii. Variation of selectivity toward the target products: Although some processes like xylene isomerization are affected negatively in terms of selectivity due to the presence of mesopores in the hierarchical zeolites, in other processes like toluene disproportionation, the shorter residence time within the zeolite micropores led to a reduction in conversion of the primary products (xylene) through non-desired secondary reactions.

iv. Decrease in coke enhanced deactivation: Generally, a higher amount of coke is usually formed over hierarchical zeolites but it has a lower deactivating effect when compared with conventional zeolites. Deactivation occurs by site coverage, micropore blockage and deposition over zeolite crystals external surface. This is very prominent in zeolites with large crystal sizes, but reduced in nanocrystalline zeolites and by extension hierarchical zeolites (Zhu *et al*, 2013).

These factors all contribute to the overall effectiveness of hierarchical zeolites use over conventional zeolites provided that the substrates lead to steric or diffusion problems and the coking enhanced deactivation is significant.

3.0 HIERARCHICAL ZEOLITE SYNTHESIS

Over the last decade, a lot of research work has gone into the development of hierarchical zeolites. As has been stated earlier in introduction, there are two major sub divisions of the methods i.e. top down and bottom up. These two can be further reclassified into seven (7) different strategies viz. (Serrano *et al*, 2013):

Top Down: (a) Dealumination (b) Desilication (c) Irradiation (d) Mixed Approach.

Bottom Up:

(e) Soft Templating,

(i) Dual templating with surfactants

(ii) Silanization based methods:

Crystallization of silanized protozeolitic nanounits

Crystallization using sylilated polymers

Crystallization using amphiphilic organosilanes

(f) Zeolitization of preformed solids:

(i) Nanozeolitic assemblies by cyclic or linear diamino or diamine structure directing agents

(ii) Nanozeolite assemblies by multistep pretreatment procedures

(iii) Nanozeolite assembles from concentrated gels

(g) Hard templating methods:

(i) Carbonaceous templates

(ii) Polymeric templates

(iii) Other solid templates

3.1 Top Down approaches:

Being the earliest of all processes used in developing hierarchical zeolites, top down approaches have been widely researched upon and the zeolites thus produced have been put to industrial use (Pavol, 2011). They are thus far accepted as the cheapest and simplest route to achieving hierarchy in zeolites. They basically involve demetallation, that is, removal of frame work atoms from the zeolite crystals through acid or alkali treatment, radiation, steaming or a combination of some of the methods.

3.2 Dealumination:

This is a well-known process employed to produce zeolites with high Si/Al ratios and enhanced diffusion characteristics from high alumina zeolites. It is formed by hydrothermal treatment or chemical treatment of which high temperature steaming and acid leaching are the commonest procedures. The primary reason for dealumination was to control the concentration strength of the acid sites by increasing the Si/Al ratio of high alumina zeolites, often with the secondary porosity as a pleasant surprising consequence. As stated earlier, dealumination is used, sometimes by combination of the two procedures, to produce ultra-stable zeolite Y (USY) which is currently used as FCC catalyst. Drawbacks of this process include a partial collapse of the crystal framework and irregularity of the mesopores formed i.e. low inter-connectivity and wide size distribution (Serrano *et al*, 2013). These have led to a gradual decline in proponents for this method, although it has been suggested that this process could be used in conjunction with desilication to produce novel zeolites (Yuan *et al*, 2014).

3.3 Desilication:

Arguably the most researched upon method, desilication involves the controlled dislodgement of silica from the zeolite crystals causing a decrease in the Si/Al ratio of the crystals. The first reported case of desilication was in 2000 (Serrano *et al*, 2013). Since then, a lot of interest has been developed in this field. An optimum Si/Al ratio is required in the zeolite to be desilicated in order to prevent over leaching or little-to-no leaching and to generate enhanced mesoporosity. Leaching is usually in the presence of a base. The crystalline morphology of the zeolite used affects desilication, and hence concentration of base used as leaching agent (Moller and Bein, 2013).

The drawbacks of this method include amorphization with extreme dissolution and micropore volume loss, accompanied by a loss in crystallinity. Sometimes, in order to mitigate excess leaching, a surfactant or alternative reagents are added to the leaching base or a partial removal of the template is followed by the leaching base (Moller and Bein, 2013).

3.4 Irradiation:

This method employs the use of radiation (^{238}U) in order to create latent tracks inside the crystalline zeolite. Sequentially the irradiated zeolite is leached with diluted HF acid and washed with water. This leads to the formation of uniform meso/macropores in parallel orientation within the zeolite crystal. Notedly, neither the crystallinity or micropore volume are impinged upon by the irradiation process. Drawback of this process is the use of uranium with its attendant complexity.

3.5 Mixed approach:

This method is similar to the one reported in desilication using surfactant but it comes with a twist. It was found that, using a particular surfactant, Cetyl trimethylammonium bromide (CTAB), and NaOH as the leaching base, a rearrangement of the zeolite framework occurred (Li *et al*, 2015a). This could be tuned in such a way that you can have a completely different material, having either a bimodal micropore/mesopore structure, or a completely mesoporous material, by adjusting NaOH concentration. Another variation to conventional dealumination and desilication involves using both simultaneously (Yuan *et al*, 2014). Drawbacks of this include the toxicity of the template used and its relatively high cost.

3.6 Bottom Up approaches:

These refer to generally all hierarchical zeolite synthesis methods that utilize zeolite precursors in producing multi-modal pores in the zeolite structure. They may be grouped as hard templating, soft templating and non-templating synthesis procedures. These templating methods employ conventional hydrothermal synthesis processes for the production of the hierarchical zeolites. But, instead of using only one Structure Directing Agent (SDA), a second, larger template is also used to impart hierarchical pores on the zeolite. However, there are reports indicating the use of a single template (soft) in determining both bi-modal pores (Liu *et al*, 2014a). Non-templating synthesis procedures include the zeolitization of preformed solids.

3.7 Soft templating:

(i) Dual templating: this strategy combines both the use of SDA to build the conventional zeolite framework and subsequent addition of surfactant leading directly to the formation of micelles which serves as a template for the meso-structure. The process involves the formation of protozeolitic units, to be subsequently templated by the surfactant. This sequence was informed as a succour to the phase separations experienced when both templates were utilized simultaneously (Jin *et al*, 2014). Drawbacks of this method are the relatively high cost of templates and environmental concerns regarding its toxicity.

(ii) Silianization based methods: Organosilanes have found extensive use in research as soft templates (mesoporogens) for hierarchical zeolite synthesis. This is due to their tunability i.e. ability to transform them by addition of functional groups to enhance their zeolitization utility. Three silanization based methods have been distinguished, in accordance with the type of silanization agent used and the role it plays in zeolite crystal formation, viz.:

Crystallization of silanized protozeolitic nanounits: This method follows these synthesis steps accordingly: pre-crystallization of the zeolite synthesis gel to form protozeolitic nanounits (zeolitic seeds); functionalization of protozeolitic nanounits on their external surface from the reaction with the organosilane, forming a protective layer; crystallization to complete zeolitization of the functionalized protozeolitic units; calcination in air to remove SDA and mesoporogen leaving uniform interconnected mesopores behind (pore size typically ~2-5nm).

Crystallization using sylilated polymers: A typical synthesis procedure includes the addition of a sylilated polymer to a zeolite seed gel. This leads to the aggregation of protozeolitic units forming large crystals. Mesopores are formed due to phase segregation of the space occupied by the sylilated polymer from the zeolite (pore size range ~2-5nm).

Crystallization of amphiphilic organosilanes: Amphiphilic organosilanes were developed in response to the phase segregation witnessed when simultaneously adding both templates (micro/mesoporous) into the reaction mix. They are usually utilized following conventional synthesis procedures (pores size range ~2-20nm).

3.8 Zeolitization of preformed solids:

A lot of attention has been given to this method due to the synthesis of nanocrystalline zeolite phases in hierarchical porous materials having 2D and 3D microporous stability, large surface area, strong acidity and high absorption capacity (Yang *et al*, 2017). There are two general synthesis procedures: Vapour Phase Transport (VPT), where a mixture of water and SDA is vaporized and contacted with the dry gel; steam assisted conversion (SAC), where only water is vaporized, the SDA (non-volatile compounds) having being already included in the solid gel. This method presents a number of advantages including faster crystallization, minimal SDA use and stable SiO/M_xO_y ratio in seed and crystal. A few schemes have been identified for the synthesis of the nanozeolites, listed as follows:

(i) Nanozeolites assemblies by cyclic or linear diamino or diamine SDAs: These SDAs cause a pseudomorphic crystallization of zeolite precursor gels

into zeolite nanocrystal assemblies, maintaining the gel structural features.

(ii) Nanozeolite assembles by multiple step pretreatment procedures: In this process, pre-prepared zeolite seeds are added in small quantities to the reaction gels, thereby promoting nucleation of the desired phase. This suppresses any side products and usually significantly reduces the reaction time.

(iii) Nanozeolite assembles from concentrated gels: SAC assists in the synthesis of nanocrystals from dry synthesis gel. The drying of the precursor gel further implies a localized concentration of the constituents in the synthesis mix, an ideal condition for controlled massive nucleation.

3.9 Hard templating:

Hard templating involves the use of porous solids as matrices within which zeolitization of zeolite seeds proceeds. The process consists of 3 basic steps: impregnation of pores of the hard template with the zeolite precursor; crystallization of zeolite within the pores of the template by heat treatment; removal of template by calcination (organic templates) or dissolution (inorganic templates). Nano crystalline materials have been reportedly formed using this method (Na *et al*, 2013). The zeolite crystal size is determined by the pore size distribution of the template. Drawbacks are the relative cost of template, environmental hazards involved with template pyrolysis, and inhomogenous mix of zeolite seeds and template leading to irregular pore size distribution.

(i) Carbonaceous templates: These include carbon black, carbon nanotubes or nanofibres, ordered mesoporous carbons, carbon aerogels and mesoporous carbons, pyrolysed wood, carbonized rice husk, carbonized sugarcane bagasse, among others. The concentration and volume of the zeolite seed gel, along with the porous properties of the carbon template are very important variables in determining the final characteristics of the hierarchical zeolites formed. The use of specialized carbonated material e.g. CMK leads to narrow pore size ranged, ordered nanoporous zeolites (Fang and Hu, 2006). For carbon nanotubes and nanofibres, the procedures for incorporating the synthesis gel into the template matrix is crucial for obtaining single crystals with intraparticle mesoporosity (Serrano *et al*, 2013). Colloidal silica has also been used in producing mesoporous carbons, which are subsequently employed as templates for hierarchical zeolites (Serrano *et al*, 2013). Finally, the effect of the nature of carbon pores templates used on zeolite crystal growth was demonstrated using graphene and graphene oxide. Hydrophilic graphene oxide sheets promote zeolite crystallization, with the formation of large crystals as opposed to hydrophobic graphene sheets which act as barriers to confine zeolite crystal growth and result in smaller crystals (Zhang and Ostraat, 2016).

(ii) Polymeric templates: Polymers have also seen wide application as templates, usually as scaffolds, for hierarchical zeolite synthesis. Some materials used are polystyrene, polyurethane foams and polymeric aerogels. Natural polymeric materials (e.g. starch derived templates) have been explored for use as templates as they have the advantages of being relatively cheap and non-toxic, with good hydrophilicity. The zeolites may be synthesized by addition of starch to zeolite synthesis gel, then proceeding with conventional zeolite synthesis, followed by calcination to remove the template and hence impart mesoporosity on the zeolite formed.

(iii) Other solids as templates: other materials that have been explored for possible use as hard templates in hierarchical zeolites synthesis include $CaCO_3$, bacterial threads, natural sponges (luffa sponge) and leaves of plants. Little research work has been done in this realm, thereby leading to a paucity of data regarding critical zeolitic parameters like mechanical stability and catalytic features.

Reflectingly, it must be said that qualitatively different mesoporosity in hierarchical zeolites is created by the varying processing techniques. Tiny variations in synthesis conditions (rotating or static) can lead to vast differences in material properties (Liu *et al*, 2014b). This may be manifested in pore volume or surface area, intra or inter crystalline, inter connecting of secondary pores, or size distribution. The different methods may also indicate differences in microporosity, acidity, hydrothermal stability and crystallinity. Efforts have been made to have generalized correlations for comparing the hierarchical zeolites prepared by varying techniques.

One of these is the hierarchical factor (HF) defined as the product of S_{meso}/S_{total} and V_{micro}/V_{total} (Li *et al*, 2014a). Care has to be taken when comparing the HF obtained using different gas-adsorption determination equipment. Although this HF appears viable, its

reliability has not been confirmed, since the relationship between HF and catalytic performance is hitherto unestablished.

4.0 HIERARCHICAL ZEOLITES IN OIL REFINING

Zeolites have been regarded as one of the catalysts in high demand in the petrochemical industry owing to their excellent catalytic performance. Hierarchical zeolites were first introduced in oil refining as ultra-stable zeolite Y (USY), an accidental benefit attained as a consequence of an attempt to reduce the activity of Zeolite Y (Pavol, 2011). The perks gained include diffusion of greater molecules to strong acid centers within the zeolite crystal structure, leading to an increase in overall conversion of substrate into gasoline, in comparison with conventional zeolite Y. Over the years, there has been an intense interest in the usage of hierarchical zeolites as catalysts or catalyst supports (Li *et al*, 2013). This interest has been driven by the demand to add value to an increasing volume of less valuable substrates. In oil refining, this has become more evident as new oil sources are being discovered (Vogt and Weckhuysen, 2015). The FCC unit being at the heart of the oil refinery operations, and accounting for a great tonnage of catalyst use in the oil refining industry, has taken a central stage in the use as proposed of new hierarchical zeolites, in order to enhance gasoline and diesel yield.

Zeolite Y in its various forms has been the main component of FCC catalysts since 1964 (Vogt and Weckhuysen, 2015). ZSM-5 has also found large scale usage in FCC. It has been found to improve the yield of propylene, an important precursor of plastics. As conventional FCC feedstocks get heavier, the need to tweak the system for better functionality to enable them handle these substances is required. This may be seen as engendering increased metal tolerance, flue gas emissions control, petrochemical feedstock maximization (e.g. propylene), light cycle oil (LCO) maximization (e.g. diesel flexibility) and lowering coke yield. Some strategies employed in furthering these include using composite zeolite Y / ZSM-5 zeolites (Pavol, 2011), and having over 65% of tonnage of FCC catalysts sold in the USA containing ultra-stable zeolite Y (USY) (Li *et al*, 2013).

In a number of research applications, hierarchically porous zeolites have been found to outperform their conventional counterparts with the increase in diffusion rates of reactants and higher conversion of bulky materials deemed the reasons for this outcome. Catalyst deactivation due to coke deposition on the catalyst would hence been minimized. As an example, mesostructured zeolite Y, with ordered mesoporosity and high hydrothermal stability, prepared by a surfactant method was used as an FCC catalyst (Zhu *et al*, 2013). The mesostructured zeolite Y produced more gasoline and LCO as well as less bottoms and coke than conventional zeolite Y because the presence of mesopores allows larger molecules in the vacuum gas oil (VGO) access to active sites within the zeolite crystal.

In another instance, bimodal Zeolite Y nanoclusters were synthesized using a triblock polymer as a template (Zhu *et al*, 2013). This zeolite produced a higher yield of light fractions (53%) than conventional zeolite Y (40%) in FCC, with heavy oil as feed.

In April 2013, Rive Technology began the ongoing supply of a commercial FCC catalyst, with mesoporous Zeolite Y made by a surfactant template post-synthetic modification, heralding a new age in the commercial application of hierarchical zeolites (Li *et al*, 2014a).

Hierarchical ZSM-5 has also been used for catalytic cracking. They can be used as additives to USY in FCC for improving catalytic activity and selectivity towards light olefins without affecting the gas oil yield (Zhu *et al*, 2013). Mesopores were understood to be the key determinant to enhancing the preferential production of propylene, suppressing secondary and hydrogen transfer reactions and offering easier access to its active sites.

Similarly, two ZSM 5 mesoporous catalysts (~2.2 and 5.2nm) with intracrystal mesopores formed using organosilane polymer templates were used in cracking VGO (Zhu *et al*, 2013). They both displayed higher reactivity and selectivity towards light olefins, with gasoline yield increasing from 12% to 19% as compared to conventional ZSM %, and overall VGO conversions from 33% to 48% which was attributed to the formation of olefin precursor in small intracrystal mesopores and subsequent formation of olefins in the micropores. Finally, slurry phase catalytic cracking of n-hexadecane showed pronounced increase in activity using mesoporous ZSM 5 as catalyst than conventional ZSM 5 (Perez Page *et al*, 2016).

Reflectingly, juxtaposing the interest and research on use of hierarchical zeolites as FCC catalyst, and the fact

that most of these remain in academia, is a paradox. But with recent commercialization of hierarchically mesoporous zeolite Y by Rive Technology in the USA, and with the discovery of facile and cheaper routes for hierarchy in zeolites, it is not out of place that there remains great interest in their use.

5.0 ADVANCES IN SYNTHESIS METHODS

Due to the level of interest in hierarchical zeolites, research is abundant on synthesis methods for all the various strategies, engineering a progressive advancement reflected in the quality of synthesis product thus obtained. Carbonaceous templates so far appear the most promising of the lot, giving a viable product when all the process parameters are considered, of which cost and toxicity are included among others. Here we present a few of the more prominent strategies, and research progress made so far:

Dealumination:

Due to recent advances in hierarchical zeolite synthesis, this primary process is gradually losing its panache and importance. Most research work involving dealumination usually considers it in association with another supporting process (eg, desilication). Nevertheless, some research in recent past concerning simulations on dealumination of mordernite was conducted (Ban *et al*, 2010). It was a successful effort as the simulation results were in good agreement with experimental results from Si NMR, XRD and N_2 and Ar desorption. The effort also successfully demonstrated the enlargement of micropores and creation of mesopores in the zeolite.

Desilication:

Desilication is one of the more popular strategies, and occurs in the presence of a base. Groen *et al* (2004) tried to optimize the desilication process, by studying the influence of Si/Al on the process. It was observed that a Si/Al range of 25-50 appeared to be optimal for mesopore formation. The tetrahedrally coordinated aluminum controlled the mechanism of mesopore formation.

More recently, desilication takes place in the presence of template (e.g. surfactant). In view of this, Wang *et al* (2015) produced mesoporous ZSM-5 zeolites using NaOH and a small molecular organic amine (piperidine). The piperidine added successfully prevented the excessive leaching of the zeolite by the base. From N_2 adsorption measurements, noticed was a significant change in micropore volume (from 0.16 to $0.11 cm^3 g^{-1}$) in the NaOH treated ZSM-5 without piperidine (PI) as compared to minimal change in that obtained with various molar volumes of piperidine at the same NaOH concentration, while still having a greater mesopore volume at low PI loading. Catalytic cracking of n-hexane over conventional ZSM-5, NaOH treated ZSM-5 and piperidine+NaOH treated ZSM-5 was investigated, with the PI treated showing a better overall performance over the others in this order: PI+NaOH ZSM-5> ZSM-5> NaOH ZSM-5.

Tarach *et al* (2016) preferred tetrabutylammonium hydroxide (TBAOH) as low-leaching template i.e. mixing it with NaOH. The TBAOH + NaOH treated ZSM-5 zeolites were less leached than those treated with NaOH alone, showing the protection offered by the template. The mesopore size distribution was also narrower than TBAOH+NaOH treated ZSM-5 as opposed to NaOH treated, which had a longer range. Cracking of n-decane, TIPB and VGO was investigated on the 3 catalysts. Parent ZSM-5 showed the best n-decane values, followed by TBAOH + NaOH ZSM-5. This was attributed to the greater activity of the parent ZSM-5, decreasing in that order. In TIPB, greater accessibility to the acid sites lead to a better conversion for the treated zeolites than parent ZSM-5, with TBAOH + NaOH ZSM-5 giving the highest values. VGO cracking produced inconclusive results, with the major standout point being the preference of olefinic components observed for the treated zeolites.

Finally, in congruence with the work by Tarach *et al* (2016), Wan *et al* (2006) found a significant difference in the degree of leaching when using tetrapropylammonium hydroxide (TPAOH) with NaOH, as opposed to only NaOH. This was attributed to size distribution of mesopores formed in both cases, with TPAOH + NaOH ZSM-5 having a shorter range of size and smaller mesopores. The catalysts performance was then studied with cracking of methanol. Even though their conversion was comparable, the TPAOH+ NaOH ZSM-5 had greater catalytic longevity than parent ZSM-5 and NaOH ZSM-5. This was attributed to the mesopores which prevented retention of coke precursors within its pores by shortening diffusion pathways. The increased external surface area in TPAOH + NaOH ZSM-5 was indicated as being responsible for its better longevity as compared with NaOH ZSM-5, though also mesoporous.

Mixed Approach:

Mixed methods were developed in order to mitigate the problems associated with desilication and dealumination. Yuan *et al* (2014) produced hierarchical ZSM5 by acid leaching of parent ZSM-5 mixed with sodium aluminate ($NaAlO_2$), varying a number of process conditions (e.g. treatment time, temperature). The doubly treated ZSM-5 showed greater mesopore volume than parent ZSM-5, and greater crystallinity when compared with a NaOH treated ZSM-5, under similar conditions. This indicates that even though mesopores are formed in the doubly treated ZSM-5, their formation is controlled so as to largely maintain its crystal structure. From micro reaction activity tests, doubly treated ZSM-5 showed greater catalytic activity than the parent ZSM-5 accounted for by the reduction in diffusion restrictions.

Li *et al* (2015a), instead of using PI as in Wang *et al* (2015), replaced PI with an ammonium surfactant (cetyltrimethylammonium bromide (CTAB)), but as a recrystallization template. N_2 adsorption measurements showed an increase in specific surface area, as compared with the parent ZSM-5, an indication of the formation of mesopores. The zeolites were transformed into a ZSM-5/MCM-41 composite due to partial recrystallization of the zeolites enhanced by the surfactant. The composite zeolites thus formed exhibited superior performance in the catalytic cracking of n-dodecane, when compared with untreated zeolites.

Sun *et al* (2017) went a step further, in trying to propose a scheme by which mesoporous zeolites produced by mixed approach (sequential desilication and dealumination) can be put into commercial use. They used NaOH instead of $NaAlO_2$ as the leaching base, retaining HCl as the leaching acid. The scaled up process (50L) was found to show the formation of mesopores leading to a corresponding rise in specific surface area. In cracking VGO, a remarkable rise in preferred products (gasoline, propylene) is noticed when compared with parent ZSM-5, an increase in coke yield not affecting the overall conversion.

Zeolitization:

Efforts are underway for meso-template-free synthesis of zeolites. These have been hailed for their 'green' outlook, since they don't involve the use of mostly toxic templates. Ding *et al* (2013) synthesized hierarchical ZSM-5 zeolite from rectorite without the use of template. Undissolved rectorite debris acted as seed crystals and played a structure directing role, effectively substituting templates. N_2 adsorption measurements showed an increase in mesopore volume, along with attendant increase in specific surface area, which is attributed to the aggregation of nanorods that make large spherical ZSM-5 particles, and consequent intercrystal mesopores. Hierachical ZSM-5 (Hc ZSM-5) showed greater hydrothermal stability when juxtaposed with conventional ZSM5 (R ZSM-5), as buttressed by its higher crystallinity after steam treatment. To test the catalytic performance of the zeolites, 1,3,5-tri-isopropylbenzene (TIPB) was cracked over both Hc ZSM5, R ZSM-5, and desilicated ZSM-5, with Hc ZSM-5 coming out tops in conversion. Heavy gas oil was then cracked over the three candidate catalysts above, with Hc ZSM-5 being better than the rest, with a reduction in coke and dry gas yield. Wang *et al* (2014a) synthesized Hc ZSM-5 by a CO_2-in-water microemulsion method. The Hc ZSM-5 formed had a wide mesopore range (10-40nm) with a greater pore volume than R ZSM-5. It also took much less time to crystallize than R ZSM-5 with similar crystallinity.

Yuan *et al* (2014) synthesized Hc ZSM-5 by depolymerization and subsequent rearrangement of the synthesis mix containing one aluminium-rich (diatomite) and silicon-rich (rectorite) aluminosilicate mineral. It had a greater hierarchical factor (HF) than R ZSM-5. The crystallization follows a similar scheme as Wang *et al* (2014a), producing primary nanocrystals, and then nanosheets after aggregation. Cracking of TIPB and Heavy gas oil (HGO) were all more favorable on the Hc ZSM-5 when compared with commercial ZSM-5, with a boost in gasoline/diesel and propylene yield, and reduction in coke formation.

Zheng *et al* (2016) also produced nanocrystalline mesoporous zeolite following a traditional hydrothermal route, while adjusting parameters resulting in higher degree of supersaturation and nucleation to growth rates. As expected, the total pore volume and specific surface area (SSA) of the Hc ZSM-5 surpassed that of R ZSM-5. Cracking of TIPB over both catalysts was undertaken, with Hc ZSM-5 showing better conversion. Though the acid sites in R ZSM-5 are stronger than those in Hc ZSM-5, increased access to the interior of the Hc ZSM-5 catalyst led to a better conversion. This work is similar to that by Li *et al* (2015b), the main difference being the use of different silica types as precursors.

Finally, kinetic regulation was propounded by Ding *et al* (2015), implying the possible regulation of nucleation kinetics to form nanocrystalline MFI zeolites. The main

idea was to avoid Ostwald ripening at lower temperatures, allowing the retention of defects generated in the oriented attachment process. When tested for cracking as a composite with USY zeolite in the FCC unit, a higher gas oil conversion, and less coke formation was observed, with increased olefin selectivity, as compared with R ZSM-5.

Surfactants:

Surfactants are a group of complex compounds that have gotten wide use in synthesis of zeolites. There have been reports of surfactants being used in controlled desilication, and commercial quantities of the zeolites have been produced (Li *et al*, 2014a).

In 2011, Na *et al* synthesized $C_{n\text{-}6\text{-}6}$ Br_2 (n=12, 16 or 22) surfactants for use as SDA for the synthesis of Hc MFI zeolites to from unilamellar, and after aging under specific conditions, multilamellar crystals sequentially. The unilamellar crystals showed great mechanical stability under pressure, giving promise for possible use in high pressure environment (FCC). $C_{22\text{-}6\text{-}6}$ was found to have the largest pore volume, showing a large mesopore volume and hence, better prospects for use. Liu *et al* (2014b) studied the effect of synthesis conditions (rotation or static) on the nature of Hc ZSM-5 produced using a dual porogenic surfactant (C_{22}-N_4-C_{22}). The Hc ZSM-5 produced with rotation during synthesis produced the most mesopores when compared with Hc ZSM-5 Static and R ZSM-5. Thus, Hc ZSM-5 rotation was adjudged to have the best diffusion characteristics.

A gemini surfactant ($C_{18\text{-}3\text{-}18}$) was synthesized by Wang *et al* (2014b) for use as SDA to produce Hc ZSM-5. Hc ZSM-5 crystals formed had a small range of pore size distribution, as is common with surfactant SDAs. A relatively low crystalline temperature was required for the crystallization process. Liu *et al* (2014a) used bolaform quarternary ammonium surfactants ($C_{6\text{-}6\text{-}diphe}$) as SDAs. They work in such a way that allows crystal growth only along certain planes, due to the nature of functional groups that make them up. The Hc ZSM-5 crystals produced were arranged in a multilamellar form. Jin *et al* (2014) used cetyl trimethylammonium bromide (CTAB) as the only SDA in synthesis of Hc ZSM-5. This was achieved through the self-assembly of zeolites seeds with the help of CTAB. The crystals produced were in nanoscale (10nm). The CTAB prevents aggregation of the nanoparticles into larger crystals. Finally, Keoh *et al* (2016) used simple diquarternary ammonium SDA (Prediquat-5) to synthesize hierarchically and sequentially intergrown ZSM-5, giving thin crystalline plates.

Silanization:

Organosilanes are a group of recently developed templates used as SDAs in hierarchical zeolite synthesis. They are characterized as having the silane group. Being surfactants, their functionality is similar to those of that group. Guo *et al* (2011) synthesized Hc ZSM-5 using organosilanes by two methods: A sequential addition of template to the zeolite seeds before crystallization; and making the template part of the reaction solution. The Hc ZSM-5 thus produced indicated the presence of mesopores of 2.8nm size and supermicropores of 1.4nm size. This process, like surfactant use, leads to the formation of nanocrystals, with their attendant benefits. The two synthesis schemes employed didn't exhibit any deviation in the functionality of Hc ZSM-5 synthesized by their routes. 3-Aminopropyltrimethoxysilane (APTMS) was found to give the best crystallinity, indicating the formation of excellent nanosized crystals.

Zhu *et al* (2011) produced some Hc ZSM-5 nanocrystals (12nm) using another silane (hexadecyltrimethoxysilane) dissolved in ethanol solution containing zeolite precursors. The Hc ZSM-5 produced had trimodal pores, increasing its SSA and pore volume, as compared with R ZSM-5. Uniquely, the nanozeolites formed shared the same crystalline orientation. Hc ZSM-5 microspheres were synthesized by Xiao *et al* (2013), leaving the nanocrystalline trend for surfactants. The silane used, 3-aminopropyltriethoxysilane (APTES), plays a retarding role in the development of crystallinity of Hc ZSM-5, leading to the formation of microspheres.

He and Liu (2014) synthesized Hc ZSM-5 with chain-like morphology with the help of a carbamate linked organosilane. TEM images and N_2 adsorption measurements were used to confirm the formation of mesopores in the Hc ZSM-5 crystals, with SSA of $378m^2/g$ and mesopore volume of $0.3cm^3/g$ respectively.

Zhu *et al* (2016) followed up their 2011 work with the use of a mesoporogen, an organosilane, with a gemini type structure to synthesize Hc ZSM-5. The mesopores formed are quite irregular, but can be tuned by changing organosilane/silica ratio, showing organosilane flexibility. The mesopore volume increased with increased SDA/silica ratio. Mesopore size distribution is 10-30nm. Wang and Liu (2016) used an organosilane (TABDPI) with double oxycarbonyl carbon chains in the

synthesis of Hc ZSM-5. N_2 adsorption measurements discovered a mesopore size distribution at about 4nm. Porous volume was 0.2cm^3/g. Well organized crystals were formed, leading to the formation of mesopores.

Finally, nanocrystalline aggregates were produced from the hydrothermal synthesis from zeolite precursors (mesoporous silica) in the presence of an organosilane phenylaminopropylmethoxysilane (PHAPTMS) following a conventional synthesis method (Wang *et al*, 2017). Tunability of mesopore volume was also found to be viable by this process. Pore size distribution was found to be 2-10nm, with a concentration around 2.5nm and 5.5nm.

Polymers:

Polymers have extensive use as templates in Hc ZSM-5 synthesis. Natural polymers (Luffa sponge) have long been touted as 'green' templates for use. One such attempt at synthesis of Hc ZSM-5 with the use of polymers as templates involved block co polymers (Zhou *et al*, 2011). The co polymers act as a scaffold, supporting the synthesized zeolite, and imparting mesoporosity on the ZSM-5 crystals after removal by calcination. Steam treatment was used in the synthesis of the dried ZSM-5-in-co polymer matrix gel, dried so as to prevent phase separation between the silicon phase and template. Total pore volume of Hc ZSM-5 was far greater than that for R ZSM-5, having an average pore size of 9.8nm. The micropore volume for R ZSM-5 only slightly changed (.02cm^3/g) as compared with the Hc ZSM-5. The mesopore volume and average diameter can be tuned, as is same for most hard templates, by changing the mass of template used. TIPB was cracked over both Hc ZSM-5 and R ZSM-5, with Hc ZSM-5 showing better ratings with regards to conversion, and coke induced deactivation, accounted for by improved diffusion characteristics (nearly 100 times diffusion length reduction).

Subsequently, efforts were made to produce ordered mesostructure in Hc ZSM-5 using polymers, expecting an improvement in overall catalytic performance due to organized linkage of pores. Thus, a cationic amphiphilic copolymer was used in one such attempt (Liu *et al*, 2012), with b-aligned mesopores formed by this process. N_2 adsorption measurements gave a mesopore size distribution of 6-60nm. The Hc ZSM-5 showed great hydrothermal stability under steam treatment. From the catalytic conversion of benzaldehyde, the copolymer synthesized ZSM-5 outperformed disordered hierarchical ZSM-5 and multilamellar and unilamellar nanosheets, prompting a positive outlook with regards its use in the FCC unit.

From the success achieved with ordered mesoporous Hc ZSM-5 templated by polymers, ways by which to increase the total pore volume as a way forward were proposed. In this vein, Tao *et al* (2013) and Li *et al* (2014b) both produced Hc ZSM-5 with intracrystalline and intercrystalline mesopores using polyethylene glycol (PEG) and polyurethane (PUF) as scaffolding templates respectively. Tao *et al* (2013) successfully generated irregular intracrystalline mesopores (2-10nm) after removal of template, while intercrystalline mesopores were formed due to the aggregation of well crystallized ZSM-5 nanocrystals (50-200nm). A trimodal porosity distribution was obtained. Activity of the Hc ZSM-5 synthesized was compared with nano ZSM-5 and R ZSM-5 by the conversion of benzenaldehyde. Hc ZSM-5 (56.5%) compared favourably with nano ZSM-5 (56.7%), and outperformed R ZSM-5 (18.3%) by more than three fold.

Considering the challenges associated with separating nano ZSM-5 from product, Hc ZSM-5 appears the standalone victor in this quest. For PUF templated Hc ZSM-5, a monolithic solid crystalline structure of ZSM-5 was obtained with tetramodal porosity. Pore volume was found to be 0.21cm^3/g. Intracrystalline mesopores were created by voids formed by the initial dry precursors, which transformed and were preserved in the Hc ZSM-5 crystal.

Finally, due to problems associated with the use of binders in catalyst formulation for industrial applications, Hu *et al* (2017) set out to synthesize standalone zeolites capable of direct industrial application. Their approach involved the use of a sponge as polymeric template. The Hc ZSM-5 produced had a considerably large pore volume (0.62cm^3/g) as opposed to R ZSM-5 (0.22cm^3/g).

Carbonaceous Material:

This class of materials gives one of the classic attempts at hierarchicalization of zeolites. From carbon black to CMK, they have been widely researched on with new solutions generated by the day. One of the earliest attempts at hierarchicalization using carbonaceous materials in recent times involved the use of carbon aerogels (resorcinol-formaldehyde (RF)) (Tao *et al*, 2002). Hc ZSM-5 Synthesis followed the conventional route, with the aerogel incorporated into the process. N_2 adsorption isotherms gave an SSA of 1330m^2/g, and

mesopore volume as 0.2cm^3/g with pore size distribution of 9-13nm. Micropore volume difference between Hc ZSM-5 and R ZSM-5 is 0.03cm^3/g.

Subsequently, an attempt at making ordered Hc ZSM-5 was made using CMK, known for its monolithic ordered structure. (Fang and Hu, 2006). Al/SBA-15 (mesoporous silica) was used as zeolite precursor. N_2 adsorption measurements confirmed the creation of mesopores (5nm) in the ZSM-5 crystal. The mesopore volume was found to be 0.5cm^3/g, indicating complete crystallization of Al/SBA-15. This was supported by FTIR spectra. Hydrothermal stability of Hc ZSM-5 was determined by steam treatment, after which it remained stable, as confirmed by XRD and TEM Imagery. Finally, metal assisted Hc ZSM-5 gave better results as compared with metal assisted R ZSM-5 in the methylation of 2-methylnaphtalene with methanol.

In the pursuit of perfection, a new scheme was proposed in which the use of a specialty carbonaceous template (3DOM carbon) was used in so called 'confined' synthesis (Yoo *et al*, 2009). This involves impregnating the pores of the 3DOM carbon pieces with zeolite precursor mix and subsequent low temperature crystallization followed by calcination to remove the template. This led to formation of MFI (silicalite) nanocrystals, a rare occurrence when using carbonaceous templating methods. High precursor concentrations (nucleation dominant conditions) led to polycrystalline zeolite particles, whereas growth dominant conditions led to large single crystals.

Going further, problems associated with cost and environmental hazards associated with choice of carbonaceous template led to the search for more eco-friendly cost effective solutions. Nandan *et al* (2014) presented one such example, using glucose as a template. Hc ZSM-5 was synthesized by conventional methods. Mesopore/macropore volume was considerably higher (0.22cm^3/g) when compared with R ZSM-5 (0.10cm^3/g), although there was a significant change in micropore volume (0.07cm^3/g). It was also noticed that activity decreased with increase in glucose concentration. Catalytic conversion of phenol was found to be greatly enhanced in the Hc ZSM-5 (46.6%) as compared with R ZSM-5 (13.7%). This may be attributed to the ease of diffusion in the Hc ZSM-5, as R ZSM-5 has been proven to have more activity.

Due to irregularities in pore formation associated with the glucose templated Hc ZSM-5, more research unearthed a new template synthesized from biological material (biomass) for Hc ZSM-5 synthesis (White *et al*, 2014). This template, NDC (Nitrogen doped Carbonaceous) monolith was found to have a desirable mesopore generating length scale (12-16nm) and was successfully employed in the synthesis of Hc ZSM-5 via conventional zeolite synthesis procedure. Interestingly, N_2 adsorption measurements showed that micropore volume was not significantly altered by the presence of NDC monolith in the synthesis, as compared with R ZSM5(~0.13cm^3/g). Pore size distribution of Hc ZSM-5 had a maxima around 10-20nm considerably repeating the structure of NDC monolith in the ZSM-5 crystal to create mesopores. Volume of mesopores was found to be 0.13cm^3/g, giving a 50:50 ratio between micopores and mesopores. High crystallinity was noticed when using high resolution TEM imagery. Mesoporosity was also tunable, by varying precursor concentration, solvent volume etc. Given the 3D nature of the NDC monolith, intracrystallinity in the zeolite can be engineered by impregnation as was done with 3DOM carbon, producing nanocrystals. These NDC monoliths have prospective comparability in performance to the more acclaimed 3DOM Carbon, and are without their cost and environmental malaise.

Finally, a modification of a template that can be wittingly referred to as the old lady in hierarchicalization of zeolites using carbonaceous templates was considered, being that it was one of the more facile routes, and considering it's known environmental dynamics(Han *et al*, 2016). Carbon black was used in the synthesis of mesoporous ZSM-5 zeolites as carbonaceous template. The hydrophobic carbon black was first oxidized to gain hydrophilicity via the action of sodium hypochlorite solution. This induced the uniformity of mesopore distribution within the synthesized Hc ZSM-5. Conventional zeolite synthesis method was then followed. A narrow mesopore range (5-18nm) was identified using N_2 adsorption measurements. It was also found that changing the carbon black content regulated both the textural properties and acidity of the Hc ZSM-5, as determined by BET/SEM/TEM and NH_3 TPD measurements respectively. When used for toluene disproportionation, Hc ZSM-5 was comparable to commercial ZSM-5, having a better conversion and xylene selectivity, and almost identical p-xylene selectivity.

5.0 CONCLUSION

Considering all that has been discussed, it has been seen that all the various strategies by which hierarchical

zeolites are produced have been elaborated upon. Their application has also been reviewed when it comes to FCC operation. Finally, previous works related to hierarchicalization of zeolites, and its respective application in FCC and allied operations, with special emphasis on Hc ZSM5, have been considered. It is hoped that armed with this information, a better picture About the scope and extent of research regarding hierarchical ZSM-5 use in oil refining and FCC has been visualized. Going forward, as more research is conducted in this field, it can be appropriately deduced as adduced from the prevailing literature that an optimal strategy for Hc ZSM-5 catalyst synthesis for the process should fulfill the following: induce hydrothermal stability with excellent mechanical strength; be economically suitable; environmentally friendly; have a facile process of application; optimize catalytic activity; ingrain order in the catalyst; and enable tuning of catalyst parameters to suit prevailing conditions of service and extend its functionality. Accordingly, the biomass engineered template (NDC) shows great prospects for the future, although there remains a considerable gulf in quality between the optimum product and its present condition.

ACKNOWLEDGEMENT

Funding: This work was supported by the Petroleum Technology Development Fund (PTDF) Abuja, Nigeria.

ABBREVIATIONS

Hc – Hierarchical
SDA- Structure Directing Agent
VPT- Vapour Phase Transport
SAC- Steam Assisted Conversion
TIPB- (1,3,5 tri-isopropylbenzene)
CTAB- cetyltrimethylammonium bromide
PI- Piperidine
R- Conventional
HF- Hierarchical Factor
APTMS- 3-Aminopropyltrimethoxysilane
APTES- 3-Aminopropyltriethoxysilane
PHAPTMS- Phenylaminopropylmethoxysilane
RF- Resorcinol-Formaldehyde
SSA- Specific Surface Area
NDC- Nitrogen Doped Carbonaceous

REFERENCES

Ban, S., Van laak, A.N.C., Landers, J., Neimark, A.V., Jongh, P.E, and Vlugt, T.G.H. (2010) Insight into the Effect of Dealumination on Mordenite Using Experimentally Validated Simulations, *Journal of Physical Chemistry C*, 114, pp. 2056 – 2065.

Ding, J., Liu, H., Yuan, P., Shi, G., and Bao, X. (2013) Catalytic Properties of a hierarchical Zeolite Synthesized from a Natural Aluminosilicate Mineral without the use of a Secondary Mesoscale Template, *ChemCatChem*, 5, pp. 2258 – 2269.

Ding, K., Corma, A., Macia-Agullo, J.A., Hu, J.G., Kramer, S., Stair, P.C., and Stucky, G.D. (2015) Constructing Hierarchical Porous Zeolites via Kinetic Regulation, *Journal of American Chemical Society*, 137, pp. 11238 – 11241.

Fang, Y., and Hu, H. (2006) An Ordered Mesoporous Aluminosilicate with Completely Crystalline Zeolite Wall Structure, *Journal of American Chemical Society*, 128, pp. 10636- 10637.

Groen, J.C., Jansen, J.C., Moulijn, J.A., and Perez-Ramirez, J. (2004) Optimal Aluminum-Assisted Mesoporosity Development in MFI Zeolites by Desilication, *Journal of Physical. Chemistry B*, 108, pp. 13062 – 13065.

Guo, Y.P., Wang, H., Guo, Y.J., Guo, L., Chu, L., and Guo, C. (2011) Fabrication and Characterization of Hierarchical ZSM-5 Zeolites by Using Organosilanes as Additives, *Chemical Engineering Journal, Elsevier*, 166, pp. 391 – 400.

Han, S., Wang, Z., Meng, L., and Jiang, N. (2016) Synthesis of Mesoporous ZSM 5 usingHydrophilic Carbon as Hard Template, *Materials Chemistry and Physics, Elsevier*, 177, pp. 112-117.

He, D., and Liu, D. (2014) Amphiphilic Organosilane-Directed Synthesis of Mesoporous ZSM-5 Zeolite Crystals with a Chainlike Morphology, *Chemistry Letters*, 43, pp. 1616 – 1618.

Hu, T., Liu, J., Cao, C., and Song, W. (2017) Synthesis of ZSM-5 Monolith with HierarchicalPorosity through a Steam-Assisted Crystallization Method Using Sponges as Scaffolds *Chinese Journal of Catalysis*, 38, pp. 872 – 878.

Ishihara, A., Kimura, K., Onaki, A., Inui, K., Hashimoto, T., and Nasu, H. (2012) Catalytic Cracking of VGO by Hierarchical ZSM 5 Zeolite Containing Mesoporous Silica Aluminas using Curie Point

Pyrolyser, *Catalysis Communications, Elsevier*, 28, pp. 163.

Jin, L., Liu, S., Xie, T., Wang, Y., Guo, X., and Hu, H. (2014) Synthesis of Hierarchical ZSM-5 by Cetyltrimethylammonium Bromide Assisted Self-Assembly of Zeolite Seeds and its Catalytic Performances, *Reaction Kinetics Mechanisms and Catalysis, Springer*, 113, pp.575 – 584.

Keoh, S.H., Chaikittisilp, W., Muraoka, K., Mukti, R.R., Shimojima, A., Kumar, P., Tsapatsis,M., and Okubo, T. (2016) Factors Governing the Formation of Hierarchically and Sequentially Intergrown MFI Zeolites by Using Simple Diquaternary Ammonium Structure-Directing Agents, *Chemistry of Materials*, 28, pp. 8997 – 9007.

Li, B., Hu, Z., Kong, B., Wang, J., Li, W., Sun, Z., … Zhao, D. (2014b) Hierarchically Tetramodal-Porous Zeolite ZSM-5 Monoliths with Template-Free-Delivered Intracrystalline Mesopores, *Chemical Science*, 5, pp. 1565 – 1573.

Li, G., Diao, Z., Na, J., and Wang, L. (2015a) Exploring Suitable ZSM-5/MCM-41 Zeolites for Catalytic Cracking of n-dodecane: Effect of Initial Particle Size and Si/Al Ratio, *Chinese Journal of Chemical Engineering*, 23, pp. 1655 – 1661.

Li, K, Valla, J., and Martinez, J.G. (2014a) Realizing the Commercial Potential of Hierachical Zeolites: New Opportunities in Catalytic Cracking, *ChemCatChem Reviews*, 6, pp. 51, 52, 57.

Li, W., Ma, T., Zhang, Y., Gong, Y., Wu, Z., and Dou, T. (2015b) Facile Control on Inter-Crystalline Porosity in the Synthesis of Size-Controlled Mesoporous MFI Zeolites Via In Situ Conversion on Silica Gel into Zeolite Nanocrystals for Catalytic Cracking, *CrystEngComm*, 17, pp. 5680 – 5689.

Li, X., Sun, M., Rooke, J.C., Chen, L., and Su, B. (2013) Synthesis and Applications of Hierarchically Porous Catalysts, *Chinese Journal of Catalysis*, 34, pp. 22, 23.

Liu, B., Duan, Q., Li, C., Zhu, Z., Xi, H., and Qian, Y. (2014a) Template Synthesis of the Hierachical Structured MFI Zeolite with Nanosheet Frameworks and Tailored Structure, *New Journal of Chemistry*, 38, pp. 4380-4388.

Liu, B., Zheng, L., Zhu, Z., Zhang, K., Xi, H., Qian, Y. (2014b) Effect of Synthesis Conditions on the Structural and Catalytic Properties of Hierarchically Structured ZSM-5 Zeolites, *Royal Society of Chemistry Advances*, 4, pp. 13831 – 13838.

Liu, F., Willhammar, T., Wang, L., Zhu, L., Sun, Q., Meng, X., … Xiao, F. (2012) ZSM-5Zeolite Single Crystals with B-Axis Aligned Mesoporous Channels as an Efficient Catalyst for Conversion of Bulky Organic Molecules, *Journal of American Chemical Society*, 134, pp. 604 – 610.

Moller, K., and Bein, T. (2013) Mesoporosity: A New Dimension for Zeolites, *Chemical Society Reviews*, 44, pp. 3703, 3694.

Na, K, and Somorjai, G.A. (2015) Hierarchically Nanoporous Zeolites and Their HeterogeneousCatalysis: Current Status and Future Perspectives, *Catalysis Letters, Springer*, 145, pp. 193 – 213.

Na, K., Choi, M., and Ryoo, R. (2013) Recent Advances in the Synthesis of Hierarchical Nanoporous Zeolites, *Microporous and Mesoporous Materials, Elsevier*, 166, pp. 4-6.

Na, K., Park, W., Seo, Y., and Ryoo, R. (2011) Disordered Assembly of MFI Zeolite Nanosheets with a Large Volume of Intersheet Mesopores, *Chemistry of Materials*, 2, pp. 1273 – 1279.

Nandan, D., Saxena, S.K., and Viswanadham, N. (2014) Synthesis of Hierachical ZSM 5 using Glucose as a Templating Precursor, *Journal of Materials Chemistry A*, 2, pp. 1054-1059.

Pavol, H. (2011, June) *FCC Catalyst - Key Element in Refinery Technology*, Paper Prensented at the 45th International Petroleum Conference, Bratislava, Slovak Republic, pp. 9, 11.

Perez-Page, M., Yu, E., Li, J., Rahman, M., Dryden, D.M., Vidu, R., and Stroeve, P. (2016) Template-Based Synthesis for Shape Controlled Nanostructures, *Advances in Colloid and Interface Science, Elsevier*, w234, pp. 69.

Schwieger, W., Machoke, A.G., Weissenberger, T., Inayat, A., Selvam, T., Klump, M., and Inayat, A. (2016) Hierachy Concepts: Classification and Preparation Strategies for Zeolite Containing Materials

with Hierachical Porosity, *Chemical Society Reviews*, 45, pp. 3353.

Serrano, D.P., Escola, J.M., and Pizarro, P. (2013) Synthesis Strategies in Search of Hierachical Zeolites, *Chemical Society Reviews*, 42, pp. 4004, 4009.

Tao, H., Yang, H., Liu, X., Ren, J., Wang, Y., and Lu, G. (2013) Highly Stable Hierarchical ZSM-5 Zeolite with Intra- and Inter-Crystalline Porous Structures, *Chemical Engineering Journal, Elsevier*, 225, pp. 686 – 694.

Tao, Y., Kanoh, H., and Kaneko, K. (2002) ZSM-5 Monolith of Uniform Mesoporous Channels, *Journal of American Chemical Society*, 125, pp. 6044 – 6045.

Tarach, K.A., Martinez-Triguero, J., Rey, F., and Gora-Marek, K. (2016) Hydrothermal Stability and Catalytic Performance of Desilicated Highly Siliceous Zeolites ZSM-5, *Journal of Catalysis, Elsevier*, 339, pp. 256 – 269.

Vogt, E.T.C., and Weckhuysen, B.M. (2015) FCC: Recent Development on the Grand Old Lady of Zeolite Catalysis, *Chemical Society Reviews*, 44, pp. 7342 – 7370.

Wan, W., Fu, T., Qi, R., Shao, J., and Li, Z. (2016) Coeffect of Na+ and Tetrapropylammonium (TPA+) in Alkali Treatment on the Fabrication of Mesoporous ZSM-5 Catalyst for Methanol-to-Hydrocarbons Reactions, *Industrial and Engineering Chemistry Research*, 55, pp. 13040 – 13049.

Wang, C., Li, J., Yan, J., and Sun, J. (2014a) Investigation on the Morphology of Hierarchical Mesoporous ZSM-5 Zeolite Prepared by the CO2-in-Water Microemulsion Method, *Korean Journal of Chemical Engineering*, 31, pp. 1547 – 1552.

Wang, D., Zhang, L., Chen, L., Wu, H., and Wu, P. (2015) Post-synthesis of Mesoporous ZSM-5 Zeolite by Piperidine Assisted Desilication and its Superior Catalytic Properties in Hydrocracking, *Journal of Materials Chemistry A.*, 3, pp. 3511-3521.

Wang, Q., Wei, Y., Xu, S., Zhang, M., Meng, S., Fan, D., … Liu, Z. (2014b) Synthesis of Mesoporous ZSM-5 Using a New Gemini Surfactant as a Mesoporous Directing Agent: A Crystallization Transformation Process, *Chinese Journal of Catalysis*, 35, pp. 1727 – 1739.

Wang, Y., and Liu, D. (2016) Synthesis of Mesoporous ZSM-5 Zeolite Crystals by a NewOrganosilane Template with Double-Oxycarbonyl Carbon Chains, *Chemistry Letters*, 45, pp. 1012 – 1014.

Wang, Y., Ma, J., Ren, F., Du, J., and Li, R. (2017) Hierarchical Architectures of ZSM-5Nanocrystalline Aggregates with Particular Catalysis for Larger Molecule Reaction, *Microporous and Mesoporous Materials, Elsevier*, 240, pp. 22 – 30.

Wei, Y., Parmentier, J.E., de Jong, K.P., and Zecevic, J. (2015) Tailoring and Visualizing the Pore Architecture of Hierachical Zeolites, *Chemical Society Reviews*, 44, pp. 7234-7261.

White, R.J., Fischer, A., Goebel, C., and Thomas, A. (2014) A Sustainable Template for Mesoporous Zeolite Synthesis, *Journal of American Chemical Society*, 136, pp. 2715-2718.

Xiao, Q., Yao, Q., Zhuang, J., Liu, G., Zhong, Y., and Zhu, W. (2013) A Localized Crystallization to Hierarchical ZSM-5 Microspheres Aided by Silane Coupling Agent, *Journal Colloid and Interface Science, Elsevier*, 394, pp. 604 – 610.

Yang, X.Y., Chen, L.H., Li, Y., Rooke, J.C., Sanchez, C., and Su, B.L. (2017) Hierachically Porous Materials: Synthesis Strategies and Structure Design, *Chemical Society Reviews*, 46, 481, pp. 493.

Yoo, W.C., Kumar, S., Penn, R.L., Tsapatsis, M., and Stein, A. (2009) Growth Patterns and Shape Development of Zeolite Nanocrystals in Confined Syntheses, *Journal of American Chemical. Society*, 131, pp. 12377 – 12383.

Yuan, E., Tang, Z., and Mo, Z. (2014) A New Method to Construct Hierarchical ZSM-5 Zeolites with Excellent Catalytic Activity, *Journal of Porous Materials, Springer*, 21, pp. 957 – 965.

Yue, Y., Liu, H., Yuan, P., Li, T., Yu, C., Bi, H., and Bao, X. (2014) From Natural Aluminosilicate Minerals to Hierarchical ZSM-5 Zeolites: A Nanoscale Depolymerization-Reorganisation Approach, *Journal of Catalysis, Elsevier*, 319, pp. 200-210.

Zhang, K., and Ostraat, M.L. (2016) Innovations in hierarchical Zeolite Synthesis, *Catalysis Today, Elsevier*, 264, pp. 3, 6.

Zheng, J., Zhang, H., Liu, Y., Wang, G., Kong, Q., Pan, M., Tian, H., Li, R. (2016) Synthesis of Wool-Ball-Like ZSM-5 with Enlarged External Surfaces and Improved Diffusion: A Potential Highly-Efficient FCC Catalyst Component for Elevating Pre-Cracking of Large Molecules and Catalytic Longevity, *Catalysis Letters, Springer*, 146, pp. 1457 – 1469.

Zhou, J., Hua, Z., Lin, Z., Wu, W., Zhu, Y., and Shi, J. (2011) Direct Synthetic Strategy of Mesoporous ZSM-5 Zeolites by Using Conventional Block Copolymer Templates and the Improved Catalytic Properties, *ACS Catalysis*, 1, pp. 287 – 291.

Zhu, H., Abou-Hamaad, E., Chen, Y., Saih, Y., Liu, W., Samal, A.K., and Basset, J. (2016)Organosilane with Gemini-Type Structure as the Mesoporogen for the Synthesis of the Hierarchical Porous ZSM-5 Zeolite, *Langmuir*, 32, pp. 2085 – 2092.

Zhu, J., Meng, X., and Xiao, F., (2013) Mesoporous Zeolites as Efficient Catalyst for Oil Refining and Natural Gas Conversion, *Frontiers of Chemical Science and Engineering*, 7(2), pp. 233 – 248.

Zhu, K., Sun, J., Liu, J., Wang, L., Wan, H., Hu, J., … Nie, Z. (2011) Solvent Evaporation Assisted Preparation of Oriented Nanocrystalline Mesoporous MFI Zeolites, *ACS Catalysis*, 1, pp. 682 – 690.

JOURNAL OF THE NIGERIAN SOCIETY OF ENGINEERS
INSTRUCTION TO AUTHORS

1. TYPES OF PUBLICATION

The Journal of the Nigerian Society of Chemical Engineers will publish articles on the original research on the Science and Technology of Chemical Engineering. Preference will be given to articles on new processes or innovative adaptation of existing processes. Critical reviews on current topics of Chemical Engineering are encouraged and may be solicited by the Editorial Board. The following types of articles will be considered for publication:

a. Full length **articles or review papers**.
b. **Communication** – a preliminary report on research findings.
c. **Note** – a short paper describing a research finding not sufficiently completed to warrant a full article.
d. **Letter to the Editor** – comments or remarks by readers and/or authors on previously published materials.

The authors are entirely responsible for the accuracy of data and statements. It is also the responsibility of authors to seek ethical clearance and written permission from persons or agencies concerned, whenever copyrighted material is used.

2. MANUSCRIPT REQUIREMENTS

a. The **Manuscript** should be written in clear and concise English and typed in Microsoft Word using double spacing on A4-size paper, Times New Romans font and 12 point. A full length article or review should not exceed 15 pages. Margin should be Normal (i.e. 2.54cm for Top, Bottom, Left & Right margins).
b. The **Manuscript** should be prepared in the following format: Abstract, Introduction, Materials and Methods, Results, Discussion, Conclusion, Acknowledgements, and References..
c. The **Manuscript** must contain the full names, address and emails of the authors. In the case of multiple authorship, the person to whom correspondence should be addressed must be indicated with functional email address. As an examples, authors' names should be in this format:
Momoh, S. O., Adisa, A. A. and **Abubakar, A. S.**
If the addresses of authors are different, use the following format:
***Momoh, S. O.[1], Adisa, A. A.[2]** and **Abubakar, A. S.[3]**
Use star * to indicate the corresponding author.

d. **Symbols** should conform to America Standard Association. An abridged set of acceptable symbols is available in the fourth edition of Perry's Chemical Engineering Handbook. Greek letters, subscripts and superscripts should be carefully typed. A list of all symbols used in the paper should be included after the main text as **Nomenclature**.
e. All **Units** must be in the SI units (kg, m, s, N, etc).
f. The **Abstract** should be in English and should not be more than 200 words. The Abstract should state briefly the purpose of the research, methodology, results, major findings and major conclusions. Abstracts are not required for Communications, Notes or Letters.
g. **Citation** must be in the Harvard Format i.e. (Author, Date). Examples are (Smith, 1990) or (Jones et al, 2011). (Kemp, 2000) demonstrated that …..; (Mbuk, 1985; Boma, 1999; Sani, 2000) if more than two authors. (Telma, 2001a), (Telma, 2001b); etc if the citation have the same author and year of publication.
For more information on Harvard Referencing: Guide visit http://www.citethisforme.com/harvard-referencing
h. **References** must also be in the Harvard Format i.e. (Author, Date, Title, Publication Information). References are listed in alphabetical order. Examples are shown below:
Haghi, A. K. and Ghanadzadeh, H. (2005). A Study of Thermal Drying Process. *Indian Journal of Chemical Technology*, Vol. 12, November 2005, pp. 654-663
Kemp, I.C., Fyhr, C. B., Laurent, S., Roques, M. A., Groenewold, C. E., Tsotsas, E., Sereno, A. A., Bonazzi, C. B., Bimbernet, J. J. and Kind M.(2001). Methods for Processing Experimental Drying Kinetic Data. *Drying Technology*, 19: 15-34.
i. **Tables** should contain a minimum of descriptive materials. Tables should be numbered in Arabic numerals (1, 2, 3, etc), and should be placed at the referenced point with captions (centralised) placed at the top of the table.
j. **Figures**, charts, graphs and all illustrations should be placed at the referenced point, numbered in Arabic numerals (1, 2, 3, etc) and incorporated in the text. Caption for Figures should be placed at the bottom of the Figure (centralised). Lettering set or symbols should be used for all labels on the figures, graphs, charts, photographs even when drawn in colours. (Note that figures drawn in colours may be unreadable if printed in black and white).
k. **Equations** should be typed using MS Word Equation Editor and should be centred with number (in Arabic numeral) at the right margin.
l. Wherever possible, **Fractions** should be shown using the oblique slash. E.g. x/y
m. **Footnotes** should not be incorporated in the text.
n. **Acknowledgements** should appear at the end of the paper, before the list of references.

3. SUBMISSION OF MANUSCRIPTS

Manuscripts should be submitted by sending a Microsoft Word document (taking into account the Manuscript Requirements described in section 2 above) to the following email address: **nschejournal@yahoo.com** and copy **stevmomoh@yahoo.com.**
All correspondences are directed to the Editor-in-Chief using the submission emails addresses: nschejournal@yahoo.com and copy stevmomoh@yahoo.com.

4. ACCEPTED PAPERS

On acceptance, authors will be required to submit a copy of their manuscripts using Microsoft Word by emails to **nschejournal@yahoo.com** and copy **stevmomoh@yahoo.com**.

The following additional information should be observed for accepted papers: (i) Typed in Microsoft Word using 1.15 spacing on A4-size paper, Times New Romans font and 10 point; (ii) Margin should be 2.54cm for Top & Bottom; 2.20cm for Left & Right margins; (iii) The abstract should be one column document while the body of the manuscript should be double columns with 0.5cm gutter spacing except some tables and figures that may have to go in for one column document.

5. PUBLICATION

Full NSChE Journal edition in hard copy will be published twice annually.

6. REPRINT

Reprints are available on request at a moderate fee per page. Orders must be placed before the paper appears in Print.

7. READER'S INFORMATION

The papers are wholly the view of their author(s) and therefore the publishers and the editors bear no responsibility for such views.

8. SUBSCRIPTION INFORMATION

The subscription price per volume is as follows:

a. Individual Reader - ₦3,000.00
b. Institutions, Libraries, etc. - ₦5,000.00
c. Overseas Subscription - $100.00

Request for information or subscription should be sent to the Editor-in-Chief through the following emails addresses: nschejournal@yahoo.com and copy stevmomoh@yahoo.com.

9. COPYRIGHT NOTICE

Copyright of published material belongs to the journal

10. PRIVACY STATEMENT

The names and email addresses entered in this journal site will be used exclusively for the stated purposes of this journal and will not be made available for any other purpose or to any other party.

GENERAL ANNOUNCEMENT

As from the next edition (March/April 2020), a fee will be charged for paper review and publication; and this will be borne by the authors.

1. **Manuscript Review charges = ₦6,500 payable by both Members and Non-Member.**
2. **Publication Charges = ₦10,000 payable by Non-Members and Members who are not financially up-to-date.**
3. **Members would only get one (1) Journal free and buy the other if they so wish.**
4. **Corresponding Author whose paper is published on a particular edition would get one (1) free copy on behalf of all the co-authors. Other co-authors will buy if they so wish.**